EUROPEAN SCHOOL OF MOLECULAR MEDICINE
Sede di Napoli

UNIVERSITÀ DEGLI STUDI DI NAPOLI FEDERICO II

Ph.D. in Molecular Medicine
Human Genetics

Expanding AAV cargo capacity for gene therapy of Stargardt disease

Tutor
Prof. Alberto Auricchio
Medical Genetics,
Dept. of Translational Medicine,
Federico II University
TIGEM
SEMM

Ph.D. student
Mrs. Ivana Trapani
TIGEM
SEMM

Internal Supervisor
Prof. Vincenzo Nigro
Dept. of Biochemistry, Biophysics and General Pathology,
Second University of Naples
SEMM

External Supervisor
Prof. Rando Allikmets
Dept. of Pathology and Cell Biology,
Columbia University

2009 – 2013

PUBLICATIONS

1. **I. Trapani**, P. Colella, A. Sommella, C. Iodice, G. Cesi, S. de Simone, E. Marrocco, S. Rossi, M. Giunti, A. Palfi, G. Jane Farrar, R. Polishchuk, A. Auricchio. Effective delivery of large genes to the retina by dual AAV vectors. EMBO Molecular Medicine. 2014; PMID: 24150896. **APPENDIX**

2. P. Colella, **I. Trapani**, G. Cesi, A. Sommella, A. Manfredi, A. Puppo, C. Iodice, S. Rossi, F. Simonelli, M. Giunti, M. L. Bacci, A. Auricchio. Efficient gene delivery to the cone-enriched pig retina by dual AAV vectors. Gene Therapy. 2014, in press.

INDEX

LIST OF ABBREVIATIONS

IRDs: inherited retinal degenerations

PRs: photoreceptors

AAV: adeno-associated virus

RPE: retinal pigmented epithelium

STGD: Stargardt disease

ONL: outer nuclear layer

INL: inner nuclear layer

MC: Müller cells

GCL: ganglion cell layer

OPL: outer plexiform layer

IPL: inner plexiform layer

OLM: outer limiting membrane

ILM: inner limiting membrane

OS: outer segment

IS: inner segment

ABCA4: ATP-binding cassette, subfamily A, member 4

PE: phosphatidylethanolamine

ERG: electroretinogram

ITR: inverted terminal repeats

NS: normal size

OZ: oversize

OV: overlapping

TS: trans-splicing

SD: splicing donor signal

SA: splicing acceptor signal

AP: alkaline phosphatase recombinogenic region

AK: F1 phage recombinogenic region

FIGURES AND TABLES INDEX

ABSTRACT

Inherited retinal degenerations (IRDs), with an overall global prevalence of 1/2,000, represent a major cause of blindness worldwide. IRDs are mostly inherited as monogenic conditions that are caused by mutations in genes preferentially expressed in photoreceptors (PRs) and retinal pigment epithelium (RPE) cells. Gene therapy represents a promising therapeutic strategy for IRDs. Vectors derived from the adeno-associated virus (AAV) have been proven to be the most efficient and safe tools for gene delivery to the retina. Further, AAV vectors have been successfully used in pre-clinical models and clinical trials focused on the treatment of IRDs. The major limitation to the use of AAVs is their packaging capacity, which is considered to be restricted to the size of the parental genome (4.7 kb) and thus hinders the treatment of certain forms of IRDs caused by mutations in genes whose coding sequence exceeds 5 kb in length, including the gene mutated in Stargardt disease (STGD), *ABCA4*. Thus, different strategies to overcome AAV cargo limitation have been investigated. One strategy for large gene transfer is based on "forced" packaging of large genes into AAV capsids (oversize AAV); this strategy, however, results in the production of viruses with a heterogeneous genome and thus may not be easily translated to the clinical arena due to safety concerns. Alternatively, the inherent ability of AAV genomes to undergo intermolecular concatemerization can be exploited to transfer large genes by splitting the expression cassette into two halves (<5 kb in size), each independently packaged in one of two separate (dual) AAV vectors. Dual AAV vectors can reconstitute a large gene via either splicing (dual AAV trans-splicing), homologous recombination (dual AAV overlapping) or a combination of the two (dual AAV hybrid). Dual AAV strategies have been used to efficiently delivery large genes to a number of tissues, however, the efficacy of the dual AAV systems for gene delivery to the retina remains to be investigated.

Therefore, the goals of my Ph.D. project were to:

- develop dual AAV vector-based strategies for large gene delivery to the retina;

- compare the efficiency of oversize to that of dual AAV vector strategies for the delivery of large genes both *in vitro* and *in vivo*, in the retina;
- characterize the effect of AAV-mediated large gene expression in an animal model of STGD.

To this aim, I generated oversize and dual AAV vectors encoding for either the reporter EGFP or the therapeutic ABCA4 protein to compare the efficacy of AAV vector systems *in vitro* using HEK293 cells and *in vivo* in mouse and pig eyes. I found that dual AAV vectors are more efficient than oversize vectors, both *in vitro* and in the retina. While dual AAV OV vectors are effective in transducing the RPE, dual AAV trans-splicing and hybrid approaches transduce efficiently PRs, in addition to RPE. Thus, as the PRs are the cell target for the treatment of STGD, I selected dual AAV trans-splicing and hybrid vectors as the candidate strategies to be tested in the mouse model of STGD (*Abca4-/-*). I injected subretinally one-month-old mice with dual AAV trans-splicing and hybrid vectors encoding for ABCA4 and found a significant improvement of the main STGD mice retinal abnormalities, including: lipofuscin accumulation, RPE thickening and recovery from light desensitization.

In conclusion, my data show that dual AAV trans-splicing and hybrid vectors are an attractive strategy for gene therapy of STGD as well as other retinal diseases that require the delivery of large genes.

INTRODUCTION

1. The eye and the retina

1.1 The eye

The eye is the highly specialized organ responsible for vision, the sense through which originates most of our high order neuronal activities: behaviour, learning, memory and emotions. It is composed of many specialized structures, organized into three main layers: i) the external fibrous layer, ii) the intermediate vascular layer and iii) the internal nervous layer (Blanks, 2001). The fibrous layer includes the sclera and the cornea (Fig. 1). The sclera is a dense, white, opaque, fibrous tissue that serves mainly as a protective barrier. The cornea is a transparent near-spherical dome at the front of the eye that refracts light to focus it to the internal nervous layer. The vascular layer is divided into two parts: anterior (iris and ciliary body) and posterior (choroid) (Fig. 1). The iris is a thin, circular structure responsible for controlling the diameter of the pupil and subsequently the amount of light reaching the retina. The ciliary body is important for accommodation, the process by which the eye maintains focus of an object at varying distances. The choroid provides oxygen and nourishment to the outer layers of the retina. The internal layer represents the sensory part of the eye, the retina, which is an extension of the central nervous system and is connected to the brain by the optic nerve (Fig. 1). In addition, a monolayer composed of specialized epithelial cells, the retinal pigment epithelium (RPE), separates the retina from the underlying choroid. The structures of the eye delimit three chambers of fluid: the anterior chamber (between cornea and iris), posterior chamber (between iris, zonule fibers and lens) and the vitreous chamber (between the lens and the retina). The first two chambers are filled with aqueous humor whereas the vitreous chamber is filled with a more viscous fluid, the vitreous humor (Fig. 1).

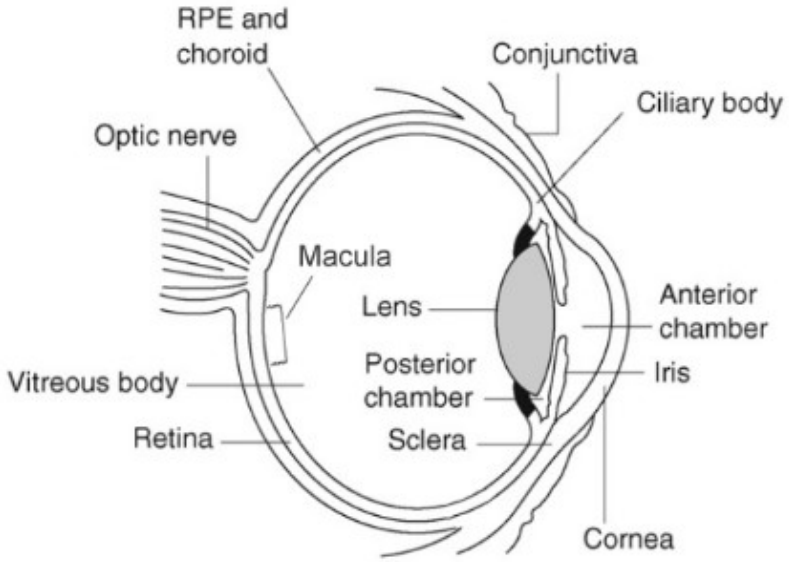

Figure 1. Schematic representation of the human eyeball
Modified from (Colella et al, 2009)

1.2 The retina

The retina represents the structural and functional basis of vision, as it is the light sensitive tissue of the eye. The retina is half a millimetre thick and is divided into three layers of cells: i) the outer nuclear layer (ONL), that contains photoreceptor (PRs) cell bodies; ii) the inner nuclear layer (INL) consisting of cell bodies of the bipolar, horizontal, amacrine and Müller cells (MCs) and iii) the ganglion cell layer (GCL, Fig. 2) (Blanks, 2001). In addition to these neuronal-derived layers, a monolayer of specialized epithelial cells, the RPE, overlays PRs. Importantly, PR cell function is intimately associated to that of the underlying RPE as this layer sustains PR cell integrity and metabolism (see section 1.4).

Neuronal interconnections (synapses) between the cells of the retina are placed in distinct histological layers. The region containing synapses between PRs and bipolar or horizontal cells is known as the outer plexiform layer (OPL), while the area where bipolar and amacrine cells connect to the ganglion cells is the inner plexiform layer

(IPL, Fig. 2) (Blanks, 2001). Fine processes of MCs, the major glial cells of the retina, envelop, at least partially, all the neurons within the retina. These processes extend as radial fibres spanning from the ONL to the GCL. In the ONL, adherent junctions between MCs and PRs form the outer limiting membrane (OLM), while in the GCL the expanded MCs vitreal processes (end-feet) and the basement membrane (a surface modification of the vitreous body) form the inner limiting membrane (ILM, Fig. 2). The OLM and the ILM form diffusion barriers between the neural retina and the subretinal space or vitreous humour, respectively.

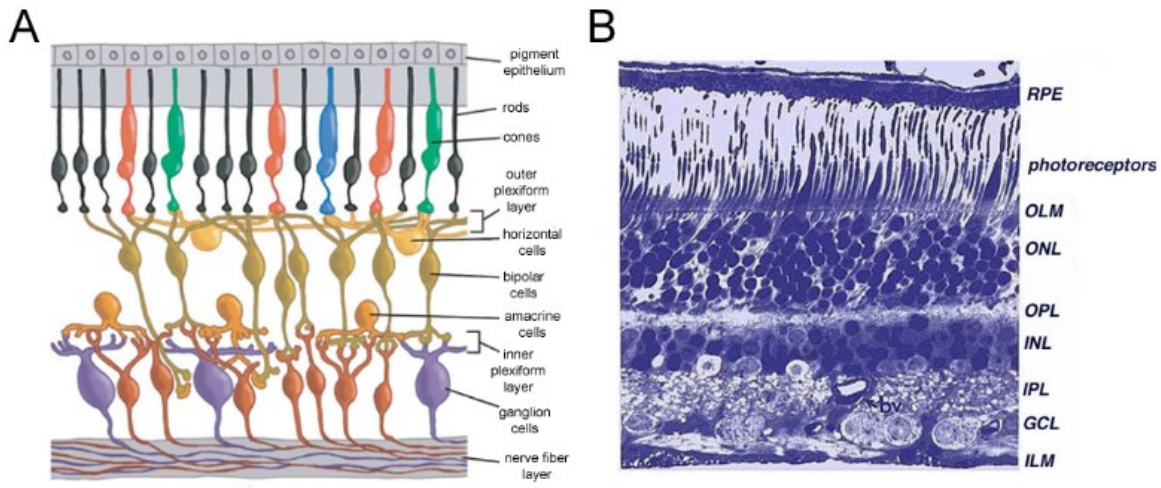

Figure 2. Organization of the retina
(A) A diagram that shows the schematic organization of the retina. Taken from (Abramoff et al, 2010). (B) Light micrograph of a vertical section through a human retina. Taken from http://webvision.med.utah.edu.

The process of vision begins at the level of PRs, the light sensitive cells of the retina. Light rays focused through the lens must pass through the entire retina before reaching the PRs, which convert photons into a chemical stimulus through the process of phototransduction (see section 1.4). This stimulus is then integrated and processed by interneurons (bipolar, horizontal and amacrine cells) and transmitted to GCs through

synapses in the IPL. Finally, GC axons, which project towards the optic nerve head, carry the signal to the visual centres of the brain (Blanks, 2001).

1.3 The photoreceptors: rods and cones

PRs are highly specialized sensory neurons able to capture light stimuli (electromagnetic radiation/photons) and to convert them into an electrochemical signal. There are two types of PRs in the retina: rods and cones, which differ in their sensitivity to light (Blanks, 2001). Rods mainly function under low-light conditions, being a hundred-fold more sensitive than cones, and are responsible for peripheral and night vision (Fu, 1995). Cones respond to bright light, provide visual acuity and mediate colour vision. In the retina of vertebrates, rods represent the majority of PRs, reaching a rod:cone ratio of 35:1 in mice, 18:1 in humans and 8:1 in pigs. The human retina contains approximately 6 million cones predominantly located in the macula, a small and highly sensitive region near the centre of the retina, responsible for central vision (Fig. 1) (Ahnelt, 1998). Specifically, the cones are most densely packed within the central portion of the macula, the fovea. In the central portion of the fovea the blood vessels, GCL, INL and IPL are displaced and this allows light to reach cones with minimal distortion to allow for acute and detailed vision. In addition to cones, there are approximately 125 million rods, which are spread throughout the peripheral retina. Structurally, both rods and cones can be divided into four functional segments: the outer segment (OS), the inner segment (IS), the nucleus and the synaptic body (Fig. 3) (Blanks, 2001). The OS is a modified cilium constituted by an elaborate system of stacked membranous discs (1,000/PR) that derive from invaginations of the plasma membrane during development. In rods most of these invaginations become separated from the plasma membrane, while discs remain connected to the outer membrane in cones. The membranous sacs disintegrate near the apical surface of the cell and their

cellular debris are removed through phagocytosis by the adjacent RPE (Young, 1976). Newly formed discs that originate near the base of the OS gradually replace the older discs (Hinton, 2001). The degradation and phagocytosis of the sloughed OS follows a diurnal rhythm. The IS contains the cytoplasm and the organelles of the cells and it is linked to the OS through the connecting cilium. The connecting cilium is responsible for the intracellular transport and turnover of proteins from and to the OS. The synaptic body connects PRs to subsequent neuronal cells, the horizontal and bipolar cells, which represent the next stages in the vision cascade.

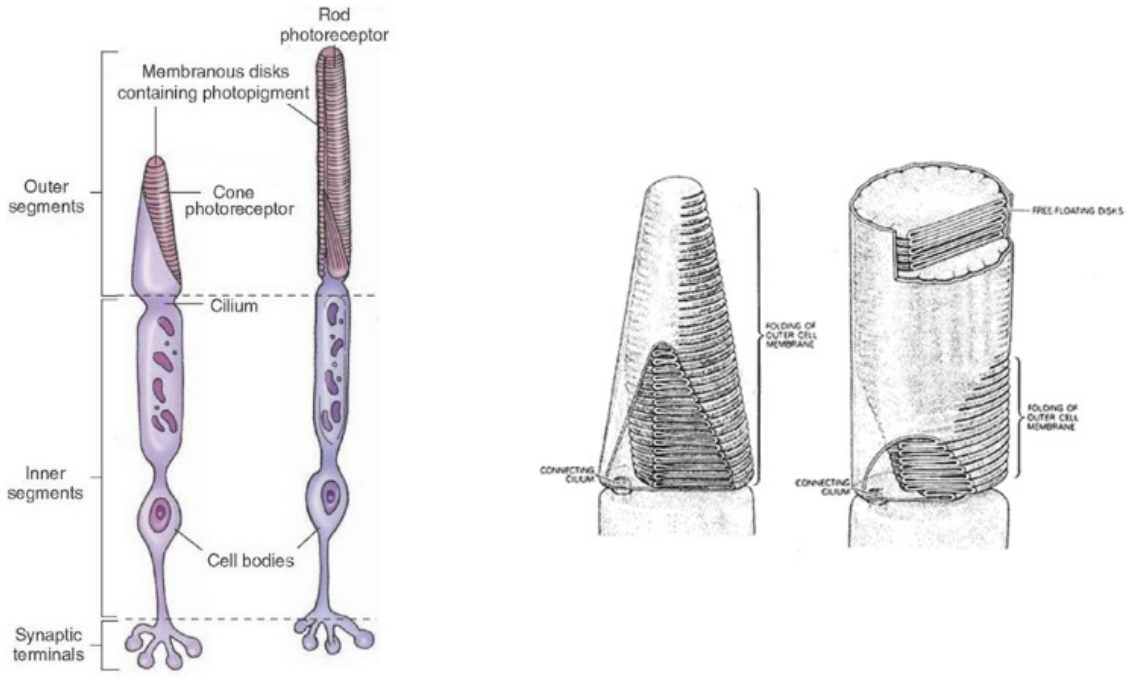

Figure 3. Structure of the PRs cell (left panel) and differences between the rod and cone OS structures (right panel)
Taken from http://what-when-how.com/neuroscience (A) and http://www.cis.rit.edu (B)

Visual pigments and other key players of the phototransduction pathway localize to the OS discs where the conversion of light energy into electrochemical signals occurs (Blanks, 2001). The visual pigments expressed in the OS, named opsins, determine the light-sensitivity of the PRs. Opsins are light-sensitive, membrane-bound G protein-

coupled receptors of the retinylidene protein family that covalently bind to a vitamin A-based retinaldehyde chromophore, which undergoes photoisomerisation following the absorption of a photon. Rods contain the photopigment rhodopsin (max absorbance 500nm). Cones contain one of three colour pigments that are uniquely sensitive to a particular wavelength of light: blue (445nm), green (535nm) or red (570nm).

1.4 Phototransduction and the visual cycle

Phototransduction is the biochemical pathway that takes place in OS discs, which mediates the conversion of photons into an electrochemical signal (Flannery, 2001). Phototransduction has been extensively studied in rods. In the absence of light, rhodopsin is bound to the 11-cis-retinal chromophore forming inactive rhodopsin (R) and the basal activity of the guanynyl cyclase keeps cGMP levels in the cell high(Fig. 4). Both Na^+ and Ca^{2+} enter the membrane channels leading to high Ca^{2+} levels and to the activation of guanylate-cyclase-activating protein (GCAP). The Ca^{2+}-bound calmodulin (CaM) confers high cGMP affinity to cGMP-gated channels in the OS plasma membrane keeping them open and thus the PRs depolarized. Photons reaching PRs induce the isomerization of the 11-cis-retinal to all-trans-retinal, activate rhodopsin (R*), that releases all-trans-retinal and activates the G protein transducin (αβγ subunits) by catalyzing a GDP to GTP exchange. The dissociated α-subunit of transducin subsequently activates cGMP-phosphodiesterase 6 (PDE6), which rapidly hydrolyzes the cytoplasmic cGMP. The decreased cGMP concentration causes the closure of the cGMP-gated cation channels on the plasma membrane thus reducing the Ca^{2+} influx (Fig. 4). As a result, rods are hyperpolarized and release fewer glutamate transmitters from the synaptic region of the PRs to the connected bipolar cells. This initial signal is transmitted via second-order retinal neurons to the optic nerve and ultimately to the brain. Additional proteins are required to shut off the cascade. In the recovery phase

photoactivated rhodopsin (R*) is desensitized by phosphorylation, which is mediated by the binding of the rhodopsin kinase protein (RHOK) and arrestin. Retinal guanylyl cyclase (GC) and guanylate cyclase activating protein (GCAP) replenish cGMP levels in a Ca^{2+}-dependent manner while the Na/Ca-K exchanger that resides on the plasma membrane, regulates Ca^{2+} homeostasis. All the components of the phototransduction cascade are arranged in close proximity at the disc membrane and at the plasma membrane of PRs (Fig. 4) (Flannery, 2001).

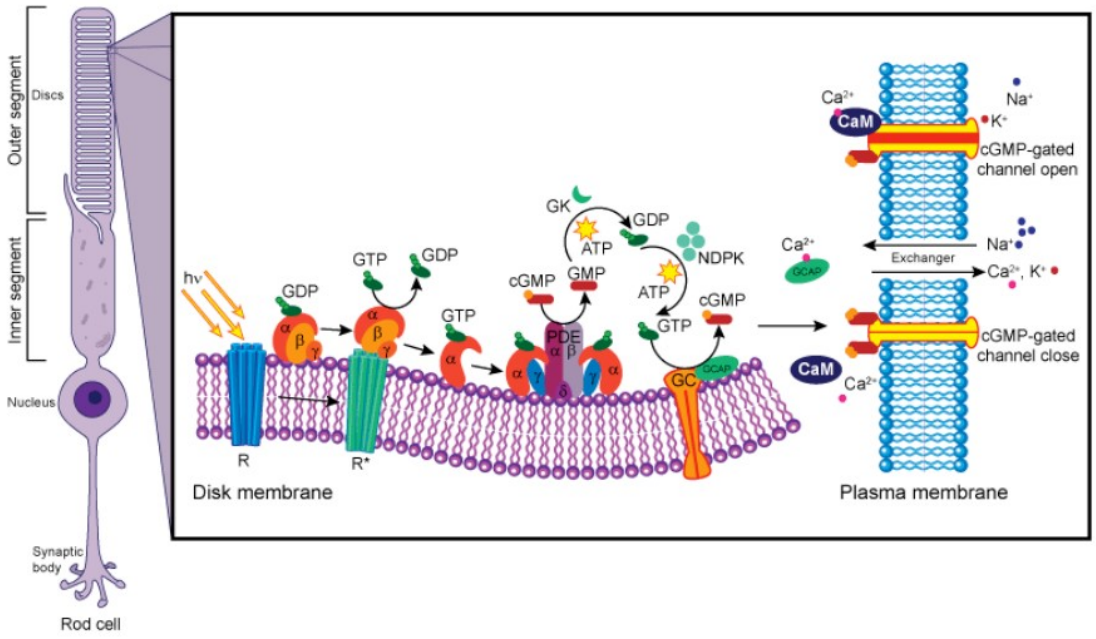

Figure 4. Phototransduction pathway in rod PRs
R: rhodopsin; R*: photoactivated rhodopsin; PDE6: phosphodiesterase 6; GCAP: guanylate cyclase activating protein; GC: guanylyl cyclase. Taken from http://mutagenetix.utsouthwestern.edu/phenotypic/phenotypic_rec.cfm?pk=282

The phototransduction cascade is closely associated with the visual cycle, an enzymatic pathway that starts in the rod OS yet is completed in RPE, where retinoids that are isomerized by light are "recycled" back to the PRs (Fig. 5) (Hinton, 2001).

As previously described, photoisomerization in rods converts the 11-cis-retinal to all-trans-retinal, which is then released from rhodopsin, conjugated with the membrane

lipid phosphatidylethanolamine (PE) and transported by the ATP-binding cassette, subfamily A, member 4 (ABCA4) from the lumen side of the disc to the OS cytoplasm. Here it is converted to all-trans retinol by a retinol dehydrogenase (RDH). The all-trans retinol is then released from the OS and taken up by the RPE, thanks to the transport mediated by retinoid-binding proteins, such as interphotoreceptor retinoid-binding protein (IRBP), that are involved in the transport of the hydrophobic retinoids in aqueous environments (Fig. 5). In the RPE the all-trans-retinol undergoes a series of enzymatic reactions to be converted back to 11-cis-retinal. All-trans-retinol is esterified to a fatty acyl group by lecithin retinol acyltransferase (LRAT) to form all-trans-retinyl ester, which in turn is subjected to trans-isomerization to 11-cis-retinal through the actions of two enzymes (RPE65 and 11-cis retinol dehydrogenase). Finally, 11-cis-retinal returns back to the OS where it is re-combined with the rhodopsin to form a new molecule of light-sensitive rhodopsin, completing the visual cycle (Fig. 5).

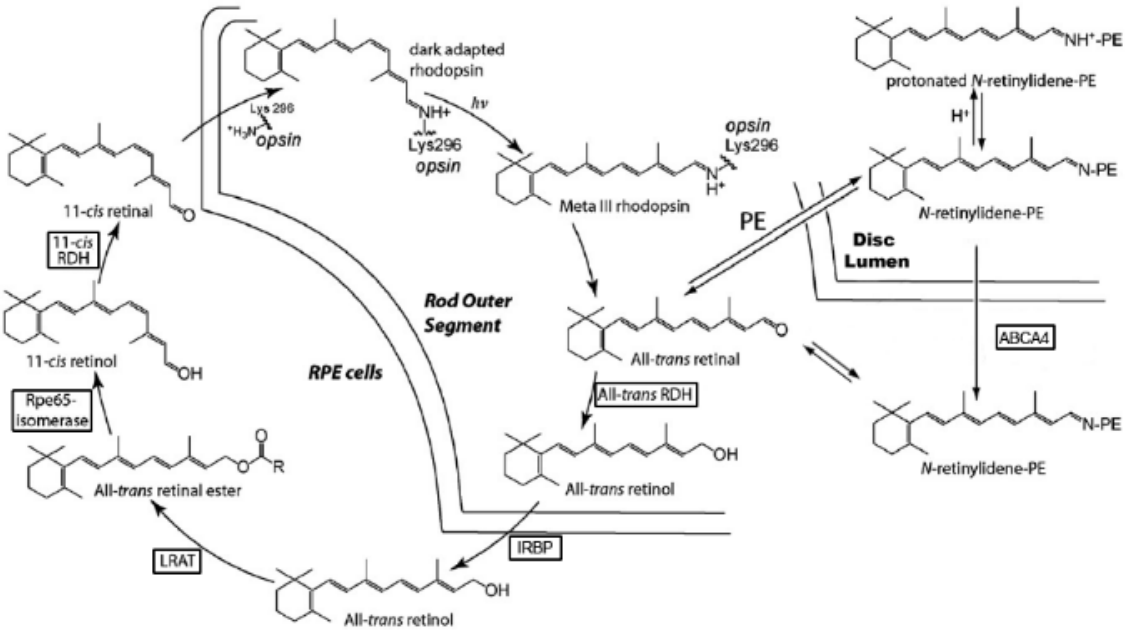

Figure 5. The visual cycle
RDH: retinol dehydrogenase; ABCA4: ATP-binding cassette, subfamily A, member 4; IRBP: interphotoreceptor retinoid-binding protein; LRAT: lecithin retinol acyltransferase; PE: phosphatidylethanolamine. Modified from (Molday & Zhang, 2010)

2. Inherited retinal degenerations and Stargardt disease

2.1 Inherited retinal degenerations (IRDs)

Maintenance of the complex PR-RPE connections requires the tight regulation of highly specialized intracellular protein interactions and the harmonic activity of several hundred gene products, of which most can lead to retinal dysfunction or cell death when mutated. Thus, it is not surprising that many genetic disorders manifest in the eye. IRDs have an overall global prevalence of 1/2,000 (Sohocki et al, 2001) and represent a significant cause of blindness worldwide. They are mostly inherited as Mendelian traits and are characterized by extensive genetic and clinical heterogeneity, however, they share a common pathological landmark: progressive degeneration ultimately resulting in PRs cell death. Genetic defects in more than 200 genes, including a myriad of functions, are known to underlie the etiology of IRDs (Fig. 6, http://www.sph.uth.tmc.edu/retnet/).

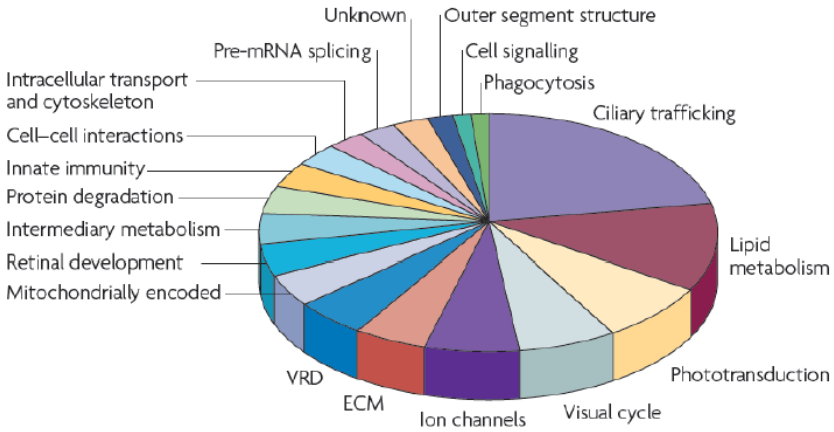

Figure 6. IRDs causative genes grouped by function
Pie chart depicting the functional classification of genes implicated in PR degeneration. The data are from the Retinal Information Network (RetNet). ECM: extracellular matrix; pre-mRNA: precursor mRNA; unknown: function undetermined; VRD: vitreoretinal degeneration; EM: extra-cellular matrix. Taken from (Wright et al, 2010).

These genes are mainly expressed in rods, cones and RPE, where they perform essential functions. Due to the close interdependence between PRs and RPE, dysfunctions in either of these two cell layers can cause secondary dysfunctions to the other (Ryan 2001).

For simplicity, retinal dystrophies are typically classified into two types by their phenotypic characteristics: those that initially and primarily affect the peripheral vision, such as retinitis pigmentosa (RP), and those that primarily affect the macula, the macular degenerations including Stargardt disease (Molday & Zhang, 2010). RP affects one in 3,500 people and is typically characterized by night blindness, progressive loss of peripheral vision and subsequent loss in central vision that often leads to total loss of sight. Macular degenerations involve the loss of central vision, with varying degrees of peripheral vision deterioration, which can affect people of all ages.

2.2 Stargardt disease (STGD)

Stargardt disease (STGD1; MIM #248200), first described by the German ophthalmologist Karl Stargardt in 1909 (Stargardt, 1909) is the most common autosomal recessive, early-onset macular dystrophy with a reported prevalence of 1:8,000-1:10,000 individuals (Fujinami et al, 2013; Noble & Carr, 1979; Walia & Fishman, 2009; Weleber, 1994), although the frequency of carrier of mutations in the gene causative of the STGD is thought to be as high as 2 in 100 (Zernant et al, 2011). STGD patients experience significant bilateral loss of central vision, photophobia and color vision abnormalities, parafoveal scotoma and slow dark adaptation (Allikmets, 2007; Fishman et al, 1991; Walia & Fishman, 2009; Westerfeld & Mukai, 2008). The age of onset of the vision decrease is highly variable, however, it mainly occurs between childhood and adolescence/early adulthood and rapidly progresses. Visual acuity at presentation may range from as good as 20/20 to as bad as <20/200, with prior visual

acuity frequently being normal, and very few patients have further deterioration of their vision to finger counting or hand motions level (Rotenstreich et al, 2003). The prognosis for visual outcome is highly dependent on the age of disease onset. Typically, the first diagnostic approach for STGD can simply be made by direct ophthalmoscopy. STGD affects the macula with variable centrifugal expansion but fundus examination is frequently normal early in the disease's progression, even if visual loss has already begun (Noble & Carr, 1979). Characteristic fundus manifestations arise later in the course of the disease and include pigment mottling, frank macular atrophy, a bull's-eye appearance and fundus flecks. Fundus flecks are pisciform, dot-like, yellow-white lesions typically found in STGD patients (Fig. 7) (Allikmets, 2007; Anderson et al, 1995; Stargardt, 1909).

Figure 7. Fundus of a patient diagnosed with STGD
Fundus photograph of the eye from a STGD patient showing the characteristic yellowish flecks around the macula and a defined area of central macular degeneration. Taken from (Allikmets, 2007)

Fundus flecks are manifestations of lipofuscin accumulation in the RPE but may also represent areas of regional depigmentation and atrophy (Molday & Zhang, 2010). Lipofuscin deposits are composed of a heterogeneous mixture of oxidized lipids, di-retinoids and other components derived from the incomplete degradation of phagocytized PR OS (Delori et al, 1995; Eldred & Lasky, 1993). Electroretinographic (ERG) measurements are variable and are not usually considered diagnostic for the disease (Genead et al, 2009; Lois et al, 2001). A relatively novel diagnostic approach has been developed to determine the viability of the RPE in a non-invasive procedure: fundus autofluorescence imaging. This takes advantage of the innate fluorescence of lipofuscin to quantify its distribution throughout the RPE (von Ruckmann et al, 1995). An increase in fundus autofluorescence represents lipofuscin accumulation in the RPE. Inversely, areas of decreased fundus autofluorescence correlate to low levels of RPE metabolic activity, which normally underlies local atrophy and secondary PRs loss. Therefore, fundus autofluorescence has been proven to be a useful protocol, both in clinical practice and research, to study and diagnose STGD and one of the more efficient tools to determine the stage of disease (Gomes et al, 2009; Testa et al, 2012).

2.3. ABCA4 as STGD causative gene

In 1997, the gene for autosomal recessive STGD was first identified by the group of Allikmets and was found to encode a novel member of the ATP-binding cassette transporter superfamily (Allikmets et al, 1997). Also in 1997, the gene for the Rim protein, first identified in the late 1970's as a high molecular weight glycoprotein, highly expressed in PRs OS (Molday & Molday, 1979; Papermaster et al, 1978), was cloned and found to encode the same ABC transporter mutated in STGD (Azarian & Travis, 1997; Illing et al, 1997; Nasonkin et al, 1998). This ABC transporter, initially known as ABCR, is now more commonly called ABCA4, as it was the fourth identified

member of the ABCA subfamily of ABC transporters. The *ABCA4* gene maps to the short arm of chromosome 1. It is a large gene including 50 coding exons with an open reading frame of 6819 bp (Allikmets et al, 1997; Azarian et al, 1998). An important characteristic of ABCA4 is its extraordinarily high allelic heterogeneity and, indeed, there are over 600 disease-associated mutations that have been identified thus far (Zernant et al, 2011), that include missense, nonsense, splicesite, frameshift, small deletion and insertion and, more frequently, missense mutations (Fishman et al, 1999; Fumagalli et al, 2001; Lewis et al, 1999; Maugeri et al, 1999; Rivera et al, 2000). Given its high allelic heterogeneity, the most frequent disease-associated ABCA4 alleles (i.e., G1961E, G863A/delG863, and A1038V) have each been described in only about 10% of patients with STGD. This makes very difficult to identify causative mutations in STGD patients. Mutations in *ABCA4* are also known to cause two more severe, clinically distinct, retinal degenerative diseases known as cone-rod dystrophy and retinitis pigmentosa, as well as some forms of age-related macular degeneration. Indeed, it is now generally believed that mutations in *ABCA4* result in a spectrum of related retinal dystrophies, the severity of which depends on: i) the type of mutation and, subsequently, its effect on protein function (Fig. 8); ii) age of diagnosis; iii) stage of the disease; iv) genotypic variation of the patient (Cideciyan et al, 2009b; Maugeri et al, 1999; Shroyer et al, 1999; van Driel et al, 1998).

Stargardt-like diseases are typically recessively inherited, though dominant forms have been reported, which involve mutations in structural genes found on chromosomes six and four (STGD3, OMIM entry #600110 and STGD4, OMIM entry #603786) (Kniazeva et al, 1999; Stone et al, 1994).

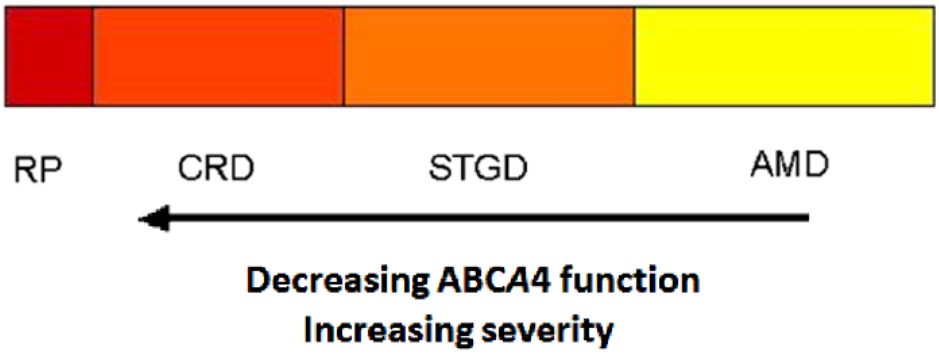

Figure 8. Spectrum of ABCA4-related phenotypes
Decreasing function of ABCA4 is thought to be associated with age-related macular degeneration (AMD) in some heterozygote mutations. Stargardt (STGD) patients have at least one missense allele, however, in cone-rod dystrophy (CRD) and retinitis pigmentosa (RP) patients are homozygous for severe mutations. Modified from (Dean, 2003)

2.3.1 ABCA4 structure and localization

ABC transporters include a superfamily of proteins that typically transport a wide variety of compounds across cell membranes using ATP hydrolysis as an energy source (Dean & Annilo, 2005). The ABC superfamily is organized in seven subfamilies, ranging from ABCA to ABCG (Dean & Allikmets, 2001). The ABCA subfamily of ABC transporters consists of 12 members (Kaminski et al, 2006). The human *ABCA4* gene encodes a 2273 amino acid protein having a molecular mass of 256 kDa with the mature protein organized in tandem halves. Each half contains a transmembrane domain, consisting of six membrane-spanning, and a nucleotide binding domain; a large glycosylated exocytoplasmic domain separates the first membrane-spanning segment from a cluster of five transmembrane segments (Fig. 9) (Molday & Zhang, 2010). The two transmembrane domain form the substrate binding site, while the nucleotide binding domains are the sites for the ATP binding and hydrolysis.

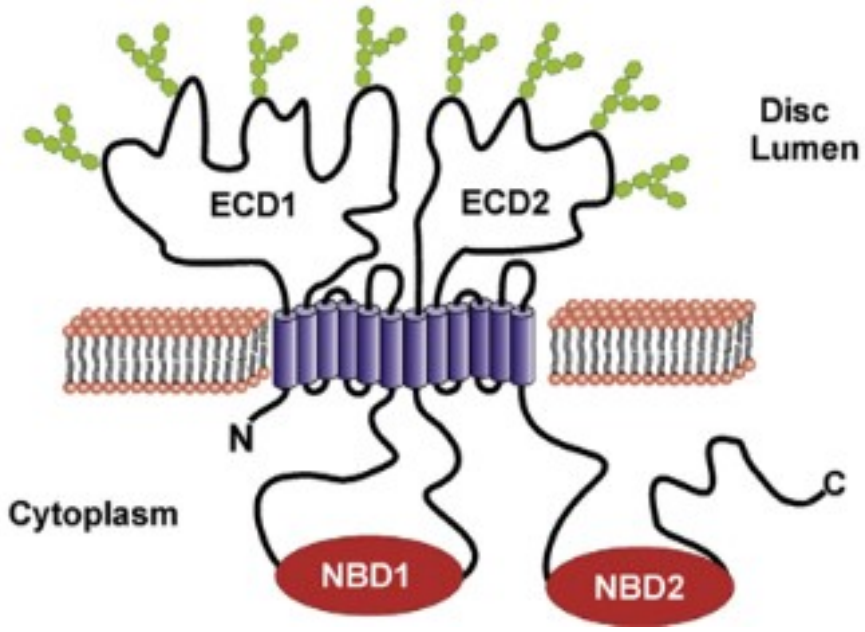

Figure 9. Structural features of the ABCA4 transporter
Topological model showing the organization of ABCA4 in the membrane. Each exocytoplasmic domain contains multiple N-linked oligosaccharide chains (hexagons) exposed to the lumen side of the disc membrane. ECD: exocytoplasmic domain; NBD: nucleotide binding domain. Taken from (Molday & Zhang, 2010)

ABCA4 is almost exclusively expressed in the retina and in particular in PRs (both rods and cones) OS (Allikmets et al, 1997; Illing et al, 1997; Molday et al, 2000; Sun & Nathans, 1997). Immunoelectron microscopic studies have localized ABCA4 to the rim and incisures of the disc membrane in amphibian PR cells (Fig. 10) (Papermaster et al, 1982). The initial finding that ABCA4 is localized to OS disc membranes together with its link to STGD provided the first evidence that ABCA4 may play a central role in PRs OS function. Biochemical and animal model studies have since established a critical role of ABCA4 in the visual cycle rather than in PR morphogenesis or structure.

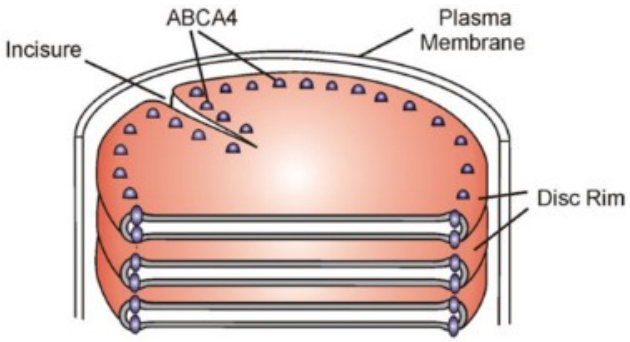

Figure 10. ABCA4 localization on discs
Schematic representation of a cutout portion of the rod outer segment with the stack of discs surrounded by the plasma membrane and the location of ABCA4 in the rim and incisure regions of the disc membrane. Modified from (Molday & Zhang, 2010)

2.3.2 The Abca4-/- mouse sheds light on the role of ABCA4 in the visual cycle and on STGD pathogenesis.

The first identification of ABCA4 as a member of the ABC transporter superfamily suggested its involvement in the transport of an unknown substrate in the PR OS. All-trans retinal, the isoform of rhodopsin chromophore, was identified as a potential substrate of ABCA4 as it has the ability to stimulate ATP hydrolysis in reconstituted ABCA4 protein *in vitro*, which suggested that this could also be the *in vivo* substrate for ABCA4 (Sun et al, 1999). Studies of *Abca4* knockout mice supported this hypothesis. This data suggested that ABCA4 functions as a "flippase" of the complex of all-trans retinal and PE across the disc membrane. *Abca4* knockout mice were generated in 1999 by the Travis group, through targeted gene disruption of the *Abca4* locus (Weng et al, 1999). This mouse model, however, did not fully recapitulate the phenotypes of STGD. These animals exhibited healthy PRs that did not show PRs degeneration under normal lighting conditions. However, recent reports found that in mice bred onto an albino background, which are more susceptible to light because of the absence of pigmentation, degeneration became evident at advanced ages (8-9 month) (Wu et al, 2010a). The initial study also suggested that delayed dark adaptation, a symptom of

STGD, was demonstrated in *Abca4-/-* mice and that it was initiated by delayed clearance of all-trans-retinal, known to re-associate with opsin and activate the phototransduction cascade. Biochemical analyses of retinoid compounds and lipids from ocular tissues revealed alterations consistent with the presumed role of ABCA4 as the transporter of all-trans-retinal and/or N-retinylidene-PE. Indeed, these animals exhibited elevated levels of all-trans-retinal in OS following light exposure, elevated PE and N-retinylidene-PE in the retina and accumulation of lipofuscin deposits in the RPE cells (Mata et al, 2000; Weng et al, 1999). Lipofuscin deposits in *Abca4-/-* mice showed elevated levels of several fluorescent diretinoid compounds, including A2E, the final product of condensation of all-trans-retinal and N-retinylidene-PE (Fig. 11), and similar potentially toxic photoreactive compounds (Ben-Shabat et al, 2002; Kim et al, 2007; Mata et al, 2001; Mata et al, 2000; Radu et al, 2004; Sparrow & Boulton, 2005; Wu et al, 2009). Accumulation of A2E in the macular region of RPE, as well as many of the other compounds previously mentioned, is the hallmark of STGD and age-related macular degeneration (Mata et al, 2000).

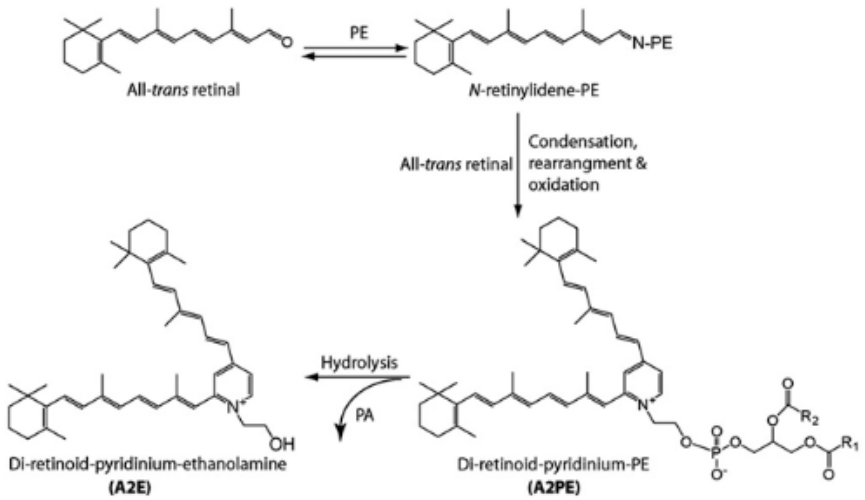

Figure 11. Reactions involved in the formation of A2E
All-trans-retinal reacts with phosphatidylethanolamine (PE) to form N-retinylidene-PE. This condenses with all-trans retinal to produce the di-retinoid pyridinium-PE compound (A2PE) in outer segments. Upon phagocytosis from the RPE, A2PE can be hydrolyzed by lysosomal enzymes to A2E and phosphatidic acid (PA). Modified from (Molday & Zhang, 2010)

The results of the characterization of *Abca4-/-* mice have definitively supported the concept that ABCA4 plays an essential role in the visual cycle and, specifically, the possible role of ABCA4 in the regeneration of the all-trans-retinal chromophore.

All-trans-retinal has to be reduced to all-trans-retinol by the retinol dehydrogenase (RDH8), localized in the cytoplasmic side of the discs, before it can be recycled. However, it is know that a fraction of all-trans-retinal reversibly reacts with PE in the disc membrane to form N-retinylidene-PE (Fig. 12A) (Anderson & Maude, 1970; Poincelot et al, 1969). This adduct cannot cross the membrane by itself and thus is trapped on the lumen side of the disc where it is no longer accessible to RDH8. In this context, ABCA4, works as a lipid transporter and "flips" N-retinylidene-PE to the cytoplasmic side of the disc membrane, utilizing ATP hydrolysis as an energy source. Once in the cytoplasm, N-retinylidene-PE can dissociate and be converted to all-trans retinol, thus re-entering the visual cycle (Fig. 12A).

In this model, ABCA4 functions to remove all-trans-retinal and related retinoid compounds from PR OS. Compatibly with this model, ABCA4 loss would result in the accumulation of A2E-containing lipofuscin granules in RPE, one of the characteristic features of STGD. Indeed, in the absence of ABCA4, N-retinylidene-PE and all-trans-retinal accumulate inside the disk, as observed in *Abca4-/-* mice, and subsequently, the levels of A2PE, the product of their condensation, also greatly increase in PR OS (Eldred & Lasky, 1993; Mata et al, 2001; Mata et al, 2000) (Fig. 12A). OS phagocytosis by RPE cells results in an increase in A2E content via lysosomal enzyme-mediated A2PE hydrolysis (Sparrow et al, 2008). As A2E and related diretinoids cannot be readily metabolized, they progressively accumulate in RPE cells, forming the fluorescent lipofuscin deposits seen in STGD patients and *Abca4-/-* knockout mice (Fig. 12B). The accumulation of A2E in RPE cells negatively affects RPE cell function and viability. Indeed, A2E has been reported to act as a detergent that disrupts intracellular

membranes, a photosensitizer resulting in free radical production that can adversely affect DNA and membrane lipids, an inhibitor of RPE phagocytosis and degradative functions, as well as an inhibitor of cholesterol efflux from RPE cells (Eldred & Lasky, 1993; Finnemann et al, 2002; Holz et al, 1999; Lakkaraju et al, 2007; Molday & Zhang, 2010; Sparrow et al, 2003; Sparrow et al, 2008; Sparrow et al, 2000; Vives-Bauza et al, 2008).

Due to the close interdependence between RPE and PR, the degeneration of RPE cells caused by the A2E related damages, will consequently result in PRs death (Fig.12B), ultimately causing the loss in the vision experienced by STGD patients.

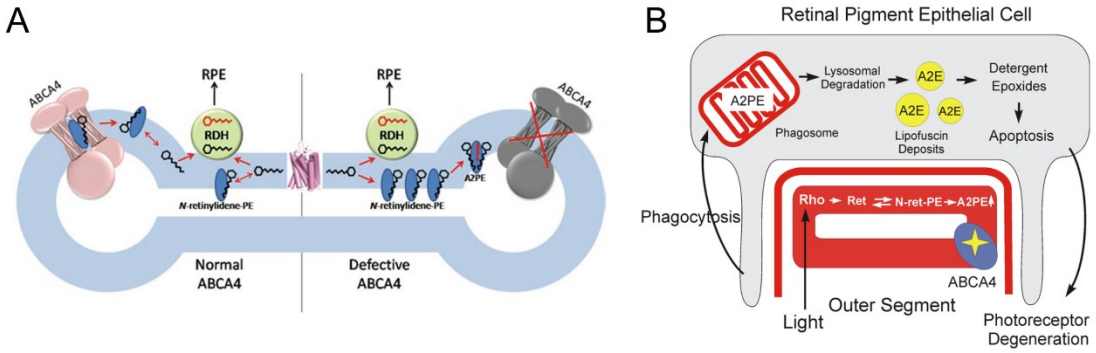

Figure 12. Proposed biological role of ABCA4 and mechanism responsible for STGD
(A) Illustration of the proposed biological role of ABCA4. The left part of the diagram represents a rod OS disk with a functional ABCA4, whereas the right part represents a rod OS disk with an inactive ABCA4. Hexagons with carbon backbone represent all-trans-retinal (black) and all-trans-retinol (red). RDH: all-trans-retinol dehydrogenase 8. RPE: retinal pigment epithelium. Modified from (Tsybovsky et al, 2010). (B) Diagram showing how the loss in the function of ABCA4 as N-retinylidene-PE transporter results in PR degeneration and vision loss. Modified from (Molday & Zhang, 2010).

3. Gene therapy strategies for IRDs

3.1 The eye as target for gene therapy

Effective treatments for IRDs are currently unavailable. However, during the past three decades, the identification of the genes causative of many IRDs has paved the way to the development of gene therapy-based strategies.

Gene therapy aims to deliver corrective nucleic acids (DNA/RNA) to a cell, tissue or target organ, in order to treat and ultimately cure a disease. The eye is a suitable target for gene transfer thanks to several features. It is small and enclosed, thus allowing for the use of small vector/transgene doses to achieve a therapeutic effect. It is an immuno-privileged site, as tight junctions between RPE cells and the presence of the blood-retina barrier limit the spreading of the vector in the circulation, thus, minimizing the activation of the immune system against either the vector components or transgene product (Bainbridge et al, 2006). The effects of gene delivery can be monitored closely, frequently and non-invasively; specifically, retinal morphology can be assessed by optical coherence tomography (OCT) while retinal function can be assessed by electroretinograms (ERGs), visual evoked potentials (VEPs) and measurement of afferent pupillary light responses (PLRs). Many ocular diseases are bilaterally symmetrical allowing a unique environment to compare the effects of vector/gene delivery to disease progression in the contralateral eye. Finally, surgical procedures have been adapted for the transfer of genetic material into specific ocular compartments, as to preferentially target a particular ocular cell type. The two most common methods of delivery are intravitreal and subretinal injection (Stieger et al, 2011). Intravitreal injection consists of the release of the therapeutic agent in the vitreous and results in the exposure of the anterior retina (GC and INL). Subretinal injection, alternatively, deposits the vector below the retina, in a virtual space between the RPE and the PRs,

inducing a regional and reversible detachment called a bleb. Subretinal vector delivery, though more invasive than the intravitreal, exposes the outer retina to the therapeutic agent and is currently the most efficient method for targeting PRs and RPE cells, which are the cell types mainly affected by many forms of IRDs.

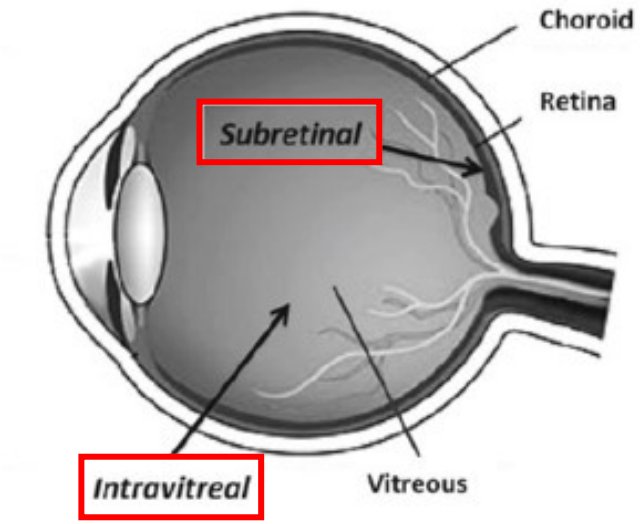

Figure 13. Routes of injection for ocular gene delivery
Modified from (Stieger et al, 2011)

Gene therapy-based strategies recently developed for the treatments for IRDs have shown promising results in several animal models of retinal degeneration and in recent clinical trials have confirmed their efficacy and safety in humans, thus suggesting that gene therapy is a valuable and viable therapeutic option for otherwise untreatable diseases that cause blindness (Allocca et al, 2006; Bainbridge et al, 2008; Cideciyan et al, 2009a; Colella et al, 2009; Maguire et al, 2009; Maguire et al, 2008; Simonelli et al, 2010; Vandenberghe & Auricchio, 2012).

3.2 AAVs as tools for gene transfer to the eye

Nucleic acids do not readily cross cell membranes, consequently it is necessary to envelope the genetic material in a delivery vehicle that can be either viral or non-viral (polymeric or lipidic complexes). Non-viral gene transfer efficiency has increased over the last several years, however, the resulting transfection rate remains low and the expression of the transgene is short lived. Consequently, many studies have demonstrated higher transduction efficiency in the retina using viral gene delivery rather than non-viral (Andrieu-Soler et al, 2006). Viral vectors commonly used for ocular gene transfer are derived from adenoviral, lentiviral or adeno-associated (AAV) viruses (Kumar-Singh, 2008; Lipinski et al, 2013). Among these, vectors derived from AAVs are currently the most used and promising vehicles for therapeutic gene delivery to the retina, given their favourable safety profile and the long-term gene expression that is observed after a single AAV administration (Stieger et al, 2011; Vandenberghe & Auricchio, 2012).

AAV is a small (20-25 nm in diameter), non-enveloped, icosaedric virus, native to humans and non-human primates, that packages a single strand DNA genome of 4.7 kb (Berns & Giraud, 1996) (Fig. 14). It belongs to the Parvoviridae viral family and it is a dependovirus, because it can replicate in the nucleus of target cells only in the presence of helper viruses. In fact, it was originally isolated as a contaminant of adenoviral cultures and thus given the name adeno-associated virus. The AAV genome is flanked by two palyndromic inverted terminal repeats (ITRs) that are 145 nucleotides in length and includes two open reading frames, rep and cap (Daya & Berns, 2008). Rep encodes for proteins involved in the replication of the viral DNA, the packaging of newly synthesized single stranded AAV genomes and the genome integration in the AAVS1 locus on human chromosome 19. Cap encodes for the VP1, 2 and 3 proteins that form the AAV capsid. In the AAV vector genome, the only viral sequences that are required

in cis are the ITRs, while the sequences encoding rep and cap can be exchanged with the exogenous DNA of choice (Daya & Berns, 2008). Rep and cap are instead required for the production of AAV vectors and, therefore, they are provided in trans to the packaging cells together with the adenoviral helper functions. Recombinant AAV vectors can be produced at high yields by transient triple transfection of mammalian cells or by infecting packaging eukaryotic or insect cells (Wright, 2008; Zolotukhin, 2005).

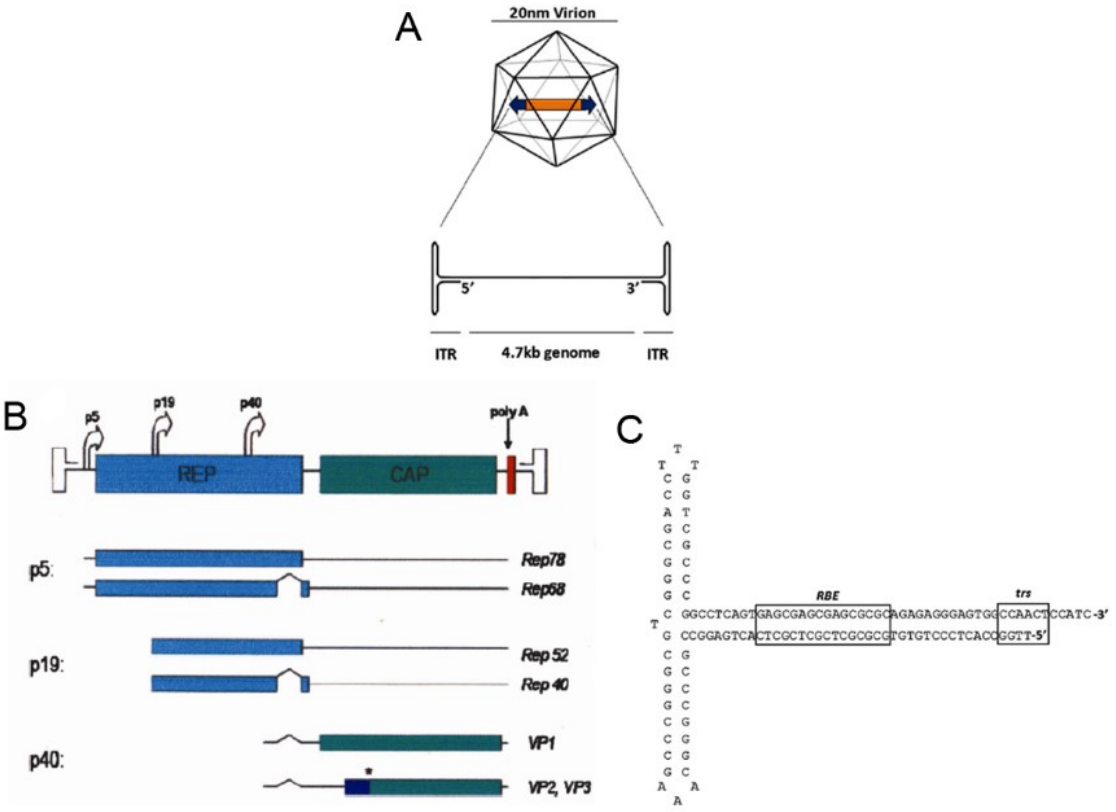

Figure 14. Schematic representation of the structure and genome of AAV vectors
(A) 20 nm icosahedral capsid of the AAV virion containing a single-stranded DNA AAV genome; (B) Rep and cap genes flanked by ITRs. The different rep and cap transcripts are produced from their respective promoters (P5 and P19 for rep and P40 for cap). The asterisk indicates the alternative ACG codon used to produce VP3; (C) Secondary structure of one ITR from AAV2 showing the rep binding elements (RBEs) and the terminal resolution site (TRS). These sequences are used by the viral regulatory protein Rep during AAV replication to process the double-stranded intermediates. Taken from (Lipinski et al, 2013) (A, C) and (Daya & Berns, 2008) (B).

The triple trasfection method is the most commonly used method of AAV production and is based on co-transfection of three plasmids into permissive cells (usually human embyonic kidney 293 cells): one containing the gene of interest flanked by the ITRs, the second a packaging plasmid encoding for the rep and cap proteins, and the third plasmid encoding the adenoviral helper genes. Column chromatography or CsCl- gradient centrifugation is used to purify cellular and viral (empty capsid) contaminants.

AAVs transduction occurs through a cascade of steps beginning with an interaction of the viral capsid with specific receptors on the cell surface; internalization of the virion is subsequently mediated by endocytosis and intracellular trafficking through the endocytic/proteasomal compartments. Finally, the virion reaches the nucleus, where it is uncoated allowing the single stranded genome to be transcribed creating double-stranded DNA, ultimately resulting in transcription of the transgene (Wu et al, 2006). In the absence of Rep proteins, the recombinant AAV genomes remain episomal and random integration occurs at very low efficiency (Smith, 2008).

Dozens of different AAV variants (serotypes) have been identified to date, either isolated as naturally occurring infectious agents or as molecular clones (Vandenberghe et al, 2009). The availability of many serotypes is one of the major strengths of the AAV vector platform, as the versatility of the AAV vectors production system allows the easy exchange of capsids among various AAV variants. This exchange creates hybrid vectors that contain a genome with the same AAV ITRs (i.e., those from AAV2) and the capsid from a different variant (Auricchio, 2003). AAVs obtained through this transcapsidation system are named AAV2/n, where the first number refers to the ITRs and the second to the capsid (Fig.15).

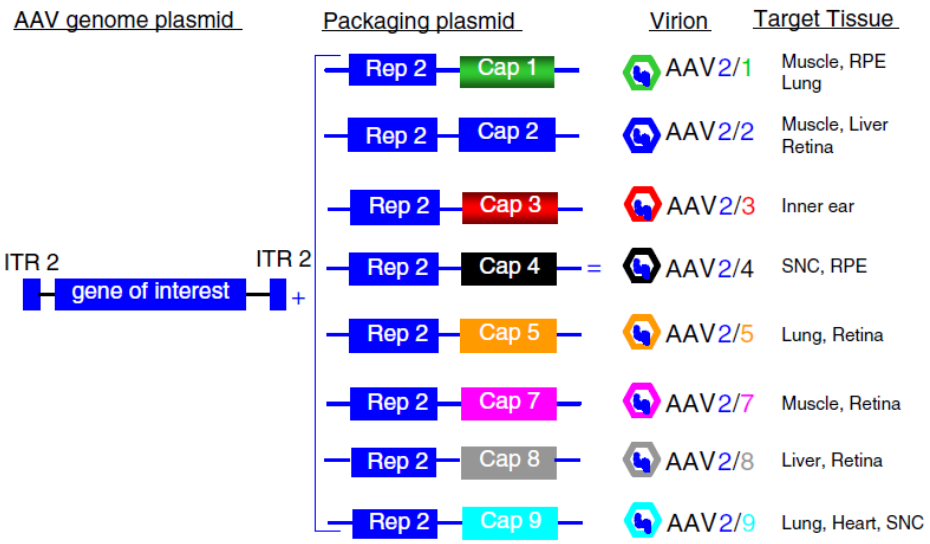

Figure 15. Scheme of the generation of AAV vectors from various AAV serotypes
Transfection of packaging cells with plasmids containing the AAV genome (with the gene of interest flanked by the AAV2 ITRs) and the packaging sequences (the cap gene encoding for the capsid proteins and the rep gene from serotype 2 to allow the most efficient packaging of a viral genome with the AAV2 ITRs) results in the production of recombinant AAV vectors. The tropism of the hybrid virions containing the genome of one serotype (i.e. AAV2) and a different capsid (AAV2/1–9) mainly depends on the capsid. Taken from (Surace & Auricchio, 2008).

Each AAV serotype has unique transduction characteristics (i.e target cells, kinetic of transgene expression) because different AAV capsids interact with different receptors on target cells and impact the post-entry transduction steps and this allows the user to choose the most appropriate AAV serotype for the disease/organ of interest (Vandenberghe et al, 2009; Wu et al, 2006). For example, the AAV2 capsid proteins interact with membrane-associated heparin sulphate proteoglycans, with avb5 integrin (Summerford et al, 1999), fibroblast growth factor-1 (Qing et al, 1999), hepatocyte growth factor (Kashiwakura et al, 2005) and laminin (Akache et al, 2006) as coreceptors. By contrast, AAV1 capsid interacts with alpha2,3 and alpha2,6 sialic acids that are present on N-linked glycoprotein receptors (Vandenberghe et al, 2009), AAV4 and AAV5 bind preferentially to a 2,3 sialic acid or platelet-derived growth factor (Di

Pasquale et al, 2003) (Kaludov et al, 2002) and AAV3, AAV8 and AAV9 bind laminin (Akache et al, 2006).

3.3 AAV serotypes for PR transduction

The transduction efficiency of the different retinal cell types by numerous AAV serotypes has been extensively documented using several reporter proteins (Allocca et al, 2007; Auricchio et al, 2001b; Lebherz et al, 2008). AAV vectors often have a broad tropism (Table 1), however, when evaluating the transduction capability of a serotype, it is important to take into account that the viral capsid is only one of several factors that determine specificity and efficacy of retinal cell transduction; cell transduction and targeting is also influenced by the route of vector administration.

rAAV serotype	Mouse	Rat	Dog	Primate
rAAV2/1	RPE	–	–	–
rAAV2/2	RPE, PR	RPE, PR	RPE, PR	RPE, PR
rAAV2/3	–	–	n.d.	n.d.
rAAV2/4	–	RPE	RPE	RPE
rAAV2/5	RPE, PR	RPE, PR	RPE, PR	RPE, PR
rAAV5/5	RPE, PR	n.d.	n.d.	RPE, PR
rAAV2/6	RPE	n.d.	n.d.	n.d.
rAAV2/7	RPE, PR	n.d.	n.d.	n.d.
rAAV2/8	RPE, PR	RPE, PR, INL, GC	RPE, PR, INL, GC	n.d.
rAAV2/9	RPE, PR, MC, INL	n.d.	n.d.	n.d.

Table 1. AAV serotype tropism in various species following subretinal injection
RPE: retinal pigmented epithelium, PR: photoreceptors, MC: Muller cells, INL: inner nuclear layer, GC: ganglion cells, n.d.: not determined. Modified from (Stieger et al, 2011).

Following subretinal injection, most AAV serotypes efficiently transduce RPE cells, with AAV2/1, AAV2/4 and AAV2/6 being the most efficient in various animal models (Auricchio et al, 2001a; Dinculescu et al, 2005; Rabinowitz et al, 2002; Yang et al,

2002). This efficient transduction could result from an inherent permissiveness of the RPE to AAV infection (specifically, the presence of AAV receptors and co-receptors at the RPE cell membrane) or from the phagocytic properties of the RPE that could facilitate entry of AAV particles (Vandenberghe & Auricchio, 2012). Conversely, the levels of PRs transduction vary significantly among different serotypes. The first evidence that AAV can target PRs in addition to the RPE was provided using AAV2/2 (Ali et al, 1996), however, transduction was relatively inefficient. Since the majority of mutations causing IRDs, including STGD, occur in genes expressed in PRs (Dryja, 2001), this concern prompted the search for AAV serotypes able to overcome this limitation. AAV2/5, 2/7, 2/8 and 2/9 have all been demonstrated to efficiently transduce PRs, in addition to RPE (Allocca et al, 2007; Auricchio et al, 2001b; Lotery et al, 2003) with AAV2/8 being the most efficient serotype in mice (Allocca et al, 2007), pigs (Mussolino et al, 2011), dogs (Stieger et al, 2008) and non-human primates (Vandenberghe et al, 2011) (Fig. 16).

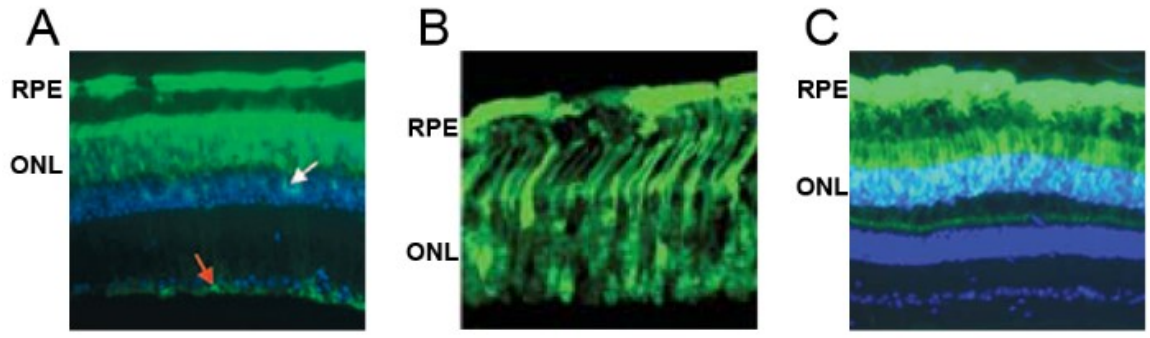

Figure 16. AAV2/8 transduction in mouse, pig and non-human primates retinas
Subretinal administration of AAV2/8 expressing EGFP in C57BL/6 mice (A), pig (B) and non-human primates (C). RPE: retinal pigmented epithelium, PR: photoreceptors. White arrows: Müller cell nuclei, red arrows: Müller cell endfoot membranes. Modified from (Allocca et al, 2007) (A), (Mussolino et al, 2011) (B), (Vandenberghe et al, 2011) (C).

In contrast, AAV vectors of any serotype have lower transduction efficiency when delivered intravitreally and AAV2/2 and AAV2/6 are currently the only serotypes found

capable of transducing retinal cells from the vitreous, with a pattern mainly restricted to GC and MC (Fig. 17).

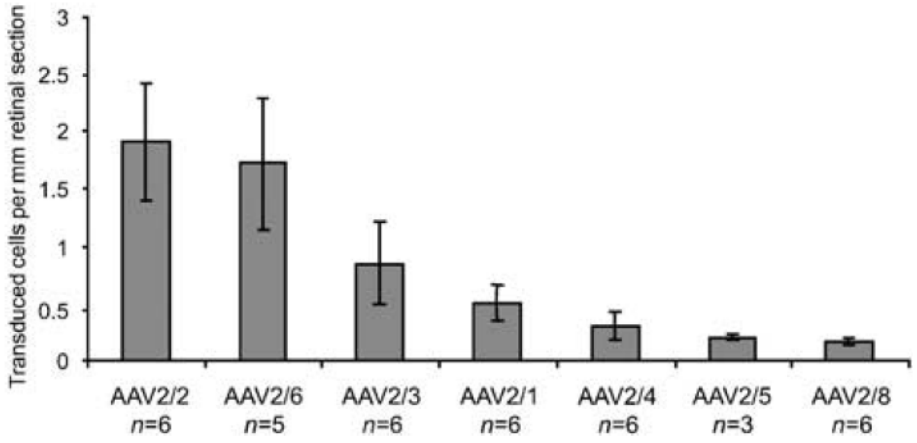

Figure 17. Transduction efficiency of the rAAV serotypes following intravitreal injection
Taken from (Hellstrom et al, 2009).

One of the reasons for the limited efficiency of AAV vectors to transduce retinal cells after intravitreal injection is the presence of the ILM at the junction of neuroretina and vitreous, which forms a structural and biochemical barrier for AAVs, likely due to the presence of specific receptors that sequester the viruses (Stieger et al, 2011). Accordingly, it has been shown that when the ILM is disrupted, either by progression of a retinal degeneration or by digestion with nonspecific proteases, it becomes possible to achieve a broader pattern of expression after intravitreal injection. Indeed, Dalkara et al. have shown that following ILM digestion, the AAV serotypes 2/1, 2/2, 2/5, 2/8, and 2/9, were all capable of transducing retinal cells, although to a variable degree, with the AAV2/5 serotype being the most efficient (Dalkara et al, 2009).

In recent years, the potential of AAV vectors for the treatment of IRDs has been greatly enhanced by the development of new AAV serotypes, either through *in vitro* evolved or rationally-modified AAV capsids. Among these new serotypes, multiple tyrosine

mutants have shown significantly enhanced transduction properties, both by subretinal and, more importantly, intravitreal delivery. These mutants were developed by the Srivastava group in an attempt to redirect the intracellular trafficking of AAVs to obtain higher levels of transduction by escaping the proteasomal-mediated degradation. Basic trafficking studies suggested that capsid tyrosine residues could be phosphorylation sites that predestine AAV capsids for ubiquitination and subsequent proteosomal degradation, and thus by mutating these residues could result in increased transgene expression. To test this hypothesis, different AAV serotypes containing one or more tyrosines to phenylalanine substitution(s) were generated and demonstrated increased gene transfer efficiency in various *in vitro* and *in vivo* settings (Petrs-Silva et al, 2009; Zhong et al, 2008). In particular, they found that the single (Y444F, Fig. 18A) and triple mutants of AAV2/2 (Y444, 500, 730F) and 2/8-Y733F (Fig. 18A) had both stronger and more widespread transduction compared to their wild type counterparts when delivered subretinally in mice (Petrs-Silva et al, 2009). Strikingly, quadruple and pentuple tyrosine-mutant AAV2/2 vectors (Fig. 18B) have demonstrated efficient transduction of PRs following intravitreal delivery (Petrs-Silva et al, 2011).

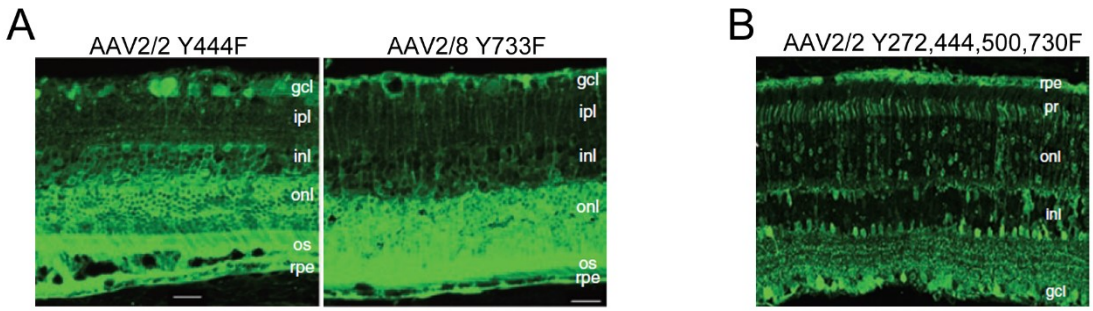

Figure 18. Transduction profiles of the AAV2/2 and AAV2/8 tyrosine mutants
(A) Representative sections depicting EGFP fluorescence throughout the retina after subretinal delivery of AAV2/2 Y444F or AAV2/8 Y733F. Modified from (Petrs-Silva et al, 2009). (B) Immunostaining for GFP protein expression in retinal sections after intravitreal delivery of AAV2/2 quadruple mutant (Y272, 444, 500, 730F). Modified from (Petrs-Silva et al, 2011).

This last finding is particularly attractive for the treatment of IRDs, as intravitreal delivery of AAV vectors would allow for a more widespread and homogeneous transgene expression and would reduce the risk of surgical morbidity.

Similar widespread retinal transduction after intravitreal delivery has been recently obtained from Dalkara and co-workers with a new AAV variant (7m8) identified through *in vivo*–directed evolution (Dalkara et al, 2013). Importantly, this vector provided therapeutic amounts of transduction of PR cells and RPE in both normal murine retina and in murine models of human retinal diseases. In addition, Dalkara and co-workers showed that intravitreal delivery of 7m8 vector results in PRs transduction also in the nonhuman primate retina, in which the ILM is a significantly thicker physical barrier to the retina than in rodent. In contrast, the 7m8 mediated RPE transduction in non human primate seemed to be impaired from the thick ILM, as they could not detect transgene expression in the RPE.

3.4 Clinical success of AAVs for ocular gene therapy

AAVs have been successfully used in dozens of proof-of-concept studies, both in small and large animal models that have demonstrated efficacy of AAV-mediated gene therapy for the treatment of recessive and dominant IRDs (Stieger et al, 2011). Historically, however, AAV-mediated gene delivery has been more effective in the treatment of IRDs caused by mutations in genes expressed in the RPE (Dejneka et al, 2004; Gargiulo et al, 2009; Smith et al, 2003; Surace et al, 2005), rather than those caused by mutations in genes expressed in PRs (Bennett et al, 1996) (Allocca et al, 2011; Schlichtenbrede et al, 2003), probably because of the above described features of the RPE (i.e. transducibility), the need for finely regulated transgene expression in PRs and/or the different rate of retinal degeneration that is usually faster in PRs diseases

(Smith et al, 2009). In fact, among the proof-of-concept studies, the most successful and advanced have been those performed in the Briard dog model of Leber Congenital Amaurosis type 2 (LCA2), which is homozygous for a null mutation in the RPE65 gene that encodes the RPE-specific all-trans retinol isomerase responsible for regenerating visual pigment after light exposure (Acland et al, 2001). Different groups have, indeed, proved that AAV2-mediated subretinal delivery of the RPE65 gene restores vision in this dog model (Acland et al, 2005; Le Meur et al, 2007; Narfstrom et al, 2003). This extraordinary result has opened the doors to three independent clinical trials tasked to test the safety and efficacy of subretinal administrations of AAV2 in LCA2 patients (Bainbridge et al, 2008; Hauswirth et al, 2008; Maguire et al, 2008). Notably, despite some differences among the various clinical trials (i.e. differences in regulatory sequences included in the vector, in the process of vector production and purification, independent selection and follow up of the patients, and independent surgical delivery), all trials have shown similar positive results. Importantly, these trials suggest that retinal gene therapy with AAV is safe and well tolerated in humans, that vision can be improved in patients that have suffered from severe visual function impairment, in some cases for decades, and that re-administration of AAV to the subretinal space is feasible, effective and safe.

3.5 Overcoming AAV's limits

Despite these important successes in pre-clinical and clinical studies, AAV is still excluded for gene therapy of many diseases. This is primarily due to its major limitation: the packaging capacity, which is considered to be restricted to the size of the parental genome (4.7 kb). This hinders the treatment of certain forms of IRDs caused by

mutations in genes whose cDNA exceeds 5 kb, such as *ABCA4* (Table 2). Thus, various strategies are being investigated to overcome AAV cargo limitations.

DISEASE	CAUSATIVE GENE	CELL AFFECTED	cDNA SIZE (kb)
USH1F	Protocadherin-related 15 (**PCDH15**)	Neurosensory retina	5.9
CSNB2	Calcium channel, voltage-dependent, L type, alpha 1F subunit (**CACNA1**)	Photoreceptors	5.9
ad RP	Small nuclear ribonucleoprotein 200 kDa (**SNRNP200**)	Photoreceptors and RPE	6.4
ad or ar RP	Retinitis pigmentosa 1 (**RP1**)	Photoreceptors	6.5
USH1B	Myosin 7A (**MYO7A**)	Photoreceptors and RPE	6.7
STGD1	ATP-binding cassette, sub-family A, member 4 (**ABCA4**)	Photoreceptors	6.8
ad RP	Pre-mRNA processing factor 8 homologue (**PRPF8**)	Photoreceptors and RPE	7.0
Occult macular dystrophy	Retinitis pigmentosa 1-like 1 (**RP1L1**)	Photoreceptors	7.2
LCA10	Centrosomal protein 290 kDa (**CEP290**)	Photoreceptors	7.5
USH1D	Cadherin 23 (**CDH23**)	Neurosensory retina	10
USH2A and RP	Usherin (**USH2A**)	Neurosensory retina	15.6
ad macular dystrophy	Hemicentin 1 (**HMCN1**)	Photoreceptors and RPE	17
USH2C	G-coupled receptor 98 (**GPR98**)	Neurosensory retina	18.9

Table 2. Examples of large genes associated with IRDs
USH1F: Usher syndrome type IF; CSNB2: congential stationary night blindness type 2; RP: retinitis pigmentosa; ad: autosomal-dominant; ar: autosomal recessive; USH1B: Usher syndrome type IB; STGD1: Stargardt disease; LCA10: Leber congenital amaurosis type 10; USH1D: Usher syndrome type ID; USH2A: Usher syndrome type IIA; USH2C: Usher syndrome type IIC.

Several groups have attempted to "force" large genes into one of the many AAV capsids available by developing the so-called oversize AAV vectors (Fig. 19) (Allocca et al, 2008; Grieger & Samulski, 2005; Hirsch et al, 2010). Notably, oversize AAVs have been successfully used to achieve therapeutically-relevant levels of transgene expression in rodent and canine models of human inherited diseases (Grose et al, 2012; Lopes et al, 2013; Monahan et al, 2010), including the retina of the *Abca4-/-* mice, resulting in significant and stable morphological and functional improvement of diseased cells (Allocca et al, 2008). However, the mechanism underlying oversize AAV-mediated PR transduction remains elusive. In contrast to what was originally proposed (Allocca et al, 2008; Grieger & Samulski, 2005; Wu et al, 2007), oversize AAV vectors do not contain a pure population of intact, large genomes but rather a heterogeneous population of mostly truncated genomes (≤5 kb in length) (Dong et al, 2010a; Lai et al, 2010; Wang et al, 2012; Wu et al, 2010b). Following infection, re-assembly of these truncated genomes in the target cell nucleus has been proposed as a mechanism for oversize AAV vector transduction (Dong et al, 2010a; Hirsch et al, 2010; Hirsch et al, 2013a; Lai et al, 2010; Wu et al, 2010b). Independent of transduction mechanism and *in vivo* efficacy, the heterogeneity of oversize AAV genomes remains a major limitation for their application in human gene therapy.

Alternatively, the inherent ability of AAV genomes to undergo intermolecular recombination at their ITRs to form concatemeres (Duan et al, 1998) has been exploited to transfer large genes *in vivo* by splitting a large gene expression cassette into halves (<5 kb in size), each contained in one of two independent (dual) AAV vector (Duan et al, 2001; Ghosh et al, 2008; Yan et al, 2000). In the dual AAV trans-splicing strategy, the transgene is divided into two parts, at either an endogenous intron or an engineered synthetic intron, and a splice donor (SD) signal is placed at the 3' end of the 5'-half vector and a splice acceptor (SA) signal at the 5' end of the 3'-half vector (Fig. 19).

Upon co-infection of the same cell by the dual AAV vectors and ITR-mediated tail-to-head concatemerization of the halves, trans-splicing results in the production of a mature mRNA that encodes a full-size WT protein (Yan et al, 2000). Trans-splicing has been successfully used to express large genes in muscle and retina (Lai et al, 2005; Reich et al, 2003). However, the transduction efficiency of this system was found to be lower than that of a single intact AAV vector, as it is impacted by a number of factors: (i) gene splitting site, as the sequences surrounding exon/intron junction can influence the splicing efficiency; (ii) levels of co-infection reached in the cells; (iii) formation of the concatemers in the tail-to-head orientation; and (iv) transcription and splicing across the complex structure formed by the ITRs upon concatemerization.

Alternatively, the halves of a large transgene expression cassette contained in dual AAV vectors may contain homologous overlapping sequences (at the 3' end of the 5'-half vector and at the 5' end of the 3'-half vector, termed dual AAV overlapping), which, in a cell co-infected by both vectors, could mediate the reconstitution of a single large genome by homologous recombination (Duan et al, 2001). The success of this strategy, however, largely depends on the recombinogenic properties of the transgene overlapping sequences. Thus, only if a gene contains a highly recombinogenic region it will be possible to achieve therapeutic levels of expression (Ghosh et al, 2006). To overcome this problem, a third dual AAV strategy (hybrid) was developed by the group of Ghosh. This strategy is based on the addition of a highly recombinogenic region from an exogenous gene (i.e. alkaline phosphatase, AP (Ghosh et al, 2011; Ghosh et al, 2008) to the trans-splicing vector to increase recombination between the dual AAVs. The exogenous region is placed downstream of the SD signal in the 5'-half vector and upstream of the SA signal in the 3'-half vector (Fig. 19). Importantly, the efficiency of this strategy is transgene-independent as the reconstitution of the full-length cassette relies on the recombination mediated by the exogenous homology region.

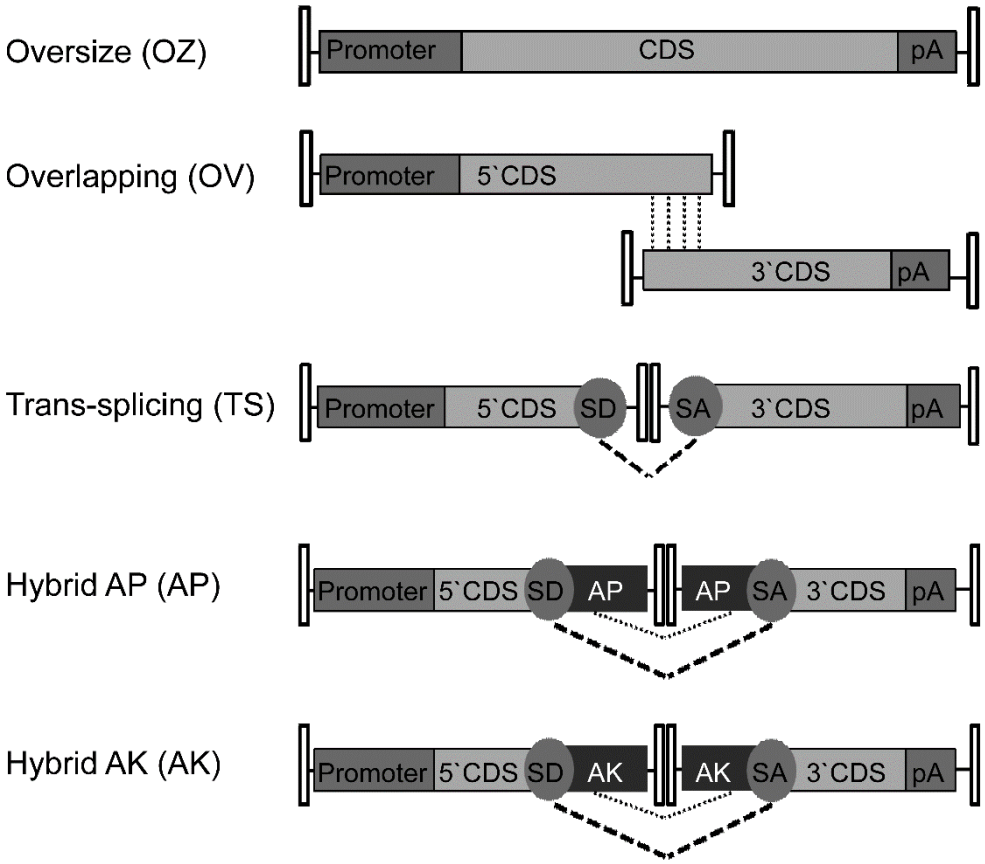

Figure 19. Schematic representation of AAV-based strategies for large gene transduction

CDS: coding sequence; pA: poly-adenylation signal; SD: splicing donor signal; SA: splicing acceptor signal; AP: alkaline phosphatase recombinogenic region (Ghosh et al, 2011); AK: F1 phage recombinogenic region. Pointed lines show overlapping regions available for homologous recombination, dotted lines show the splicing between SD and SA.

AIMS

My Ph.D. project was aimed at overcoming the major limitation to the use of AAV vectors, the limited packaging capacity, for the treatment of IRDs such as STGD that are due to mutations in large (>5 kb) genes. IRDs are mainly due to mutations in genes expressed in PRs and, among the available gene transfer vectors, those based on AAV are the most efficient at targeting PRs and have been demonstrated to be safe and effective in humans. However, AAV small cargo capacity limits the application of AAV gene therapy approaches for common IRDs that are caused by mutations in genes whose coding sequence (CDS) is larger than 5 kb. The identification of AAV-based strategies that allow the delivery of large genes to the retina would thus expand the applicability of AAVs to these otherwise untreatable diseases.

Accordingly to this, the specific aims of my project were to:

- develop dual AAV vector-based strategies for large gene delivery to the retina;
- compare the efficiency of oversize to that of dual AAV vectors strategies for the delivery of large genes both *in vitro* and *in vivo*, in the retina;
- compare the transduction efficiency of dual AAV vectors to that of a single normal size AAV vector;
- characterize the effect of the AAV-mediated large gene expression in animal models of STGD.

To this end, I generated oversize and dual AAV vectors encoding for either the reporter EGFP or the therapeutic ABCA4 protein. The efficiency of the various systems was first evaluated *in vitro*, in HEK293 cells, by Western blot (WB) analysis on lysates from cells infected with the vectors from each approach. The strategies subsequently found to be the best performing were tested *in vivo*, by subretinal injection in C57BL/6 mice and in pigs. Analysis of retinal cryosections and WB analysis of retinal lysates from eyes

injected with vectors coding for EGFP or ABCA4, respectively, were used to evaluate the relative efficiency of the AAV vector strategies. The transduction efficiency of the best performing dual AAV vectors was also evaluated, both *in vitro* and *in vivo*, in comparison to that of a single normal size AAV vector, by either WB analysis on cellular lysates or ELISA on retinal lysates of C56BL/6 mice. Finally, to assess the efficacy of dual AAV vector-mediated large gene delivery to the retina, I injected subretinally the most effective *in vivo* performing AAV vector approaches in the mouse model of the STGD (the *Abca4-/-* mouse) and evaluated the rescue of the retinal phenotypes.

MATERIALS AND METHODS

Generation of AAV vector plasmids

The plasmids used for AAV vector production were derived from either the pZac2.1 (Gao et al, 2000) or pAAV2.1 (Auricchio et al, 2001a) plasmids that contain the inverted terminal repeats (ITRs) of AAV serotype 2 (Table 3). Normal size and oversize AAV vector plasmids contained full-length expression cassettes including the promoter, the full-length transgene CDS and the poly-adenylation signal (pA) (Table 3). The two separate AAV vector plasmids (5' and 3') required to generate dual AAV vectors contained either the promoter followed by the N-terminal portion of the transgene CDS (5' plasmid) or the C-terminal portion of the transgene CDS followed by the pA signal (3' plasmid). Normal size EGFP plasmids were generated by cloning the EGFP CDS of pAAV2.1-CMV-EGFP plasmid (720 bp) (Auricchio et al, 2001a) in pZac2.1 (Gao et al, 2000); oversize EGFP was generated from pAAV2.1-CMV-EGFP (Auricchio et al, 2001a) by inserting a DNA stuffer sequence of 3632 bp from human *ABCA4* (NM_000350.2, bp 1960-5591) upstream of the CMV promoter and a second DNA stuffer sequence of 3621 bp, composed of: murine *ABCA4* (NM_007378.1, 1066-1 and 7124-6046 bp; 2145 total bp) and human *Harmonin* (NM_153676.3 131-1606 bp; 1476 total bp), downstream of the pA signal. To generate dual AAV vector plasmids, the EGFP CDS (720 bp) was split into two constructs: one containing the N-terminal CDS (PMID: 9759496, bp 1-393) and the other containing the C-terminal CDS (PMID: 9759496, bp 394-720). The stuffer sequences flanking the EGFP expression cassette in the EGFP OZ plasmid were used to generate dual AAV-TS-L and dual AAV-AK-L plasmids (Table 3) with a combined (5'+3') genome length similar to the EGFP OZ construct size.

The oversize *ABCA4* plasmids contained the full-length human *ABCA4* CDS (NM_000350.2, bp 105-6926). To generate plasmids for dual AAV OV vectors the *ABCA4* CDS was split into two constructs, one containing N-terminal CDS (NM_000350.2, bp 105-3588) and the other containing C-terminal CDS (NM_000350.2, bp 2819-6926). Therefore, the region of homology shared by overlapping vector plasmids was 770bp. To generate trans-splicing and hybrid vector plasmids the *ABCA4* CDS was split between exons 19-20 (5' half: NM_000350.2, 105-3022 bp; 3' half: NM_000350.2, bp 3023-6926). The ABCA4 protein was tagged at its C-terminus with either the 3xflag or hemagglutinin (HA) tag. In addition, the ABCA4 protein was tagged at both N- (amino acidic position 590) and C-termini with the 3xflag tag for the experiments shown in Figures 34-35. The splice donor (SD) and splice acceptor (SA) signals contained in dual trans-splicing and hybrid AAV vector plasmids are as follows: 5-'GTAAGTATCAAGGTTACAAGACAGGTTTAAGGAGACCAATAGAAACTGGGCTTGTCGAGACAGAGAAGACTCTTGCGTTTCT-3' (SD); 5'-GATAGGCACCTATTGGTCTTACTGACATCCACTTTGCCTTTCTCTCCACAG-3' (SA). The recombinogenic sequence contained in hybrid AP vector plasmids was derived from alkaline phosphatase (AP) gene (NM_001632, bp 823-1100), as previously described (Ghosh et al, 2011). The recombinogenic sequence contained in hybrid AK vector plasmids was derived from the F1 phage genome (Gene Bank accession number: J02448.1; bp 5850-5926). The AK sequence is: 5'-GGGATTTTGCCGATTTCGGCCTATTGGTTAAAAAATGAGCTGATTTAACAAAAATTTAACGCGAATTTTAACAAAAT-3'. To generate the pZac2.1-CMV-RFP plasmid, the monomeric RFP CDS (Campbell et al, 2002) (675bp) was amplified and cloned in pZac2.1-CMV-EGFP plasmid using EcoRI and BamHI restriction sites.

The ubiquitous CMV promoter is that contained in pZac2.1 (Gao et al, 2000) or pAAV2.1-CMV-EGFP (Auricchio et al, 2001a); the PR-specific human RHO and RHOK promoters were derived from pAAV2.1-RHO-EGFP and pAAV2.1-RHOK-EGFP, respectively (Allocca et al, 2007); the RPE-specific VMD2 promoter (NG_009033.1, 4870-5470 bp) corresponds to the previously described EcoRI-XcmI promoter fragment (Esumi et al, 2004) and was amplified from human genomic DNA.

AAV vector production and characterization

AAV vectors were produced by the TIGEM AAV Vector Core by triple transfection of HEK293 cells followed by two rounds of $CsCl_2$ purification (Mueller et al, 2012). For each viral preparation, physical titers [genome copies (GC)/mL] were determined by averaging the titer achieved by dot-blot analysis (Drittanti et al, 2000) and by PCR quantification using TaqMan (Applied Biosystems, Carlsbad, CA, USA) (Mueller et al, 2012). The probes used for dot-blot and PCR analyses were designed to anneal with either the ITRs or regions within 1Kb from the ITRs. No statistically significant differences were found in the titers (GC/mL) of NS AAV2/2 or AAV2/8 compared to those of dual AAV OV, TS and hybrid vectors (Table 4). The alkaline Southern blot analysis shown in Figure 20 was carried out as follows: $3x10^{10}$ GC of viral DNA were extracted from AAV particles. To digest unpackaged genomes, the vector solution was resuspended in 240 µL of PBS pH 7.4 1X (GIBCO, Invitrogen S.R.L., Milan, Italy) and then incubated with 1U/µL of DNase I (Roche, Milan, Italy) in a total volume of 300 µL containing 40mM TRIS-HCl, 10mM NaCl, 6mM MgCl2, 1mM $CaCl_2$ pH 7.9 for 2 hours at 37°C. The DNase I was then inactivated with 50 mM EDTA, followed by incubation with proteinase K and 2.5% *N*-lauroyl-sarcosil solution at 50°C for 45 minutes to lyse the capsids. The DNA was extracted twice with phenol-chloroform and

precipitated with 2 volumes of ethanol 100% and 10% sodium acetate (3M, pH 7). Alkaline agarose gel electrophoresis and blotting were performed as previously described (Sambrook & Russell, 2001). Ten µL of the 1 kb DNA ladder (N3232L, New England Biolabs, Ipswich, MA, USA) were loaded as molecular weight marker. Three different double strand DNA fragments were radio-labeled with [α-32]-CTP using the Amersham Rediprime II DNA labeling System (GE Healthcare Europe, GmbH, Milan, Italy) and used as probes. The 5' probe (875 bp) was generated by digestion of the pZac2.1-CMV-*ABCA4_5'* plasmid with EagI; the 3' probe (880 bp) was generated by double digestion of the pZac2.1-*ABCA4*_3'_*3xflag*_SV40 plasmid with StuI and NcoI; the EGFP probe (735 bp) was generated by digestion of the pAAV2.1-CMV-EGFP plasmid with NotI and BamHI. Prehybridization and hybridization were performed at 65°C in Church buffer (Sambrook & Russell, 2001) for 1 hour and overnight, respectively. Then, the membrane (Whatman Nytran N, charged nylon membrane, Sigma-Aldrich, Milan, Italy) was washed for 30 minutes in SSC 2X-0.1% SDS and for 30 minutes in SSC 0.5X-0.1% SDS at 65°C, and then for 30 minutes in SSC 0.1X-0.1% SDS at 37°C. The membrane was then analyzed by X-ray autoradiography using Amersham Hyperfilm^{TM} MP (GE Healthcare Europe, GmbH, Milan, Italy).

AAV infection of HEK293 cells

HEK293 cells were maintained in Dulbecco's modified Eagle's medium (DMEM) containing 10% fetal bovine serum and 2 mM L-glutamine (GIBCO, Invitrogen S.R.L., Milan, Italy). Cells were plated in six-well plates at a density of 2×10^6 cells/well and transfected 16 hours later with 1.3 µg of pDeltaF6 helper plasmid which contains the Ad helper genes (Zhang et al, 2000) using the calcium phosphate method. After 5 hours, cells were washed once with DMEM and incubated with AAV2/2 vectors (m.o.i: $5x10^4$

GC/cell of each vector; 1:1 co-infection with dual AAV vectors resulted in of $1x10^5$ total GC/cell) in a final volume of 700 µL serum-free DMEM. Two hours later 2 mL of complete DMEM were added to the cells. Cells were harvested 72 hours following infection for Western blot analysis. To compare dual AAV to single AAV NS vectors (Figure 22) I used the same dose of each vector because I considered that one GC of the 5'-vector plus one GC of the 3'-vector of dual AAVs are required to re-constitute one full-size functional genome as that contained in one particle of AAV NS.

Animal models

Mice were housed at the Institute of Genetics and Biophysics animal house (Naples, Italy) and maintained under a 12-hour light/dark cycle (10-50 lux exposure during the light phase). C57BL/6 and BALB/c mice were purchased from Harlan Italy SRL (Udine, Italy). Albino *Abca4-/-* mice were generated through successive crosses and backcrosses with BALB/c mice (homozygous for Rpe65 Leu450) (Radu et al, 2004) and maintained inbred. Breeding was performed crossing homozygous mice. The Large White Female pigs used in this study were registered as purebred in the LWHerd Book of the Italian National Pig Breeders' Association (Azienda Agricola Pasotti, Imola, Italy).

Subretinal injection of AAV vectors in mice and pigs

This study was carried out in accordance with the Association for Research in Vision and Ophthalmology Statement for the Use of Animals in Ophthalmic and Vision Research and with the Italian Ministry of Health regulation for animal procedures. All procedures on mice were submitted to the Italian Ministry of Health; Department of Public Health, Animal Health, Nutrition and Food Safety on October 17th, 2011. The

Ministry of Health approved the procedures by silence/consent, as per article 7 of the 116/92 Ministerial Decree. Surgery was performed under anesthesia and all efforts were made to minimize suffering.

Mice (4-5 weeks-old) were anesthetized with an intraperitoneal injection of 2 mL/100 g body weight of avertin [1.25% w/v of 2,2,2-tribromoethanol and 2.5% v/v of 2-methyl-2-butanol (Sigma-Aldrich, Milan, Italy)] (Papaioannou & Fox, 1993), then AAV2/8 vectors were delivered subretinally via a trans-scleral trans-choroidal approach as described by Liang et al (Liang, 2000). All eyes were treated with 1 μL of vector solution. The AAV2/8 doses (GC/eye) delivered vary across the different mouse experiments as it is described in the "RESULTS" section. To compare dual AAV to single AAV NS vectors (Figure 29) I used the same dose of each vector because I considered that one GC of the 5'-vector plus one GC of the 3'-vector of dual AAVs are required to re-constitute one full-size functional genome as that contained in one particle of AAV NS.

AAV2/1-VMD2-*human Tyrosinase* (Gargiulo et al, 2009) (dose: 2-5x10^8 GC/eye) was added to the AAV2/8 vector solution that was delivered subretinally to albino mice (*Abca4-/-* and BALB/c). This allowed to mark the RPE within the transduced part of the eyecup, which was subsequently dissected and analysed. Subretinal delivery of AAV vectors to the pig retina was performed as previously described (Mussolino et al, 2011). All eyes were treated with 100 μL of AAV2/8 vector solution. The AAV2/8 dose was 1x10^{10} (Fig. 24) or 1x10^{11} GC of each vector/eye (Fig. 31 and Fig. 33) and co-injection of dual AAV vectors resulted in a total dose of 2x10^{10} GC/eye or 2x10^{11} GC/eye, respectively.

Western blot analysis & ELISA.

Samples [(HEK293 cells, retinas or eyecups (cups+retinas)] for Western blot analysis were lysed in RIPA buffer (50 mM Tris-HCl pH 8.0, 150mM NaCl, 1% NP40, 0.5% Na-Deoxycholate, 1mM EDTA pH 8.0, 0.1% SDS) to extract EGFP protein, or in SIE buffer (250 mM sucrose, 3 mM imidazole pH 7.4, 1% ethanol, and 1% NP-40) to extract ABCA4 protein. Lysis buffers were supplemented with protease inhibitors (Complete Protease inhibitor cocktail tablets, Roche, Milan, Italy) and 1 mM phenylmethylsulfonyl. After lysis EGFP samples were denatured at 99°C for 5 minutes in 1X Laemli sample buffer; ABCA4 samples were denatured at 37°C for 15 minutes in 1X Laemli sample buffer supplemented with 4M urea. Lysates were separated by 6% (ABCA4 samples) or 12% (EGFP samples) SDS-polyacrylamide gel electrophoresis. The antibodies used for immuno-blotting are as follows: anti-EGFP (sc-8334, Santa Cruz, Dallas, TX, USA, 1:500); anti-3xflag (A8592, Sigma-Aldrich, 1:1000); anti-β-Tubulin (T5201,Sigma Aldrich, 1:10000); anti-Filamin A (catalog#4762, Cell Signaling Technology, Danvers, MA, USA, 1:1000); anti-Dysferlin (Dysferlin, clone Ham1/7B6, MONX10795, Tebu-bio, Le Perray-en-Yveline, France, 1:500). The quantification of EGFP and ABCA4 bands detected by Western blot was performed using ImageJ software (free download is available at http://rsbweb.nih.gov/ij/). EGFP expression was normalized to β-Tubulin; ABCA4 expression was normalized to Filamin A or Dysferlin for the *in vitro* and *in vivo* experiments, respectively, while Ponceau S (P7170, Sigma-Aldrich, Sigma-Aldrich, Milan, Italy) staining was used as loading control of the Western Blot depicted in Figure 33. Different proteins were used for normalization based on the similarity of their molecular weight to those of the different transgene products. The TS (Fig. 21B), TS-L (Fig. 21D) and NS (Fig. 22B) histogram do not have standard error bars as only one TS, TS-L or NS sample has been loaded on each SDS-PAGE and used as internal reference sample in each independent experiment. To show

the internal variability of TS, TS-L and NS samples I calculated the expression of proteins as percentage relative to the AK sample (set to 100%) which are the following: Fig. 21B: TS=106±16%; Fig. 21D: TS-L=39±6%; Fig. 22B: NS=906±281%. The ELISA was performed on retina or eyecup lysates using the Max Discovery Green Fluorescent Protein Kit ELISA (Bioo Scientific Corporation, Austin, TX, USA).

Fundus photography

The fundus live-imaging was performed by dilating the eye of C57BL/6 with a drop of tropicamide 1% (Visufarma, Rome, Italy) and subsequent eye stimulation with a 300W flash. Fundus photographs were taken using a Topcon TRC-50IX retinal camera, with a FITC filter, connected to a charge-coupled-device Nikon D1H digital camera (Topcon Medical System, Oakland, NJ, USA).

Histology, light and fluorescence microscopy

To evaluate EGFP expression in histological sections, eyes from C57BL/6 mice or Large White pigs (Mussolino et al, 2011) were enucleated one month after AAV2/8 injection. Mouse eyes were fixed in 4% paraformaldehyde over-night and infiltrated with 30% sucrose over-night; the cornea and the lens were then dissected and the eyecups were embedded in optimal cutting temperature compound (O.C.T. matrix, Kaltek, Padua, Italy). Serial cryosections (10 μm thick) were cut along the horizontal meridian and progressively distributed on slides. PR co-transduction following subretinal combined delivery of AAV2/8-CMV-*EGFP* and -*RFP* vectors has been evaluated as follows: retinal cryosections from n=6 eyes were analysed under a fluorescent microscope using either the FITC (to visualize EGFP+ cells) or Rhodamine (to visualize RFP+ cells) filters. For each eye, RFP+ PRs contained in one field at 20X

magnification (at least 100) and the corresponding EGFP+ PRs (at least 200) were photographed and then counted. PRs expressing both EGFP and RFP were unequivocally identified based on their identical shape on picture micrographs of the same field taken under either the FITC or Rhodamine filter. To calculate the percentage of co-transduced PRs, the number of PRs expressing both EGFP and RFP was divided by the total number of transduced PRs, i.e. PRs expressing at least one of the two reporter genes.

Pig eyes were fixed in 4% paraformaldehyde for 48 hours, infiltrated with 10% sucrose for 4 hours, 20% sucrose for 4 hours and finally 30% sucrose overnight. Then, the cornea, the lens, and the vitreous body were dissected and the EGFP-positive portions of the eyecups were embedded in optimal cutting temperature compound (O.C.T. matrix, Kaltek). Serial cryosections (12 μm thick) were cut along the horizontal meridian and progressively distributed on slides. Retinal histology pictures were captured using a Zeiss Axiocam (Carl Zeiss, Oberkochen, Germany). Subretinal delivery in pigs of AAV vectors encoding for EGFP under the control of the Rhodopsin promoter resulted in PRs transduction in: 100% of the retinas injected with: dual AAV TS (4/4); and dual AAV hybrid AK (3/3) (Fig. 31).

Electron microscopy and immuno-gold labelling

For electron microscopy analyses, eyes were harvested from *Abca4-/-* mice 3 months after AAV injection. Eyes were fixed in 0.2% glutaraldehyde-2% paraformaldehyde in 0.1M PHEM buffer pH 6.9 (240 mM PIPES, 100 mM HEPES, 8mM $MgCl_2$, 40 mM EGTA) for 2 hours and then rinsed in 0.1 M PHEM buffer. Eyes were then dissected under the light to select the Tyrosinase-positive portions of the eyecups of albino *Abca4-/-*and BALB/c mice. The transduced portion of the eyecups was subsequently

embedded in 12% gelatin, infused with 2.3M sucrose and frozen in liquid nitrogen. Cryosections (50 nm) were cut using a Leica Ultramicrotome EM FC7 (Leica Microsystems) and extreme care was taken to align PR connecting cilia longitudinally. To avoid bias in the attribution of morphological data to the various experimental groups, measurements of RPE thickness and counts of lipofuscin granules in *Abca4-/-* eyes were performed by a masked operator (Roman Polishchuk) using the iTEM software (Olympus SYS, Hamburg, Germany). Briefly, RPE thickness was measured in at least 30 different areas along the specimen length using the "Arbitrary Line" tool of iTEM software. The "Touch count" module of the iTEM software was utilized to count the number of lipofuscin granules in the 25μm^2 areas distributed randomly across the RPE layer. The granule density was expressed as number of granules per 25μm^2. The immuno-gold analysis aimed at testing the expression of ABCA4-HA in *Abca4-/-* samples after AAV vector delivery was performed by incubating cryosections successively with monoclonal anti-HA antibody (MMS-101P-50, Covance, 1:50), rabbit anti-mouse IgG, and 10-nm gold particle-conjugated protein A.

Electrophysiological analyses

Electroretinograms (ERGs) measure the electrical response of the retina to flashes of light and are recorded with an electrode in contact with the cornea (Ogden, 2001). A single-flash with light, if the retina is dark-adapted, elicits a combined rod-plus-cone response, characterized by an initial a-wave, showing a hyperpolarization of the PRs and a subsequent b-wave resulting from a depolarization of the cells in the inner nuclear layer. The ERG were performed as previously described (Allocca et al, 2011). Briefly, ERG were evoked by 10ms flashes of different light intensities ranging from 10e-4 to 20 cd m-2 s-1 generated through a Ganzfield stimulator. To minimize the noise, three

different responses evoked by light were averaged for each luminance step (with a time interval between light stimuli of 15-30 sec). After completion of responses obtained in dark-adapted conditions (scotopic) the recording session continued with the aim to dissect the cone pathway mediating the light response (photopic). To this end, the electroretinogram in response to light of 20 cd m-2 s-1 was recorded in the presence of a continuous background light (background light set at 50 cd m-2).

To assess the recovery from light desensitization, after 180 min of dark adaptation, eyes were stimulated with 3 light flashes of 1 cd s/m^2 and then desensitized by exposure to constant light (300 cd/m^2) for 3 minutes. Then, eyes were stimulated over time using the pre-desensitization flash (1 cd s/m^2) at 0, 5, 15, 30, 45 and 60 minutes post-desensitization. The recovery of rod activity was evaluated by performing the ratio between the b-wave generated post-desensitization (at the different time points) and that generated pre-desensitization.

RNA extraction, cDNA production and reverse transcription analyses.

RNA was extracted at 72 hours after HEK293 cells infection with dual AAV2/2 TS and hybrid AK vectors encoding for either *ABCA4* (5'+3'halves) or, as negative controls, with either the 5'or 3'half of dual AAV2/2 vectors or with a single NS AAV2/2 *EGFP* vector. Total RNA was extracted using the RT-PCR RNeasy MiniKit (Qiagen, Milan, Italy). One µg of RNA was submitted to DNase I digestion (RNase Free DNase set, Qiagen) and cDNA was generated using the QuantiTect reverse transcription kit (Qiagen). To amplify the *ABCA4* mRNA region corresponding to the exon-intron junction used in dual AAV TS and hybrid AK vectors, one µL of cDNA and the following primers were used: Abca4_RT_Fw 5'-GCTGGGAAAACCACCACC-3' and Abca4_RT_Rev 5'-GTGGACACATGCCAAGGC-3'. A PCR product of the expected

size (130 bp) was then sequenced. Five µL of cDNA were insted used to amplify the full-length *ABCA4* mRNA (6.9 Kb) with a long-range PCR using TaKaRa LA Taq DNA polymerase kit (TaKaRa, Kioto, Japan), and the following primers: ATGFw*:* 5'-GGTACCTCTAGAGTCGACCCGG-3', which anneals upstream of the ATG start codon and SV40polyA-Rev 5'-ACTCATCAATGTATCTTATCATGTCTG-3'.

Statistical analysis

Statistical p values ≤0.05 were considered significant. One-way ANOVA with post-hoc Multiple Comparison Procedure was used to compare data depicted in: Figure 21 (p ANOVA= B. 0.012; D. 0.002); Figure 22B (p ANOVA=$2.3x10^{-8}$); Figure 28 (p ANOVA= A: 0.13; B: 0.16); Figure 29 (p ANOVA=$1.9x10^{-12}$); Figure 37 (p ANOVA=0.1639) Figure 40B (p ANOVA=0.00126); Figure 42 (p ANOVA=$2.2x10^{-5}$); Table 4 (2/2 preps: p ANOVA=0.0698; 2/8 preps: p ANOVA=0.0767). As the counts of lipofuscin granules (Fig. 39) are expressed as discrete numbers, these were analyzed by deviance from a Negative Binomial generalized linear models (Venables VN & Ripley BD, 2002) (p value analysis of deviance: $1.7x10^{-7}$). The statistically significant differences between groups determined with the post-hoc Multiple Comparison Procedure are the following: Figure 21B: OV vs OZ p=0.03; OV vs AP p=0.016; Figure 21D: AK-L vs OZ p=0.003; AK-L vs TS-L p=0.005; Figure 22B: NS-*EGFP* vs TS-*EGFP* p=0; NS-*EGFP* vs AK-*EGFP* p=$1x10^{-7}$; Figure 29: NS-*EGFP* vs TS-*EGFP* p=0; NS-*EGFP* vs AK-*EGFP* p=0; Figure 39: WT vs *Abca4-/-* neg p=0.016; WT vs *Abca4-/-* AK-*ABCA4* p=0.03; *Abca4-/-* neg vs *Abca4-/-* TS-*ABCA4* p=0.0005; *Abca4-/-* neg vs *Abca4-/-* AK-*ABCA4* p=$9x10^{-8}$; Figure 40: *Abca4-/-* neg vs *Abca4-/-* TS-*ABCA4* p=0.012; *Abca4-/-* neg vs *Abca4-/-* AK-*ABCA4* p=0.002; Figure 42 (60 min): *Abca4-/-* neg vs *Abca4-/-* AK-*ABCA4*: 0.05; *Abca4-/-* neg vs *Abca4-/-* TS-*ABCA4*: 0.009; *Abca4-*

/- AK-*ABCA4* vs WT: 0.002; *Abca4-/-* TS-*ABCA4* vs WT: 0.02 *Abca4-/-* neg vs WT $1x10^{-5}$.

The Student's t-test was used to compare data depicted in Figures 30, 37 and 41. The data in the manuscript are depicted as mean ± s.e.m (standard error of the mean). The s.e.m has been calculated using the number of independent *in vitro* experiments or eyes (not replicate measurements of the same sample).

RESULTS

1. Generation of normal size, oversize and dual AAV vectors.

The first part of the project was focused on the design and generation of the plasmids, and the corresponding AAV vectors, for the previously described AAV vector strategies. In addition to the vectors expressing the therapeutic *ABCA4* gene, to treat the STGD mouse model, I have decided to also use vectors expressing the reporter *EGFP* gene to compare the efficiency of the different approaches. The latter transgene allowed me the advantage of direct visualization of the layer of retinal cells expressing the reporter gene as well as the ability to compare the efficacy of dual AAVs to that of a single normal-size AAV vector. The constructs generated for AAV vector production used in this study are listed in Table 3. In particular, for the therapeutic *ABCA4* gene, I generated AAV oversize (OZ), dual AAV overlapping (OV), dual AAV trans-splicing (TS) and hybrid vectors. The recombinogenic sequences included in the dual AAV hybrid vectors were based on either a previously reported region of the alkaline phosphatase transgene (AP, dual AAV hybrid AP) (Ghosh et al, 2011) or a 77 bp sequence from the F1 phage genome (AK, dual AAV hybrid AK) that we found to be recombinogenic in previous *in vitro* experiments (Colella and Auricchio, unpublished data). Additionally, I generated AAV OZ and dual AAV vectors including the reporter EGFP with the exception of the dual AAV OV approach since its efficiency relies on transgene-specific overlaps for reconstitution (Ghosh et al, 2006) and, therefore, can not be extrapolated from one gene to another. For EGFP I also generated single AAV vectors of normal size (NS) to compare levels of transgene expression from the various strategies. I used AAV2/2 vectors for the *in vitro* experiments, with the ubiquitous cytomegalovirus (CMV) promoter, which efficiently transduce HEK293 cells (Dong et

al, 2010b). In the experiments performed *in vivo* in the retina, I used AAV2/8 vectors, which efficiently transduce RPE and PRs (Allocca et al, 2007; Mussolino et al, 2011; Vandenberghe et al, 2011) but poorly infect HEK293 cells, and either the ubiquitous CMV promoter (Mussolino et al, 2011), the RPE-specific vitelliform macular dystrophy 2 (VMD2) (Esumi et al, 2004), or the PR-specific Rhodopsin (RHO) and Rhodopsin kinase (RHOK) promoters (Allocca et al, 2007).

	Plasmid	Size ITR- ITR (bp)	AAV serotype	
			2/2	2/8
Normal Size (NS)	pZac2.1-CMV-*EGFP*-SV40	3006	**X**	**X**
	pZac2.1-CMV-*RFP*-SV40	2653		**X**
	pZac2.1-RHO-*EGFP*-SV40	2900		**X**
Oversize (OZ)	pAAV2.1-CMV-*EGFP*-9.9-SV40	9954	**X**	**X**
	pZac2.1-CMV-*ABCA4*_3xflag-SV40	8619	**X**	
Overlapping (OV)	pZac2.1-CMV-*ABCA4*_5'	4900	**X**	**X**
	pZac2.1-RHO-*ABCA4*_5'	4805		**X**
	pZac2.1-RHOK-*ABCA4*_5'	4169		**X**
	pZac2.1-VMD2-*ABCA4*_5'	4658		**X**
	pZac2.1-*ABCA4*_3'_3xflag_SV40	4740	**X**	**X**
Trans-splicing (TS)	pZac2.1-CMV-*ABCA4* _5'TS	4431	**X**	
	pZac2.1-CMV-3xflag-*ABCA4* _5'TS	4497	**X**	**X**
	pZac2.1-RHO-*ABCA4*_ 5'TS	4321		**X**
	pZac2.1-*ABCA4* _3'TS_3xflag_SV40	4587	**X**	**X**
	pZac2.1-CMV-*EGFP*_5'TS	1906	**X**	**X**
	pZac2.1-CMV-*EGFP*_5'TS-L	4016	**X**	**X**
	pZac2.1-RHO-*EGFP*_5'TS	1802		**X**
	pZac2.1-*EGFP*_3'TS_SV40	1510	**X**	**X**
	pZac2.1-*EGFP*_3'TS_SV40-L	4551	**X**	**X**

	Plasmid	Size ITR- ITR (bp)	AAV serotype	
			2/2	2/8
Hybrid AP (AP)	pZac2.1-CMV-*ABCA4*_5'AP	4708	**X**	
	pZac2.1-*ABCA4* _3'AP_3xflag_SV40	4871	**X**	
Hybrid AK (AK)	pZac2.1-CMV-*ABCA4* _5'AK	4540	**X**	
	pZac2.1-CMV-3xflag-*ABCA4* _5'AK	4606	**X**	**X**
	pZac2.1-RHO-*ABCA4*_ 5'AK	4436		**X**
	pZac2.1-*ABCA4* _3'AK_3xflag_SV40	4702	**X**	**X**
	pZac2.1-*ABCA4*_ 3'AK_HA_SV40	4663		**X**
	pZac2.1-CMV-*EGFP*_5'AK	2015	**X**	**X**
	pZac2.1-CMV-*EGFP*_5'AK-L	4125	**X**	**X**
	pZac2.1-RHO-*EGFP*_5'AK	1911		**X**
	pZac2.1-*EGFP*_3'AK_SV40	1614	X	**X**
	pZac2.1-*EGFP*_3'AK_SV40-L	4660	**X**	**X**

Table 3. Plasmids for AAV vector production
CMV: cytomegalovirus promoter; RHO: human Rhodopsin promoter; RHOK: human Rhodopsin kinase promoter; VMD2: vitelliform macular dystrophy 2 promoter; EGFP: enhanced green fluorescent protein; RFP: red fluorescent protein; ABCA4: human ATP-binding cassette, sub-family A, member 4; SV40: simian virus 40 poly-adenilation signal; 3xflag: 3xflag tag; HA: hemagglutinin tag; AP: alkaline phosphatase recombinogenic region; AK: F1 phage recombinogenic region; L: dual AAV vectors containing a combined (5'+3') large (>5 Kb in length) genome.

As shown in Table 3, each half of the dual AAV approaches was designed to have a genome that is compatible with the packaging capacity of normal size AAV vectors. However, to better assess the genome content of these vectors and to confirm that the presence of recombinogenic region in some of these vectors did not influenced the production of the viruses, I performed Southern blot analysis of viral DNA extracted from several dual AAV OV, TS and hybrid AK viral preparations. This analysis confirmed that the genome contained in dual AAV vectors is homogeneous and has the

expected length, independent of the presence of recombinogenic elements in the dual AAV vectors (Fig. 20)

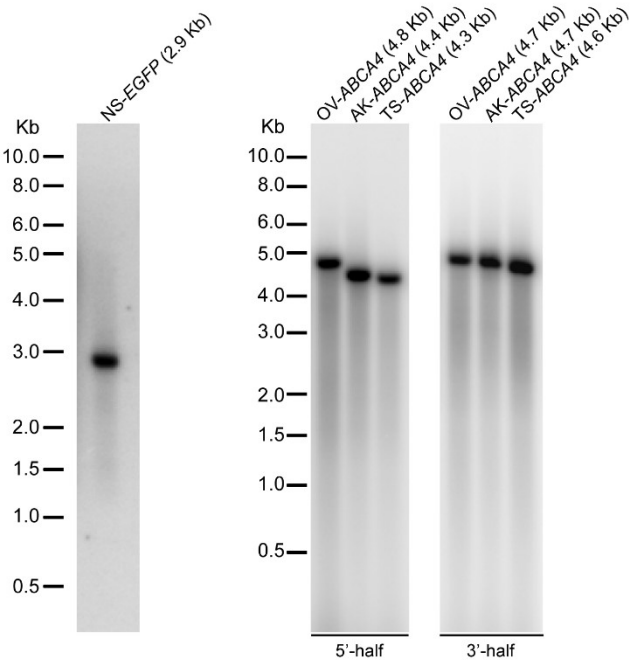

Figure 20. The genome of dual AAV RHO-ABCA4 vectors is correctly packaged in AAV capsids.
Alkaline Southern blot analysis of DNA extracted from $3x10^{10}$ genome copies of either single AAV of normal size (NS-EGFP) or dual AAV2/8-overlapping (OV-*ABCA4*), hybrid AK (AK-*ABCA4*) and trans-splicing (TS-*ABCA4*) vectors containing the RHO-*ABCA4-3xflag* expression cassette. The expected size of each genome is depicted in brackets above each corresponding lane. The molecular weight marker (kb) is shown on the left. The probes used for the hybridization are described in the Materials and Methods section.

In addition, the titers (GC/mL) of both AAV2/2 and AAV2/8 viral preparations were comparable to the titers of the regular NS AAV vectors (Table 4).

	AAV2/2			AAV2/8		
	NS[a] (GC[b]/mL)	5'-half (GC/mL)	3'-half (GC/mL)	NS (GC/mL)	5-half (GC/mL)	3'-half (GC/mL)
Average	$3.8x10^{12}$	$8.3x10^{12}$	$4.2x10^{12}$	$9.8x10^{12}$	$1.1x10^{13}$	$6.7x10^{12}$
s.e.m.[c]	$6.8x10^{11}$	$1.6x10^{12}$	$9.6x10^{11}$	$2.3x10^{12}$	$1.3x10^{12}$	$1.4x10^{12}$
n[d] preps	20	31	19	20	47	27

Table 4. The titers of dual AAV vectors are similar to those of regular AAV vectors of normal size.
N.B. [a]NS: normal size; [b]GC: genome copies; [c]s.e.m.: standard error of the mean; [d]n: number of AAV preparations. The 5'-half sample includes single 5'-halves of dual AAV overlapping, trans-splicing and hybrid vectors; the 3'-half sample includes single 3'-halves of dual AAV overlapping, trans-splicing and hybrid vectors. No statistically significant differences using ANOVA were found in the titers of NS AAV2/2 or AAV2/8 compared to those of dual AAV vectors.

2. Dual AAV vectors allow high levels of transduction in vitro.

I initially compared the efficiency of the various OZ, dual AAV OV, TS and hybrid AP and AK strategies for AAV-mediated large gene transduction *in vitro* by infecting HEK293 cells with the AAV2/2 vectors [multiplicity of infection, m.o.i.: 10^5 genome copies (GC)/cell of each vector] under the control of the ubiquitous CMV promoter. Cell lysates were analyzed by Western blot with anti-3xflag (to detect ABCA4-3xflag, Fig. 21A) antibodies. All strategies resulted in the expression of proteins of the expected size. As predicted, no bands of the expected size were observed when only one of the dual AAV vectors was used for infection. Quantification of protein expression (Fig. 21B) showed that the dual AAV hybrid AP approach resulted in the lowest levels of transgene expression, while the dual AAV OV, TS and hybrid AK approaches were more efficient than the AAV OZ approach. I then confirmed this using the *EGFP* transgene. For this purpose I selected the best performing dual AAV strategies (TS and hybrid AK; I did not use the transgene-specific OV strategy with *EGFP*, since, as

previously mentioned, its efficiency relies on transgene-specific overlaps for reconstitution and therefore can not be extrapolated from one gene to another) and further compared them to AAV OZ. I thus produced AAV2/2-CMV-OZ-EGFP vectors and for comparison -TS- and -AK-EGFP-L in which the combined dual AAV vector genome length is similar to that of AAV OZ (Table 3).

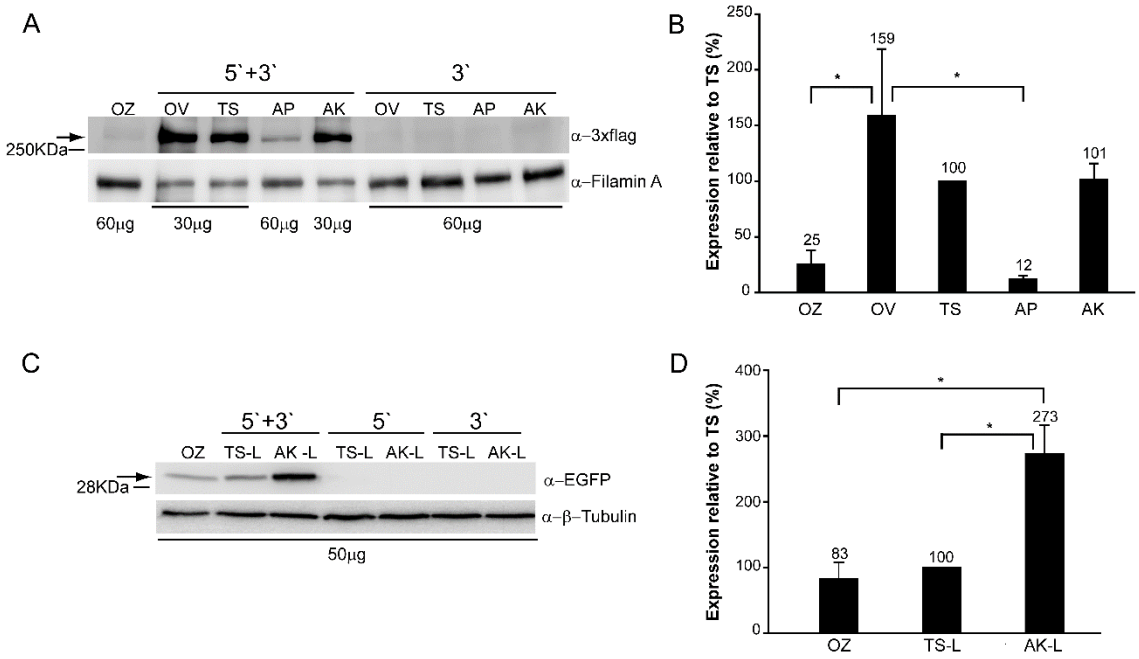

Figure 21. Dual AAV overlapping, trans-splicing and hybrid AK vectors efficiently transduce large genes *in vitro*.

Representative Western blot analysis of HEK293 cells infected with AAV2/2 vectors encoding for ABCA4 (A-B) and EGFP (C-D). (A, C) The arrows indicate full-length proteins, the micrograms of proteins loaded are depicted under each lane, the molecular weight ladder is depicted on the left. (B, D) Quantification of ABCA4 (B) and EGFP (D) protein bands. The intensity of the ABCA4 and EGFP bands was divided by the intensity of the Filamin A or Tubulin bands, respectively. The histograms show the expression of proteins as a percentage relative to dual AAV trans-splicing (TS) vectors, the mean value is depicted above the corresponding bar. Values are represented as mean ± s.e.m. (standard error of the mean). (A-D) The Western blot images are representative of and the quantifications are from n=4 independent experiments. OZ: AAV oversize; OV: dual AAV overlapping; TS: dual AAV trans-splicing; AP: dual AAV hybrid AP; AK: dual AAV hybrid AK; TS-L: dual AAV trans-splicing EGFP with a combined genome size similar to OZ-EGFP; AK-L: dual AAV hybrid AK EGFP with a combined genome size similar to OZ-EGFP; 5'+3': cells co-infected with 5'- and 3'-half vectors; 5': control cells infected with the 5'-half vector; 3': control cells infected with the 3'-half vector; α-3xflag: Western blot with anti-3xflag antibody; α-EGFP: Western blot with anti-EGFP antibody; α-β-Tubulin: Western blot with anti-β-Tubulin antibody, used as loading control; α-Filamin A: Western blot with anti-Filamin A antibody, used as loading control. *p ANOVA<0.05. More details on the statistical analysis including specific statistical values can be found in the Statistical analysis paragraph of the Materials and Methods section.

I infected HEK293 cells with AAV2/2-CMV-EGFP vectors [multiplicity of infection, m.o.i.: 10^5 genome copies (GC)/cell of each vector] and performed Western blot analysis of cell lysates with anti-EGFP antibodies (Fig. 21C). Similarly to what was observed with the ABCA4 transgene, quantification of EGFP expression (Fig. 21D) showed that dual AAV TS and hybrid AK approaches are more efficient than AAV OZ.

Then, to assess which was the *in vitro* efficiency of the dual AAV vectors relatively to a single AAV vector, I infected HEK293 cells with dual AAV TS and hybrid AK vectors encoding for EGFP [multiplicity of infection, m.o.i.: 10^5 genome copies (GC)/cell of each vector] and compared, by Western blot analysis, the levels of protein expression achieved with these vectors to those of a single AAV-NS-EGFP (Fig. 22).

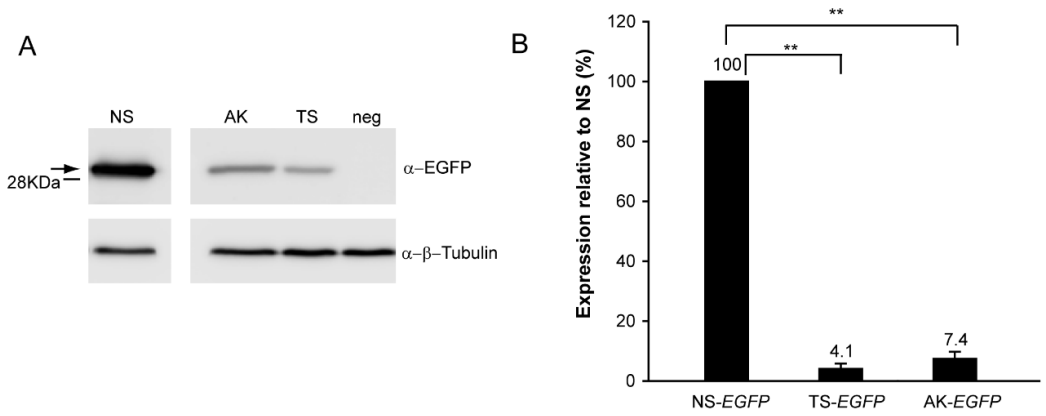

Figure 22. In vitro transduction efficiency of dual AAV trans-splicing and hybrid AK vectors compared to single normal size AAV vector.

(A) Representative Western blot analysis of HEK293 cells infected with AAV2/2 vectors encoding for EGFP under the control of the ubiquitous cytomegalovirus (CMV) promoter. The arrow indicates full-length protein, 50 micrograms of proteins were loaded in each lane, the molecular weight ladder is depicted on the left. (B) Quantification of EGFP protein bands. The intensity of the EGFP bands was divided by the intensity of the Tubulin bands. The histograms show the expression of proteins as percentage relative to single normal size AAV (NS) vector, the mean value is depicted above the corresponding bar. Values are represented as mean ± s.e.m. (standard error of the mean). The Western blot images are representative of and the quantifications are from n=3 independent experiments. NS: cells infected with normal size AAV vector; TS: cells infected with dual AAV trans-splicing vectors; AK: cells infected with dual AAV hybrid AK vectors; neg: cells infected with the 5'-half of either the dual AAV TS or hybrid AK vectors, as negative controls; α-EGFP: Western blot with anti-EGFP antibody; α-β-Tubulin: Western blot with anti-β-Tubulin antibody, used as loading control. **p ANOVA<0.001. More details on the statistical analysis including specific statistical values can be found in the Statistical analysis paragraph of the Materials and Methods section.

Quantification of EGFP expression showed that the levels achieved with dual AAV TS and hybrid AK vectors were about 13-25 folds lower (7-4%) than with AAV NS.

3. Assessment of co-transduction efficiency in mice retinas.

The enclosed and small subretinal space should favour co-infection and transduction of the same cell by two independent AAV vectors. To test this, specifically in PRs, I injected subretinally C57BL/6 mice with a mixture of AAV2/8-CMV-EGFP and -RFP vectors (dose of each vector/eye: $1.4x10^9$ GC/eye) and analysed co-transduction on retinal cryosections, which allows for the unequivocal identification of PRs from RPE (Fig. 23). I found that 24±2% of transduced PRs expressed both EGFP and RFP.

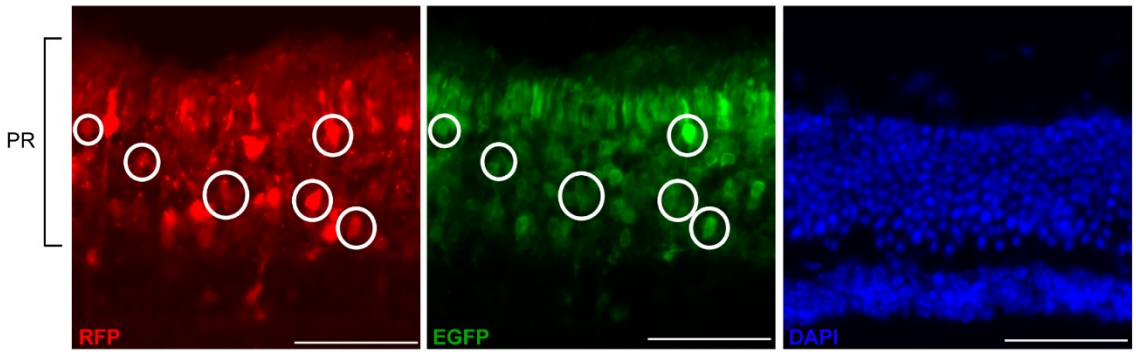

Figure 23. Photoreceptor co-transduction following subretinal combined delivery of single AAV-EGFP and -RFP vectors
Fluorescence analysis of a representative retinal cryosection from C57BL/6 mice 3 weeks following subretinal co-injection of single AAV2/8-CMV-EGFP and-RFP vectors (dose of each vector/eye: $1.4x10^9$ GC, n=6 eyes) demonstrating RFP+ cells (left panel) and EGFP+ cells (central panel) is presented. The scale bar (50 µm) is depicted in the figure. Circles highlight PRs transduced by both vectors. PR: photoreceptors; RFP: native RFP fluorescence; EGFP: native EGFP fluorescence; DAPI: 4',6'-diamidino-2-phénylindole staining.

However, since the number of RFP-single-positive cells was lower than the number of EGFP-single-postive cells, likely due to a weaker RFP fluorescence compared to EGFP, co-transduction efficiency may have been under-estimated. Indeed, considering the number of RFP+ cells that are also EGFP+, the percentage of co-transduction reaches 53±4%. This co-transduction efficiency is similar to that previously reported by Palfi and colleagues (Palfi et al, 2012).

4. Dual AAV trans-splicing and hybrid AK, but not overlapping, vectors transduce mouse and pig photoreceptors.

I evaluated the best *in vitro* performing AAV-based systems for large gene transduction in the mouse retina. To test the dual AAV OV, which is transgene-specific, I used the therapeutic *ABCA4* gene (Fig. 24), while the EGFP reporter was used to evaluate the AAV OZ and the dual AAV TS and hybrid AK approaches (Fig. 26).

Western blot analysis on retinal lysates, one month post-subretinal injection of the dual AAV OV vectors (dose of each vector/eye: $1.3x10^9$ GC) in C57BL/6 mice, expressing ABCA4-3xflag from the ubiquitous CMV promoter, revealed robust protein expression (Fig. 24A). However, as *ABCA4* is specifically expressed in PRs, I attempted to determine which cell type in the retina expressed *ABCA4*, taking advantage of the use of various promoters that restrict transgene expression to specific cell layers. I, therefore, injected subretinally C57BL/6 mice with dual AAV OV vectors (dose of each vector/eye: $1x10^9$ GC) that contained either the PR-specific RHO and RHOK, or the RPE-specific VMD2 promoters. I detected ABCA4 protein expression in retinas injected with the VMD2 but not in those containing the RHO and RHOK promoters (Fig. 24A). These results were also confirmed in the Large White pig retina. The pig

retina is an excellent model to evaluate vector efficiency because of its size, which is similar to the human retina, and because it is enriched with cones that are concentrated in a streak-like region with a cone density that is comparable to that of the primate macula (Mussolino et al, 2011). I injected Large White pig subretinally with dual AAV OV vectors encoding ABCA4-3xflag (dose of each vector/eye: $1x10^{10}$ GC), and observed ABCA4 protein expression with the CMV but not the RHO promoter (Fig. 24B).

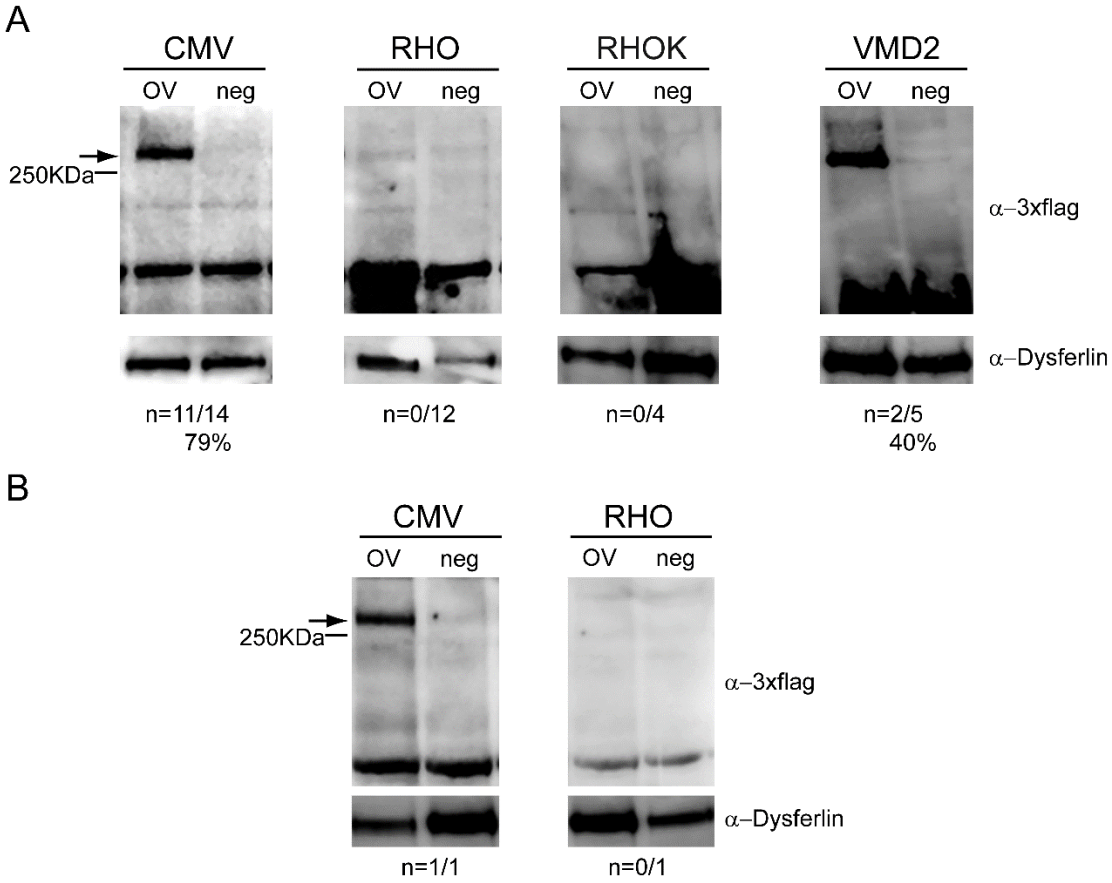

Figure 24. Dual AAV overlapping vectors transduce RPE but not photoreceptors in the mouse and pig retina.
Representative Western blot analysis of C57BL/6 (A) and Large White pig (B) retinal lysates one month following injection of dual AAV2/8 overlapping vectors encoding for ABCA4-3xflag (OV) or AAV2/8 vectors expressing EGFP (neg), under the control of the ubiquitous cytomegalovirus (CMV) promoter, the PR-specific Rhodopsin (RHO) and Rhodopsin kinase (RHOK) promoters, or the RPE-specific vitelliform macular dystrophy 2 (VMD2) promoter. The arrows indicate full-length proteins, the molecular weight ladder is depicted on the left, 150 micrograms of proteins were loaded in each lane. The number (n) and percentage of ABCA4-positive retinas out of total retinas analysed is depicted; α-3xflag: Western blot with anti-3xflag antibody; α-Dysferlin: Western blot with anti-Dysferlin antibody, used as loading control.

To rule out that this was due to a lower transcriptional activity from either the RHO or RHOK promoters compared to CMV, I injected subretinally C57BL/6 mice with $1.5x10^9$ GC/eye of AAV2/8 vectors expressing *EGFP* from each of the promoters and found that CMV and RHO drive similarly robust PR transgene expression (Fig. 25).

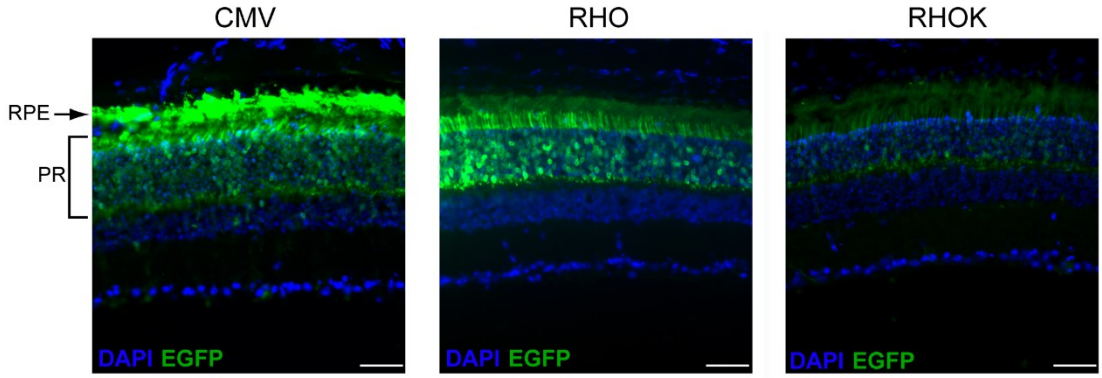

Figure 25. CMV, RHO and RHOK promoters drive transgene expression in murine photoreceptors.
Fluorescence analysis of representative retinal cryosections from C57BL/6 mice one month following subretinal injection of single AAV2/8 vectors encoding for EGFP under the control of the ubiquitous cytomegalovirus (CMV) promoter or the PR-specific Rhodopsin (RHO) and Rhodopsin kinase (RHOK) promoters. Arrow points at transduced RPE. The scale bar (50 μm) is depicted in the figure. RPE: retinal pigmented epithelium; PR: photoreceptors; DAPI: 4',6'-diamidino-2-phenylindole staining; EGFP: native EGFP fluorescence.

Overall, these data suggest that the dual AAV OV approach is more efficient for large gene transfer to RPE than to PRs, thus it is not a strategy applicable to ABCA4 delivery. To find an AAV-based strategy that efficiently transduces large genes in PRs, I compared the retinal transduction properties of the other best performing approaches *in vitro* in addition to dual AAV OV: AAV OZ and dual AAV TS and hybrid AK approaches. I used EGFP, which allowed me to easily localize transgene expression in the various retinal cell types, including PRs. C57BL/6 mice were injected subretinally with AAV OZ and dual AAV TS-L and hybrid AK-L vectors (dose of each vector/eye: $1.7x10^9$ GC), all encoding EGFP under the transcriptional control of the CMV

promoter. One month later, fundus photographs showed that the highest levels of fluorescence were obtained with the dual AAV TS and hybrid AK approaches (Fig. 26). Fluorescence microscope analysis of retinal cryosections showed that detectable levels of RPE and PR transduction could be achieved with all approaches.

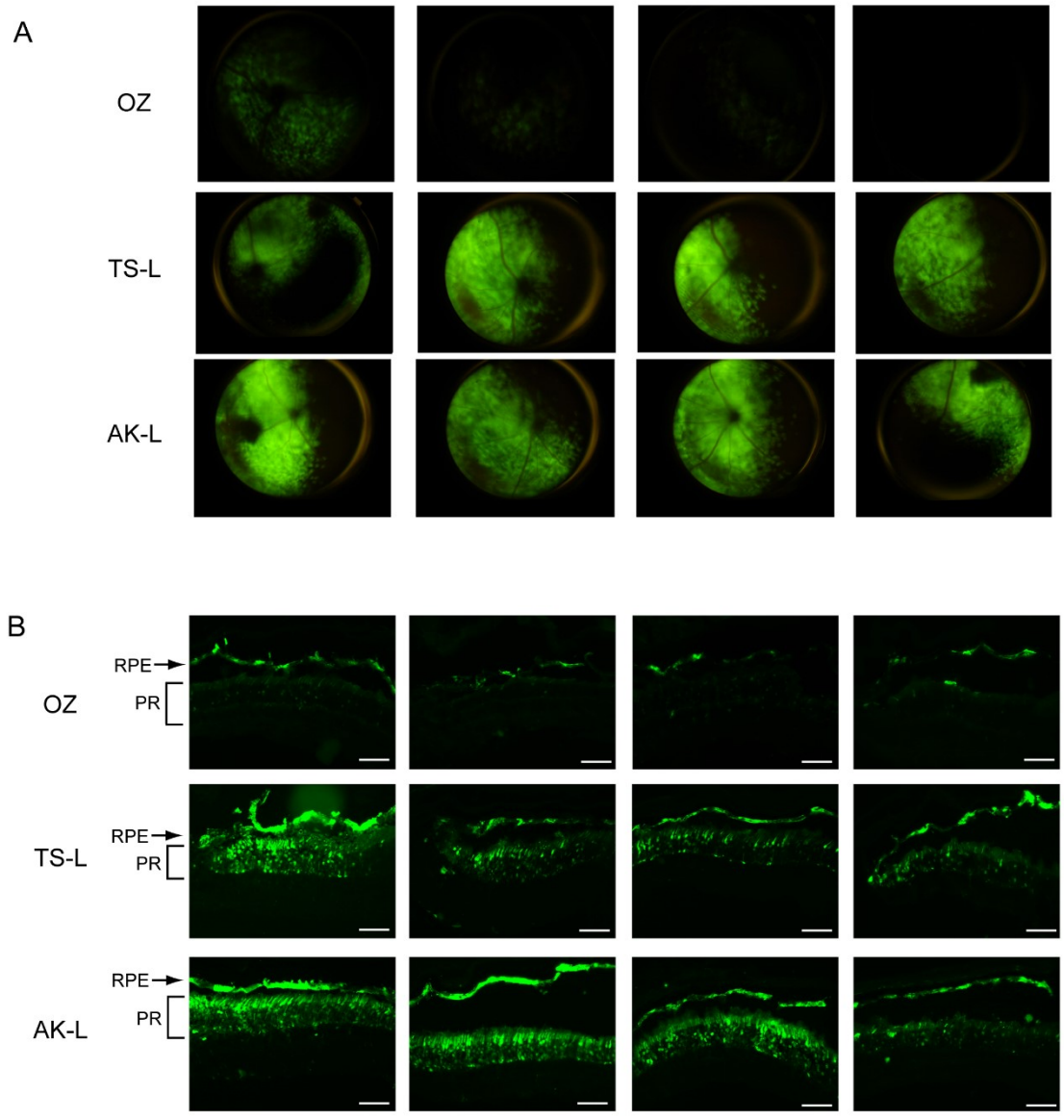

Figure 26. Dual AAV trans-splicing and hybrid AK vectors provide the most robust transduction of RPE and photoreceptors cell layers following subretinal delivery in mice.
Live-imaging fundus fluorescence (A) and fluorescence analysis of retinal cryosections (B) from C57BL/6 mice one month following subretinal injection of AAV2/8 vectors encoding for EGFP under the control of the ubiquitous cytomegalovirus (CMV) promoter. (B) Arrows point at transduced RPE. The scale bar (200 μm) is depicted in the figure. OZ: AAV oversize (n=4); TS-L: dual AAV trans-splicing EGFP with a combined genome size similar to OZ-EGFP (n=4); AK-L: dual AAV hybrid AK EGFP with a combined genome size similar to OZ-EGFP (n=4); RPE: retinal pigmented epithelium; PR: photoreceptors.

However, the levels of expression were higher, although variable, in the eyes injected with dual AAV TS-L and hybrid AK-L than in the eyes injected with AAV OZ vectors. I also confirmed that no protein expression is observed when injecting only one of the dual AAV vectors, as seen in the *in vitro* experiments (Fig. 27).

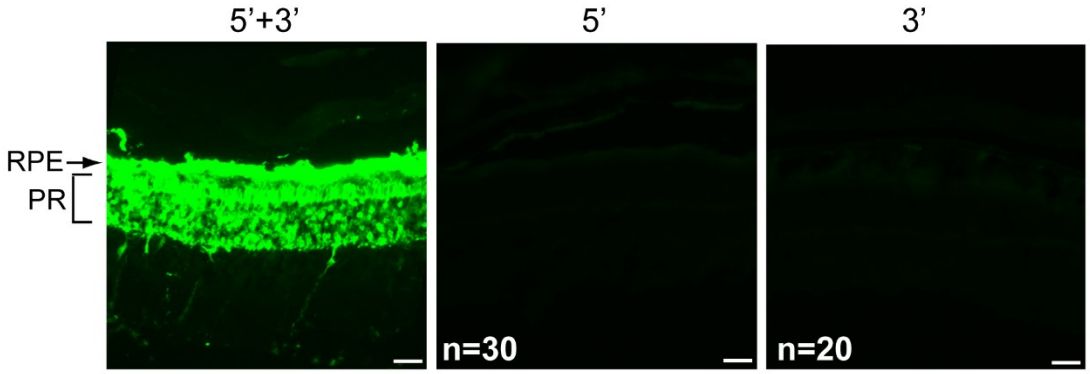

Figure 27. No detectable EGFP fluorescence in retinas injected with either the 5'- or 3'-half of dual AAV vectors.
Fluorescence analysis of representative retinal cryosections from C57BL/6 mice one month following subretinal injection of either the combination of dual AAV vectors (5'+3') encoding for EGFP or each of the single 5'- and 3'-half vectors. The eyes injected with the 5'-half include: 9 injected with CMV 5'AK, 6 injected with CMV 5'TS, 8 injected with RHO 5'AK, 7 injected with RHO 5'TS (n=30). The eyes injected with the 3'-half include: 13 injected with 3'AK and 7 injected with 3'TS (n=20). The arrow points at transduced RPE. The scale bar (20 μm) is depicted in the figure. 5'+3': retinas co-injected with 5'- and 3'-half vectors; 5': retinas injected with the 5'-half vector; 3': retinas injected with the 3'-half vector; RPE: retinal pigmented epithelium; PR: photoreceptors

To test whether the levels and consistency of dual AAV-mediated transduction obtained can be improved by varying the ratio between the 5'- and 3'-half vectors, I injected subretinally C57BL/6 mice with dual AAV TS and hybrid AK vectors with different doses of 5'- and 3'-half vectors (Fig. 28). I set as 1:1 the dose of $2.5x10^8$ GC/eye which is submaximal considering that the titers of our AAV preparations range around 10^9 GC/μL (Table 4) and that 1 μL is the maximum volume tolerated by the mouse subretinal space. Thus, $2.5x10^9$ GC/eye which is the high 1:1 dose (10:10) is the

maximum dose which is possible to administer to the murine eye. I found that none of the various ratios tested outperforms the 1:1 ratio of the high dose of vectors (10:10) used so far (Fig. 28). Therefore, I used the optimal 10:10 dose and ratio in the following experiments.

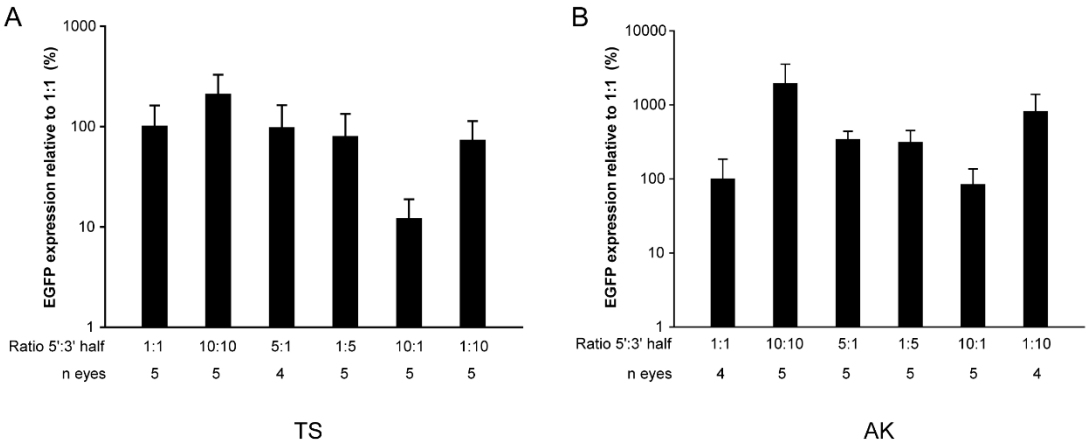

Figure 28. Murine retinal transduction with various doses and ratios of dual AAV vectors.
EGFP protein quantification by ELISA of eyecups from C57BL/6 mice one month following subretinal injection of dual AAV2/8 trans-splicing (A) and hybrid AK (B) vectors encoding for EGFP under the control of the ubiquitous cytomegalovirus (CMV) promoter. The various ratios of 5'- and 3'-half vectors used for the injections are depicted below each bar. The doses of 5'-and 3'-half vectors are the following: 1:1 [$2.5x10^8$:$2.5x10^8$ genome copies (GC)/eye]; 10:10 ($2.5x10^9$:$2.5x10^9$ GC/eye); 5:1 ($1.25x10^9$:$2.5x10^8$ GC/eye); 1:5 ($2.5x10^8$:$1.25x10^9$ GC/eye); 10:1 ($2.5x10^9$:$2.5x10^8$ GC/eye); 1:10 ($2.5x10^8$:$2.5x10^9$ GC/eye). The number (n) of eyes analysed is depicted below each bar. The histograms show EGFP expression as percentage relative to the 1:1 ratio. Values are represented as mean ± s.e.m. (standard error of the mean). TS: dual AAV trans-splicing; AK: dual AAV hybrid AK. No statistically significant differences were found using ANOVA. More details on the statistical analysis including specific statistical values can be found in the Statistical analysis paragraph of the Materials and Methods section.

Then, I sought both to better assess PR-specific transduction levels achieved with dual AAV TS and hybrid AK vectors, which appears the most promising for large gene reconstitution in PRs, and to compare them to those of a single AAV NS vector. To this aim, I injected subretinally C57BL/6 mice with dual AAV and single NS vectors (dose of each vector/eye: $2.4x10^9$ GC). All vectors encoded EGFP under the transcriptional

control of the PR-specific RHO promoter. One month after vector administration whole retina lysates were analyzed by ELISA to quantify EGFP protein levels (Fig. 29). Dual AAV TS and hybrid AK vectors reconstituted consistent EGFP expression in PRs at levels on average about 16-33 folds lower (6-3%) than with AAV NS. However, these levels were variable, similarly to what observed in retinal histological sections (Fig. 26), and some of the eyes treated with dual AAV vectors had EGFP levels in the range of those achieved with AAV NS (Fig. 29).

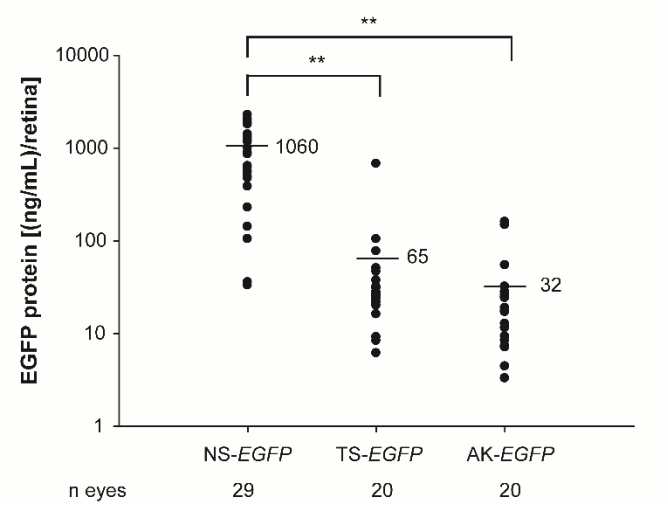

Figure 29. Dual AAV trans-splicing and hybrid AK vectors efficiently transduce mouse photoreceptors.
EGFP protein quantification by ELISA of retinas from C57BL/6 mice one month following subretinal injection of AAV2/8 vectors encoding for EGFP under the control of the PR-specific Rhodopsin (RHO) promoter. The scatter plot depicts EGFP protein levels from each retina; the mean value for each group is depicted and indicated with a solid line. The number (n) of eyes analysed is depicted under the x axis. ** p ANOVA<0.001. NS: AAV normal size; TS: dual AAV trans-splicing; AK: dual AAV hybrid AK. More details on the statistical analysis including specific statistical values can be found in the Statistical analysis paragraph of the Materials and Methods section.

As expected, no detectable EGFP expression was measured by ELISA in injected retinas when only one of the dual AAV vectors encoding for EGFP was used (n=9: 5 eyes injected with 5'-half and 4 eyes with 3'-half).

To exclude competition between dual AAV capsids at the entry step which may lead to over-estimate the efficiency of AAV NS, I evaluated EGFP expression after subretinal delivery of either $1.7x10^9$ GC of AAV2/8 NS-EGFP or $1.7x10^9$ GC of AAV2/8-NS-EGFP + $1.7x10^9$ GC of an AAV2/8 vector carrying an unrelated genome. Notably, I found no significant differences in the levels of EGFP expression whether the unrelated AAV was added or not (Fig. 30), proving that the double dose of dual AAV capsids administered when compared to AAV-NS does not affect dual AAV-mediated transduction.

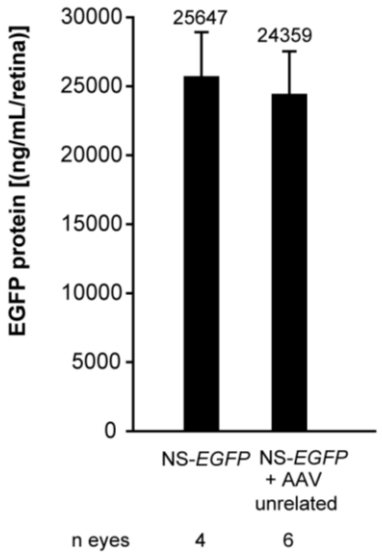

Figure 30. Similar EGFP levels following subretinal delivery of single AAV2/8-EGFP alone or in combination with the same dose of an unrelated AAV2/8 vector. ELISA quantification of EGFP protein in eyecups from C57BL/6 mice one month following subretinal injection of single AAV2/8-CMV-EGFP vector of normal size (NS-EGFP) in combination or not with the same dose of a single AAV2/8 vector of normal size carrying an unrelated transgene expression cassette (unrelated AAV2/8). The number (n) of eyes analyzed is depicted below each bar. Values are represented as: mean ± s.e.m. (standard error of the mean). No statistically significant differences were found using the Student's t-test (p=0.8).

Finally, to confirm that dual AAV TS and hybrid AK approaches transduce PRs also in pig, I injected subretinally Large White pigs with dual AAV TS and hybrid AK vectors expressing EGFP under the transcriptional control of the PR-specific RHO promoter

(dose of each vector/eye: $1x10^{11}$ GC) and I found efficient transduction of the PR cell layer (Fig. 31).

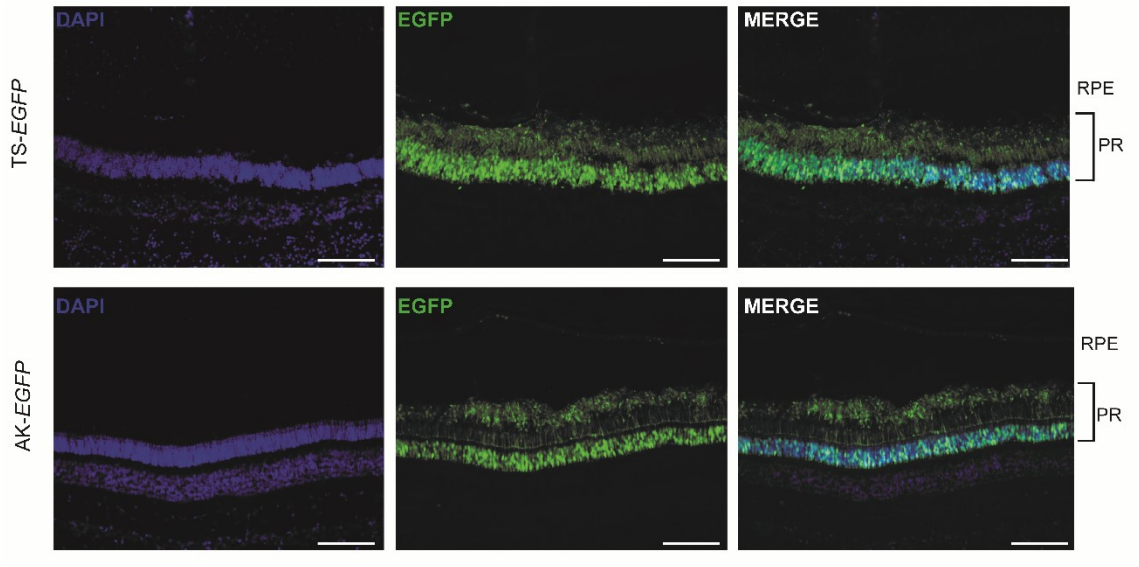

Figure 31. Dual AAV trans-splicing and hybrid AK vecotrs efficiently transduce pig photoreceptors.
Fluorescence analysis of retinal cryosections from Large White pigs one month following subretinal injection of AAV2/8 vectors encoding for EGFP under the control of the PR-specific RHO promoter. The pictures are representative of n=4 or n=3 eyes injected with dual AAV TS or hybrid AK, respectively. The scale bar (100 μm) is depicted in the figure. NS: AAV normal size; TS: dual AAV trans-splicing; AK: dual AAV hybrid AK; DAPI: 4',6'-diamidino-2-phenylindole staining; EGFP: native EGFP fluorescence; Merge: overlay of DAPI and EGFP pictures; RPE: retinal pigmented epithelium; PR: photoreceptors.

Taken together, these results show that dual AAV TS and hybrid AK strategies allow efficient PR transduction, both in mouse and in pig, although at levels which are lower than those obtained with an AAV NS.

5. Dual AAV trans-splicing and hybrid AK vectors are safe and efficient tools to deliver the large *ABCA4* gene to the mouse and pig retina.

To confirm that dual AAV TS and hybrid AK vectors can be efficiently used to deliver the large *ABCA4* gene to the retina, I generated dual AAV TS and hybrid AK vectors encoding ABCA4-3xflag under the transcriptional control of the RHO promoter and evaluated their transduction abilities in mouse and pig PRs. To this aim, I first injected them subretinally in wild-type C57BL/6 mice (dose of each vector/eye: 3-5x10^9 GC) and one month later I analysed retinas by Western blot with anti-3xflag antibodies. Both approaches resulted in robust yet variable levels of ABCA4-3xflag expression, that were more consistent in retinas treated with the dual AAV hybrid AK vectors (Fig. 32).

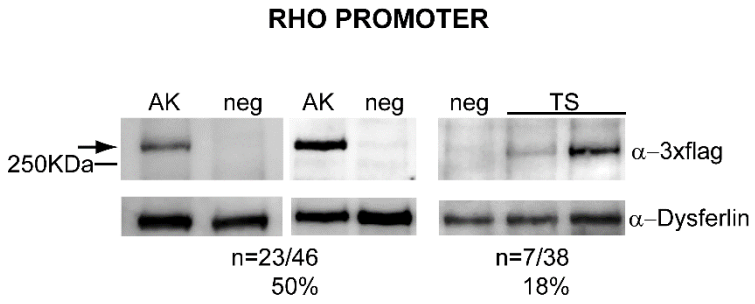

Figure 32. Subretinal administration of dual AAV vectors results in *ABCA4* expression in mouse photoreceptors.
Representative Western blot analysis of C57BL/6 retinal lysates one month following the injection of dual AAV trans-splicing (TS) and hybrid AK (AK) vectors encoding for ABCA4 under the control of the PR-specific Rhodopsin promoter (RHO PROMOTER). The arrow points at full-length proteins, the molecular weight ladder is depicted on the left, 150 micrograms of protein were loaded in each lane. The number (n) and percentage of ABCA4-positive retinas out of total retinas analysed is depicted. AK: retinas injected with dual AAV hybrid AK vectors; TS: retinas injected with dual AAV TS vectors; neg: retinas injected with AAV vectors expressing *EGFP*, as negative controls; α-3xflag: Western blot with anti-3xflag antibody; α-Dysferlin: Western blot with anti-Dysferlin antibody, used as loading control

Interestingly, this result was confirmed in pig retinas (Fig. 33). Indeed, Western blot analysis of pig retinas, one month post subretinal injection of dual AAV TS and hybrid

AK vectors, showed that both dual AAV approaches induce the expression of the full-length ABCA4-3xflag protein in PRs, although at variable levels. In addition, similarly to what observed in mice, dual AAV hybrid AK vectors resulted in more consistent *ABCA4* expression compared to dual AAV TS vectors.

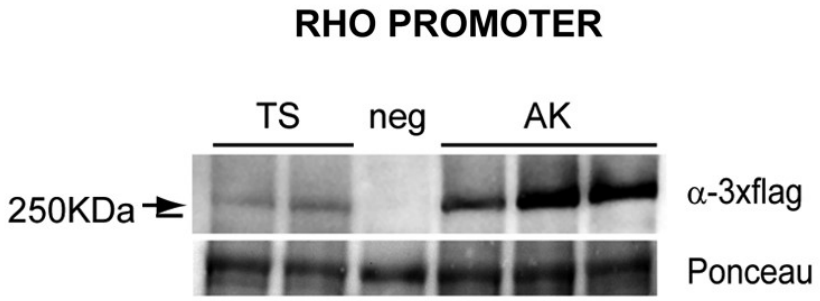

Figure 33. Subretinal administration of dual AAV vectors results in ABCA4 expression in pig photoreceptors.
Representative Western blot analysis of Large White pig retinal lysates one month following the injection of dual AAV trans-splicing (TS; n=2) and hybrid AK (AK; n=3) vectors encoding for ABCA4 or for normal size EGFP (neg), as negative control, under the control of the PR-specific Rhodopsin promoter (RHO PROMOTER). The arrows indicate full-length proteins, the molecular weight ladder is depicted on the left, 180 micrograms of proteins were loaded in each lane. α-3xflag: Western blot with anti-3xflag antibody. Ponceau staining was used as loading control.

Then, I decided to evaluate the possibility that the delivery of dual AAV vectors results in the production of aberrant proteins from both the 5'-half vectors, that contain the promoter sequence, and the 3'-half vectors, due to the low promoter activity of the ITRs (Flotte et al, 1993). To address this point, I generated 5'-halves of dual AAV vectors tagged with the 3xflag tag at the N-terminus of the ABCA4 protein and used these constructs, in combination with the 3'-halves tagged with the 3xflag tag at the C-terminus, to transduce both HEK293 cells and the C57BL/6 mouse retina. Importantly, no truncated and/or aberrant ABCA4 proteins were detected by Western blot analysis of C57BL/6 eyecups treated with dual AAV TS and hybrid AK vectors using anti-3xflag antibodies although two proteins (>100 KDa) smaller than the full length are produced

in vitro following infection with either the single 5'- or 3'-half of both dual AAV approaches (Fig. 34-35).

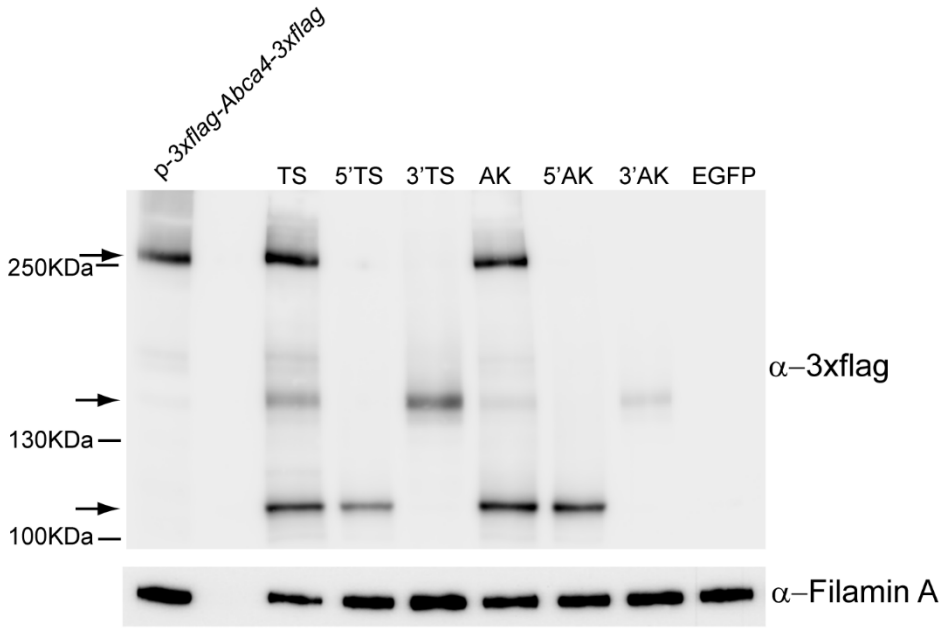

Figure 34. ABCA4 proteins smaller than expected are produced *in vitro* by dual AAV trans-splicing and hybrid AK vectors as well as by their corresponding single 5'- and 3'-half vectors.
Representative Western blot analysis of HEK293 cells infected with dual AAV2/2 trans-splicing (TS) and hybrid AK (AK) vectors encoding for ABCA4 under the control of the cytomegalovirus (CMV) promoter. Anti-3xflag antibodies recognize the 3xflag tag located at both the N- and C-termini of the ABCA4 protein. The upper arrow indicates the full-length ABCA4 protein; the lower arrows indicate the shorter products (>100 KDa) which derive from either single 5'- or 3'-half vectors. Thirty micrograms of proteins from transfected and infected cells were loaded; the molecular weight ladder is depicted on the left. The Western blot images are representative of n=3 independent experiments. p*3xflag-ABCA4-3xflag*: cells transfected with a plasmid encoding for full-length ABCA4 tagged with 3xflag at both N- and C-termini, as positive control; TS: cells infected with both 5'- and 3'-halves of dual AAV trans-splicing vectors; AK: cells infected with both 5'- and 3'-halves of dual AAV hybrid AK vectors; 5': cells infected with the 5'-half vector of either dual AAV TS (5'TS) or hybrid AK (5'AK) approaches; 3': cells infected with the 3'-half vector of either dual AAV TS (3'TS) or hybrid AK (3'AK) approaches; EGFP: cells infected with AAV vectors expressing EGFP, as negative control; α-3xflag: Western blot with anti-3xflag antibody; α-Filamin A: Western blot with anti-Filamin A antibody, used as loading control.

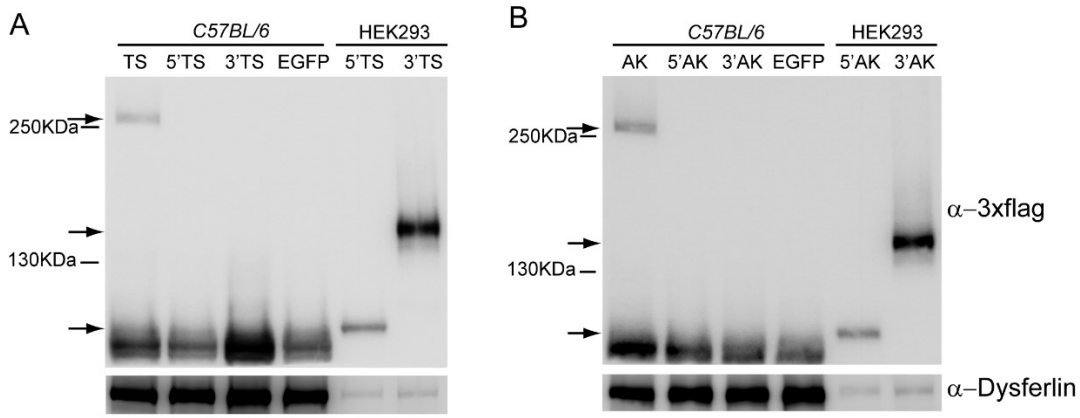

Figure 35. ABCA4 products of the expected size are detected in the eyes of C57BL/6 mice following subretinal delivery of dual AAV trans-splicing and hybrid AK vectors.

Representative Western blot analysis of C57BL/6 eyecups one month after subretinal delivery of dual AAV2/8 trans-splicing (TS; A) and hybrid AK (AK; B) vectors encoding for ABCA4 under the control of the ubiquitous cytomegalovirus (CMV) promoter. Anti-3xflag antibodies recognize the tag located at both the N- and C-termini of the ABCA4 protein. The lysates from HEK293 cells infected with single 5'- and 3'-half vectors of dual AAV2/2 TS and hybrid AK vectors were loaded as positive controls of the smaller than expected ABCA4 proteins observed *in vitro* (see Fig. 34). The upper arrow indicates the full-length ABCA4-3xflag; the lower arrows indicate the smaller products (>100KDa) which derive from either single 5'- or 3'-half vectors. Thirty or 150 micrograms of proteins from infected cells and injected eyecups were loaded, respectively; the molecular weight ladder is depicted on the left. The picture is representative of the following number of eyecups: n=10 treated with TS; n=10 treated with AK; n=5 treated with 5'TS, n=5 treated with 5'AK, n=5 treated with 3'TS, n=5 treated with 3'AK, n=7 treated with EGFP. TS: eyes injected with both 5'- and 3'-halves of dual AAV TS vectors; AK: eyes injected with both 5'- and 3'-halves of dual AAV hybrid AK vectors; 5': eyes injected or cells infected with the 5'-half of either dual AAV TS (5'TS) or hybrid AK (5'AK) vectors; 3': eyes injected or cells infected with the 3'-half of either dual AAV TS (3'TS) or hybrid AK (3'AK) vectors; EGFP: eyes injected with AAV vectors expressing EGFP, as negative control; HEK293: lysates from HEK293 cells infected with AAV; α-3xflag: Western blot with anti-3xflag antibody; α-Dysferlin: Western blot with anti-Dysferlin antibody, used as loading control.

I then tested the production of a properly spliced full-length ABCA4 mRNA by ABCA4 retrotranscription and amplification following infection of HEK293 cells with dual AAV vectors (Fig. 36). The successful amplification of the full size ABCA4 mRNA confirmed that intermolecular AAV joining and splicing occurred correctly, as expected by the size of the full-length protein detected by Western blot.

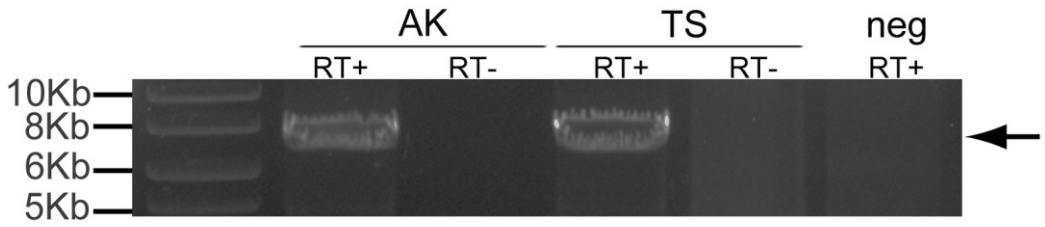

Figure 36. ABCA4 mRNA of the expected size is detected in HEK293 cells infected with dual AAV trans-splicing and hybrid AK vectors.
Amplification products of long-range PCR on cDNA of HEK293 cells infected with dual AAV trans-splicing (TS) and hybrid AK (AK) vectors or infected with vectors expressing EGFP (neg), as negative control. The arrow points at the full-length retrotranscribed *Abca4* mRNA (7 Kb). The molecular weight ladder is depicted on the left. RT+: sample from reverse transcription reaction made in the presence of the reverse transcriptase enzyme; RT-: sample from reverse transcription reaction made in the absence of the reverse transcriptase enzyme.

This data was also confirmed by the sequencing of the ABCA4 transcript region corresponding to the joining point between tail-to-head dual AAV vectors.

In addition no evident signs of retinal toxicity were observed in both C57BL/6 and *Abca4-/-* mice at 8 months after treatment with dual AAV TS and hybrid AK vectors by ERGs or conventional histological analysis, respectively (Fig. 37).

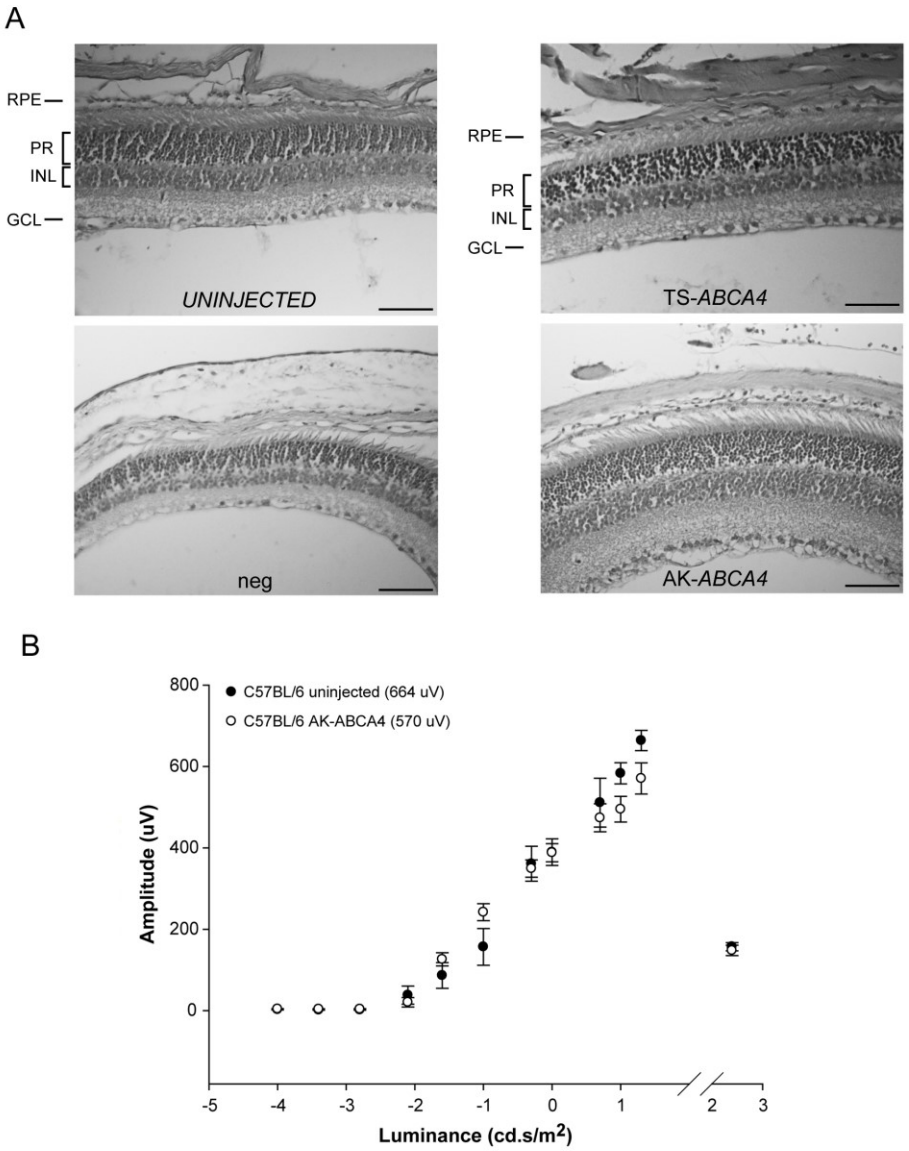

Figure 37. Normal retinal histology and function following subretinal delivery in mice of dual AAV trans-splicing and hybrid AK vectors

(A) Representative paraffin-embedded sections of *Abca4-/-* retinas either uninjected (n=2) or treated at one month of age with dual AAV2/8-RHO-ABCA4 trans-splicing (TS-*ABCA4,* n=3), dual AAV hybrid AK (AK-*ABCA4*, n=4) or single 5'-half (neg) of either dual AAV TS (n=1) or hybrid AK (n=2; neg total n=3). Eyes were harvested 8 months after treatment and retinal sections were stained with hematoxylin and eosin. The scale bar (50 μm) is depicted. RPE: retinal pigmented epithelium; PR: photoreceptors; INL: inner nuclear layer; GCL: ganglion cell layer. (B) Mean b-wave amplitude (μV) as a function of luminance in 9 months old C57BL/6 mice either uninjected or 8 months after subretinal injection of dual AAV hybrid AK vectors. The mean amplitude at 20 cd.s/m^2 is depicted. C57BL/6 uninjected: eyes from WT mice not injected (n=6); C57BL/6 AK-*ABCA4*: eyes from WT mice injected with dual AAV hybrid AK vectors (n=12). Values are represented as mean ± s.e.m (standard error of the mean). No statistically significant differences were found neither using ANOVA nor using Student's t-test on mean amplitudes at 20 cd.s/m^2 (p=0.13). More details on the statistical analysis including specific statistical values can be found in the Statistical analysis paragraph of the Materials and Methods section.

6. Subretinal delivery of dual AAV vectors improves the retinal phenotype of a mouse model of STGD.

To understand whether the levels of PR transduction obtained with the dual AAV TS and hybrid AK approaches may be therapeutically relevant, I investigated them in the retina of the mouse model of STGD.

As previously mentioned (see section 2.3.2), although the *Abca4-/-* mouse model does not undergo severe PR degeneration (Wu et al, 2010a), the absence of the ABCA4-encoded all-trans retinal transporter in PRs OS (Illing et al, 1997; Sun & Nathans, 1997) causes an accumulation of lipofuscin in PRs as well as in RPE, as result of PRs phagocytosis by RPE (Mata et al, 2001; Weng et al, 1999). As a consequence, both the number of lipofuscin granules in the RPE and the thickness of RPE cells are greater in *Abca4-/-* mice than in control mice (Allocca et al, 2008; Conley et al, 2012; Han et al, 2012; Ma et al, 2011; Radu et al, 2008). In addition, *Abca4-/-* mice also show delayed recovery from light desensitization (Allocca et al, 2008; Han et al, 2012; Maiti et al, 2006; Radu et al, 2008; Weng et al, 1999).

To evaluate the biological and therapeutic activity of the recombinant ABCA4 protein produced by dual AAV vectors, one month-old albino *Abca4-/-* mice were injected subretinally with the dual AAV TS and hybrid AK RHO-*ABCA4*-HA vectors (dose of each vector/eye: 1-3x10^9GC). Three months later, eyes were harvested and immuno-electron microscopy analysis with anti-hemagglutinin (HA) antibodies of retinal sections confirmed that immunogold particles were correctly localized in PRs OS only in animals that were injected with the combination of 5' and 3' dual AAV TS and hybrid AK vectors (Fig. 38).

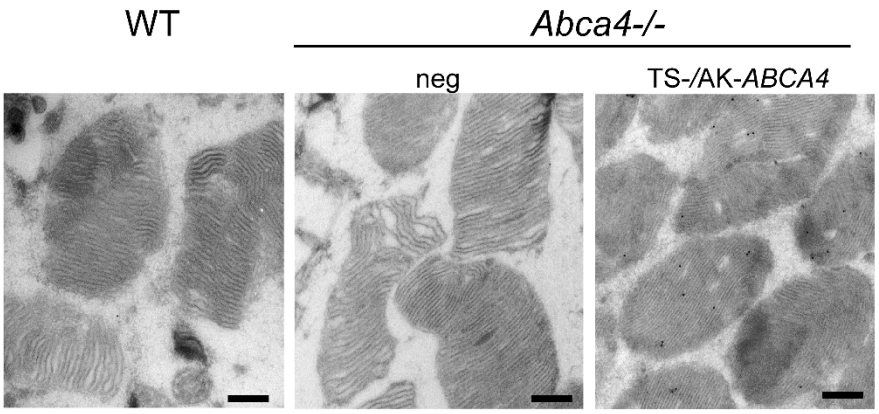

Figure 38. Subretinal administration of dual AAV vectors results in ABCA4 expression in *Abca4-/-* photoreceptors.
Representative pictures of transmission electron microscopy analysis with anti-HA antibody of retinal sections from wild-type BALB/c (WT) and *Abca4-/-* mice injected with dual AAV trans-splicing (TS-*ABCA4*) and hybrid AK vectors (AK-*ABCA4*) or with either AAV vectors expressing *EGFP* or 5'-or 3'-half of the dual hybrid AK vectors (neg), as negative controls. The black dots represent the immuno-gold labelling of the ABCA4-HA protein. The scale bar (200 nm) is depicted in the figure.

To assess the functionality of the ABCA4 protein expressed by the dual AAV vectors, I measured *Abca4*-/- retinal lipofuscin accumulation and recovery from light desensitization. To assess the former I performed transmission electron microscopy analysis to measure the number of RPE lipofuscin granules (Fig. 39) and RPE thickness (Fig. 40). Both were greater in the retina of *Abca4 -/-* mice injected with control vectors (independently of the size of the control constructs, Fig. 41) than in the retina of wild-type, age-matched BALB/c controls, and were significantly reduced or normalized in the eyes injected either with the therapeutic dual AAV TS or hybrid AK vectors (Fig. 39 and Fig. 40).

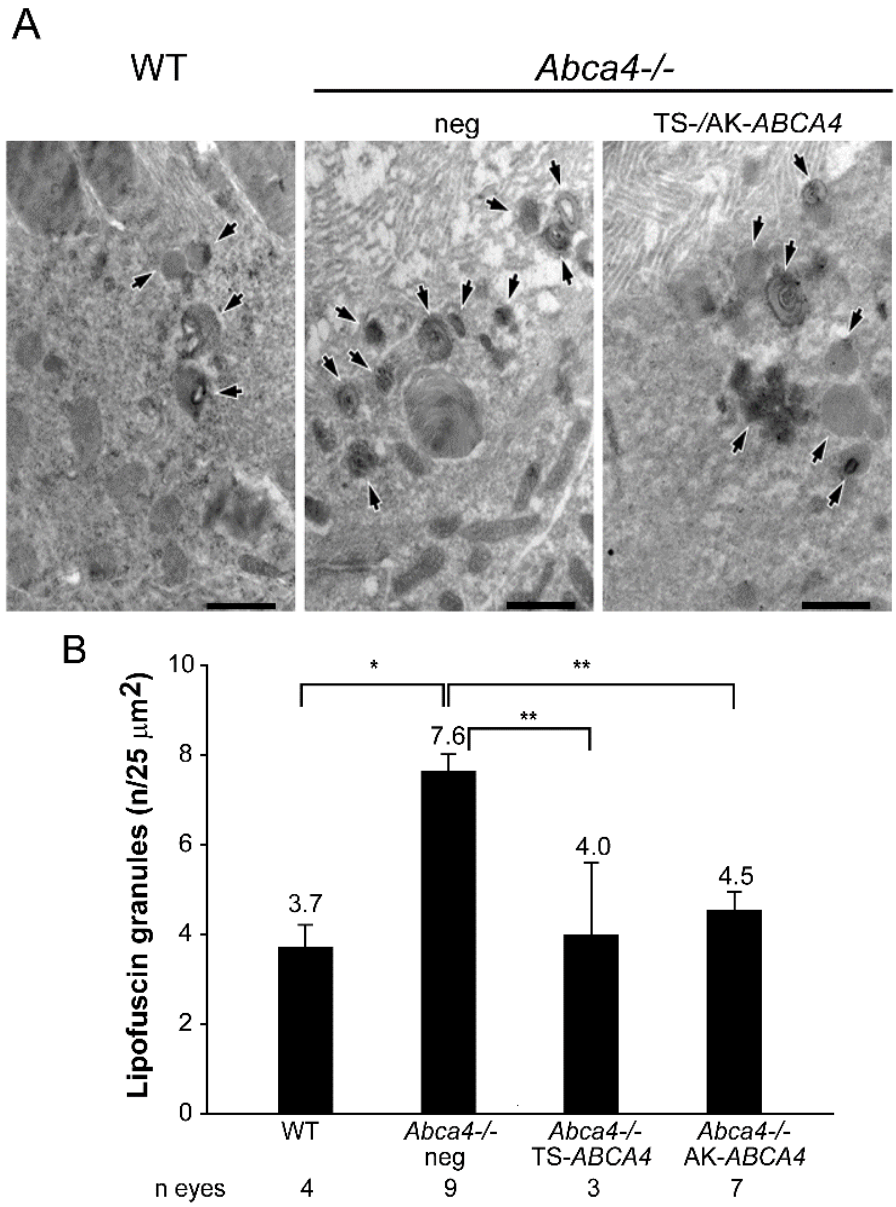

Figure 39. Subretinal administration of dual AAV vectors results in reduction of lipofuscin granule accumulation in *Abca4-/-* mice.

(A) Representative pictures of transmission electron microscopy analysis showing lipofuscin granules content in the RPE of WT and *Abca4*-/- mice injected with either dual AAV or negative control vectors. The black arrows indicate lipofuscin granules. The scale bar (1.6 μm) is depicted in the figure. (B) Quantification of the mean number of lipofuscin granules counted in at least 30 fields (25μm^2) for each sample. The number (n) of eyes analysed is depicted below each bar. The mean value is depicted above the corresponding bar. Values are represented as mean ± s.e.m. (standard error of the mean). *p ANOVA<0.05; **p ANOVA<0.001. WT: BALB/c eyes; *Abca4-/-* neg: *Abca4-/-* eyes injected with either AAV vectors expressing EGFP (n=2) or the 5'- (n=3) or 3'- (n=4) half of the dual AAV hybrid AK vectors, as negative controls (neg total n=9); *Abca4-/-* TS-*ABCA4*: mice injected with dual AAV TS vectors; *Abca4-/-* AK-*ABCA4*: mice injected with dual AAV hybrid AK vectors. More details on the statistical analysis including specific statistical values can be found in the Statistical analysis paragraph of the Materials and Methods section.

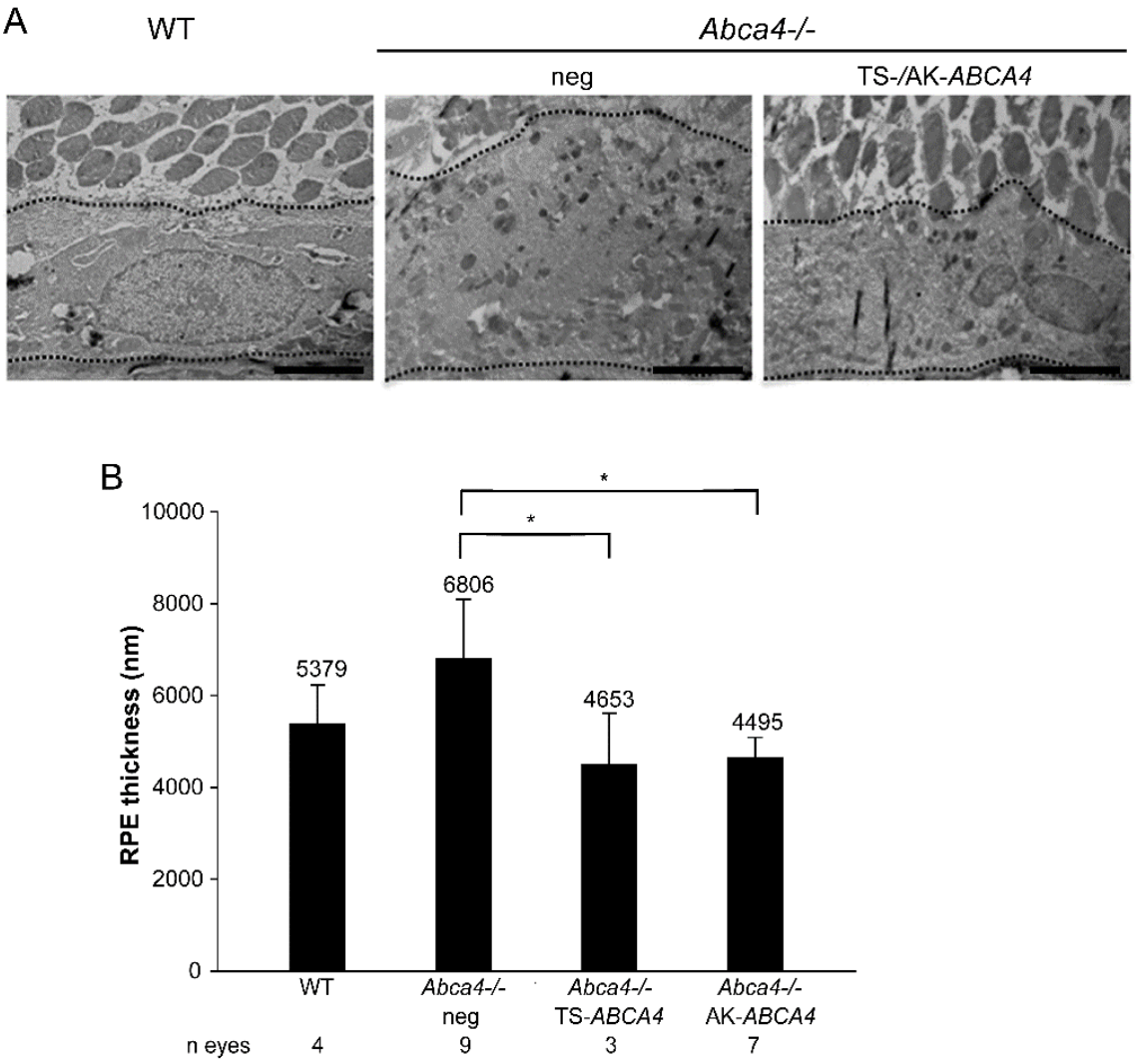

Figure 40. Subretinal injection of dual AAV vectors reduces the thickness of the RPE.

(A) Representative pictures of transmission electron microscopy analysis of retinal sections from wild-type BALB/c (WT) and *Abca4-/-* mice injected with dual AAV trans-splicing (TS-*ABCA4*) and hybrid AK vectors (AK-*ABCA4*) or with either AAV vectors expressing *EGFP* or 5'-or 3'-half of the dual hybrid AK vectors (neg), as negative controls. The dotted lines indicate the edges of RPE cells. The scale bar (3.8 μm) is depicted in the figure. (B) Quantification of the mean RPE thickness counted in at least 30 fields for each sample. The number (n) of eyes analysed is depicted below each bar. The mean value is depicted above the corresponding bar. Values are represented as mean ± s.e.m (standard error of the mean). *p ANOVA<0.05. *Abca4-/-* neg includes *Abca4-/-* mice injected with either AAV vectors expressing *EGFP* (n=2) or 5'- (n=3) or 3'- (n=4) half of the dual hybrid AK vectors (neg total n=9); *Abca4-/-* TS-*ABCA4*: mice injected with dual AAV TS vectors; *Abca4-/-* AK-*ABCA4*: mice injected with dual AAV hybrid AK vectors. More details on the statistical analysis including specific statistical values can be found in the Statistical analysis paragraph of the Materials and Methods section.

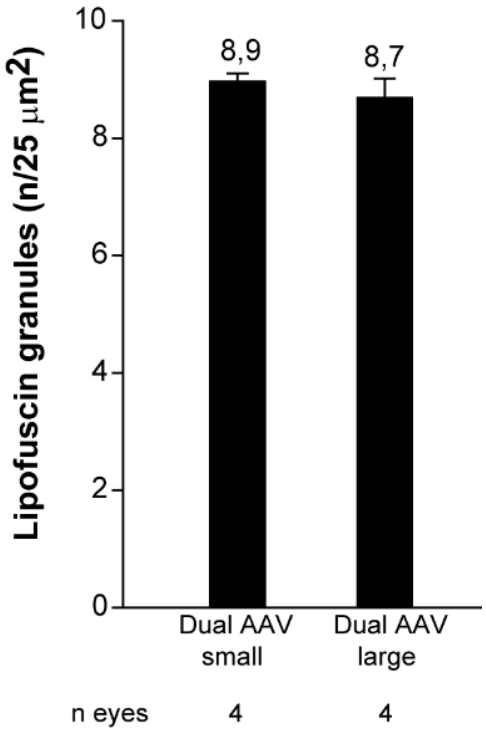

Figure 41. Similar lipofuscin granules accumulation in the retina of *Abca4-/-* mice independently of the AAV control vector genome size.
Quantification of lipofuscin granules in *Abca4-/-* mice injected subretinally with dual AAV trans-splicing and hybrid AK control vectors with a combined (5'-half+3'-half) large (8.9 Kb, dual AAV large) or small (2.7-2.9 Kb, dual AAV small) genome [dose of each vector/eye: $1.2x10^9$ genome copies (GC)]. Eyes were harvested 2 months post-injection and lipofuscin granules were counted in at least 30 fields (25 μm^2) for each sample. The number (n) of eyes analysed is depicted below each bar. Dual AAV small includes *Abca4-/-* eyes injected with either trans-splicing small (n=2) or hybrid AK small (n=2; total n=4) vectors; dual AAV large includes *Abca4-/-* eyes injected with either trans-splicing large (n=2) or hybrid AK large (n=2; total n=4) vectors. Values are represented as mean ± s.e.m. (standard error of the mean). No statistically significant differences were found using the Student's t-test (p=0.54).

Importantly, the eyes treated with dual AAV TS and hybrid AK vectors showed also improved recovery from light desensitization when compared to eyes treated with control vectors (dose of each vector/eye: $1.2x10^9$GC, Fig. 42), independently of the size of the control constructs [Student's t-test p value of dual AAV-EGFP-L (n=2 TS-L, n=4 AK-L; total n=6) vs dual AAV-EGFP (n=5 TS, n=4 AK; total n=9): 0.23)].

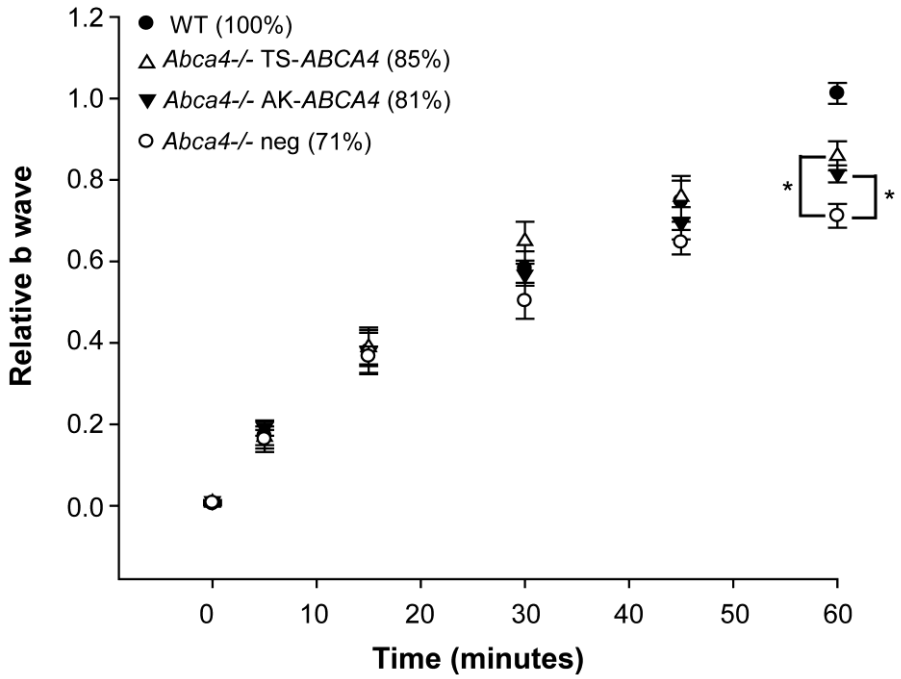

Figure 42. Subretinal injection of dual AAV vectors improves the recovery from light desensitization in *Abca4-/-* mice.
Recovery from light desensitization in 3 month-old *Abca4-/-* and BALB/c mice at 6 weeks post-injection. The relative b-wave is the ratio between the post- and the pre-desensitization b-wave amplitudes (μV) both evoked by 1 cd s/m^2. The time (minutes) refers to the time post-desensitization. The mean recovery (%) at 60 minutes is depicted. WT: BALB/c eyes (n=4); *Abca4-/-* TS-*ABCA4*: eyes injected with dual AAV TS vectors (n=5); *Abca4-/-* AK-*ABCA4*: mice injected with dual AAV hybrid AK vectors (n=5); *Abca4-/-* neg: *Abca4-/-* mice either not injected (n=2) or injected with the 5'-half of the dual AAV TS (n=3) or hybrid AK (n=2) vectors (neg total n=7). Values are represented as mean ± s.e.m (standard error of the mean). *p ANOVA<0.05. More details on the statistical analysis including specific statistical values can be found in the Statistical analysis paragraph of the Materials and Methods section.

DISCUSSION

While AAV-mediated gene therapy is effective in animal models and in patients with inherited blinding conditions (Bainbridge et al, 2008; Cideciyan et al, 2009a; Jacobson et al, 2006; Maguire et al, 2009; Maguire et al, 2008; Simonelli et al, 2010), its application to diseases affecting the retina and requiring a transfer of genes larger than 5 kb (referred to as large genes, such as ABCA4 for STGD), is inhibited by AAV limited cargo capacity. To overcome this, I compared *in vitro* and in mouse and pig retina the efficiency of various AAV-based strategies which have been recently developed for large gene transduction, including: AAV oversize (OZ), dual AAV overlapping (OV), trans-splicing (TS), hybrid AP and AK approaches.

The *in vitro* and *in vivo* results show that all the dual AAV strategies I tested (with the exception of the dual AAV hybrid AP) outperform AAV OZ vectors in terms of transduction levels. This may be explained by: i. the homogeneous size of the dual AAV genome population when compared to AAV OZ genomes, which may favour the generation of transcriptionally active large transgene expression cassettes; ii. the small volume of the subretinal space, which I show favours infection and transduction of the same cell by two independent AAV vectors. Although this has been suggested by previous work in the retina with either dual AAV TS vectors carrying the lacZ reporter gene (Reich et al, 2003) or with two single vectors encoding different fluorescent reporter proteins (Palfi et al, 2012), my study represents the first comprehensive comparison in the retina of the dual AAV strategies reported so far, as well as the first demonstration of their efficacy in animal models of common inherited blinding conditions.

Differently from what I have observed, Hirsch et al. have recently shown that AAV OZ vectors can reconstitute a large reporter gene (6.2 kb) in the retina of mice more efficiently than dual AAV TS vectors (Hirsch et al, 2013b). The following factors may account for this: i. the design of the dual AAV vectors, which may result in lower transduction levels in Hirsch et al. than in my case; ii. the purification of the AAV OZ vectors by Hirsch et al. that may promote the selection in the viral preparation of genomes with higher transduction properties; iii. the use of a shorter transgene by Hirsch et al. than by me that gives rise to genomes with longer overlaps which can positively influence AAV OZ transduction. My results also differ from those of another group that has reported that dual AAV hybrid AP outperforms TS (Ghosh et al, 2011). While I have generated the dual hybrid AP vectors based on the description provided in those publications, it is possible that minor differences in the AP sequences used may account for the different transduction levels I have observed.

The dual AAV OV approach is particularly interesting when compared to the TS or hybrid AK approaches, which appear similarly efficient *in vitro*, as dual AAV OV vectors only contain sequences belonging to the therapeutic transgene expression cassette. However, when I administered dual AAV OV vectors to the subretinal space of adult mice and pigs, I could detect expression of the large ABCA4 protein only when the ubiquitous or the RPE-specific promoters, but not the PR-specific promoters, were used. This may suggest that the homologous recombination required for dual AAV OV reconstitution is more efficient in RPE than PRs. This is consistent with the low levels of homologous recombination reported in post-mitotic neurons (Fishel et al, 2007) and may partially explain the results recently reported by Lopes and co-workers (Lopes et al, 2013), who have found dual AAV OV vectors poorly efficient in the delivery to the retina of the large gene MYO7A (see Table 2). In conclusion, subretinal administration

of dual AAV OV vectors should not be used for large gene transfer to PRs, although it is not possible to exclude that sequences that are more recombinogenic than those included in dual AAV OV *ABCA4* vectors I used may allow efficient homologous recombination in PRs.

Dual AAV TS and hybrid AK approaches efficiently transduce mouse and pig PRs, differently from what I observed with dual AAV OV. This is consistent with the knowledge that the mechanism of large gene reconstitution mediated by dual AAV TS and hybrid AK approaches may be via ITR-mediated head-to-tail rejoining (Duan et al, 1998; Ghosh et al, 2008; Yan et al, 2005) rather than homologous recombination. The transduction levels provided by the dual hybrid AK are more consistent than those of the TS approach in mouse and pig PRs. This was evident when using the large *ABCA4* but not the small *EGFP* transgene, suggesting an advantage of including the AK sequence for large transgene reconstitution in PRs.

The levels of mouse PRs transduction I achieved with dual AAV TS and hybrid AK are lower than with single NS vectors. However, these levels may be effective for treating inherited blinding conditions that require relatively low levels of transgene expression, i.e. diseases inherited as autosomal recessive. Indeed, I show that subretinal delivery of dual AAV TS and hybrid AK improves and even normalizes the retinal defects of the animal models of STGD, which is due to mutations in the large *ABCA4* gene and is an attractive target for gene therapy. Importantly, both levels and consistency of dual AAV-mediated large transgene expression could be improved by directing the productive head-to-tail genome concatemerization by either using heterologous ITRs (Yan et al, 2007) or by adding oligos to the injection solution (Hirsch et al, 2009).

Single normal size AAV vectors ensure multi-year retinal gene expression after a single vector administration (Testa et al, 2013). The data I have obtained so far from dual AAV vectors up to 4 months after retinal gene delivery, the last time point of my analysis, suggest that longevity of transgene expression may be similar between single normal size and dual AAV vectors.

The genome size of dual AAV vectors is homogeneous, which means identity and safety issues related to their use should be less considerable than those related to AAV OZ vectors, which have heterogeneous genome sizes. However, the possibility that delivery of dual AAV vectors results in the production of aberrant proteins in the retina, i.e. truncated proteins from the 5'-half vector that contains the promoter sequence and/or from the 3'-half vector due to the low promoter activity of the ITRs (Flotte et al, 1993) must be considered. The results I obtained show that proteins smaller than the full-length are produced from the 5'- and 3'-halves of dual AAV vectors *in vitro* but not *in vivo* in the retina where only full-length ABCA4 protein is detected. The production of properly spliced full length protein by dual AAV vectors is corroborated by the successful amplification of the full size *ABCA4* mRNA retro transcribed from cells infected with dual AAV TS and hybrid AK vectors. Indeed the transcript sequences confirmed that intermolecular AAV joining and splicing occurred correctly, as expected by the size of the full length proteins detected by Western blot. In addition, I detected neither ERG nor retinal histological abnormalities in both C57/BL6 and *Abca4-/-* mice that I followed up to 8 months after dual AAV vector delivery. Future long-term safety studies as well as sensitive proteomic profiling will help to better define if any toxicity derives from intraocular administration of dual AAV vectors.

CONCLUSIONS

During my Ph.D. thesis I focused my efforts on the identification of AAV-based strategies for delivery of large genes to the retina and on providing proof of principle of their efficacy in animal models of IRDs. In my study, I demonstrated that dual AAV vectors are efficient tools for large gene delivery, both *in vitro* and to the mouse and pig retina. This doubles the size of the therapeutic transcription cassette that dual AAV vectors allow to transfer when compared to a single AAV of normal size. Dual AAV OV vectors, however, efficiently transduce RPE but not PRs, and this limits the applicability of this strategy to those inherited disease that are due to mutations in genes expressed in PRs. In contrast, dual AAV TS and hybrid AK approaches drive efficient large gene reconstitution in both RPE and PRs, in mouse and pig. Importantly, although the levels of transgene expression achieved with dual AAV vectors are lower than those achieved with a single normal size AAV, they result in significant improvement of the retinal phenotype of the mouse model of STGD. These results provide evidence of the efficacy of these strategies for gene therapy for STGD and other blinding conditions, which require large gene transfer to PRs as well as RPE.

REFERENCES

Abramoff MD, Garvin MK, Sonka M (2010) Retinal Imaging and Image Analysis. *IEEE transactions on medical imaging* **3:** 169-208

Acland GM, Aguirre GD, Bennett J, Aleman TS, Cideciyan AV, Bennicelli J, Dejneka NS, Pearce-Kelling SE, Maguire AM, Palczewski K, Hauswirth WW, Jacobson SG (2005) Long-term restoration of rod and cone vision by single dose rAAV-mediated gene transfer to the retina in a canine model of childhood blindness. *Molecular therapy : the journal of the American Society of Gene Therapy* **12:** 1072-1082

Acland GM, Aguirre GD, Ray J, Zhang Q, Aleman TS, Cideciyan AV, Pearce-Kelling SE, Anand V, Zeng Y, Maguire AM, Jacobson SG, Hauswirth WW, Bennett J (2001) Gene therapy restores vision in a canine model of childhood blindness. *Nature genetics* **28:** 92-95

Ahnelt PK (1998) The photoreceptor mosaic. *Eye* **12 (Pt 3b):** 531-540

Akache B, Grimm D, Pandey K, Yant SR, Xu H, Kay MA (2006) The 37/67-kilodalton laminin receptor is a receptor for adeno-associated virus serotypes 8, 2, 3, and 9. *Journal of virology* **80:** 9831-9836

Ali RR, Reichel MB, Thrasher AJ, Levinsky RJ, Kinnon C, Kanuga N, Hunt DM, Bhattacharya SS (1996) Gene transfer into the mouse retina mediated by an adeno-associated viral vector. *Human molecular genetics* **5:** 591-594

Allikmets R (2007) *Stargardt disease: from gene discovery to therapy*, Totowa, NJ: Humana Press.

Allikmets R, Singh N, Sun H, Shroyer NF, Hutchinson A, Chidambaram A, Gerrard B, Baird L, Stauffer D, Peiffer A, Rattner A, Smallwood P, Li Y, Anderson KL, Lewis RA, Nathans J, Leppert M, Dean M, Lupski JR (1997) A photoreceptor cell-specific ATP-binding transporter gene (ABCR) is mutated in recessive Stargardt macular dystrophy. *Nature genetics* **15:** 236-246

Allocca M, Doria M, Petrillo M, Colella P, Garcia-Hoyos M, Gibbs D, Kim SR, Maguire A, Rex TS, Di Vicino U, Cutillo L, Sparrow JR, Williams DS, Bennett J, Auricchio A (2008) Serotype-dependent packaging of large genes in adeno-associated viral vectors results in effective gene delivery in mice. *The Journal of clinical investigation* **118:** 1955-1964

Allocca M, Manfredi A, Iodice C, Di Vicino U, Auricchio A (2011) AAV-mediated gene replacement, either alone or in combination with physical and pharmacological agents, results in partial and transient protection from photoreceptor degeneration

associated with betaPDE deficiency. *Investigative ophthalmology & visual science* **52:** 5713-5719

Allocca M, Mussolino C, Garcia-Hoyos M, Sanges D, Iodice C, Petrillo M, Vandenberghe LH, Wilson JM, Marigo V, Surace EM, Auricchio A (2007) Novel adeno-associated virus serotypes efficiently transduce murine photoreceptors. *Journal of virology* **81:** 11372-11380

Allocca M, Tessitore A, Cotugno G, Auricchio A (2006) AAV-mediated gene transfer for retinal diseases. *Expert Opin Biol Ther* **6:** 1279-1294

Anderson KL, Baird L, Lewis RA, Chinault AC, Otterud B, Leppert M, Lupski JR (1995) A YAC contig encompassing the recessive Stargardt disease gene (STGD) on chromosome 1p. *American journal of human genetics* **57:** 1351-1363

Anderson RE, Maude MB (1970) Phospholipids of bovine outer segments. *Biochemistry* **9:** 3624-3628

Andrieu-Soler C, Bejjani RA, de Bizemont T, Normand N, BenEzra D, Behar-Cohen F (2006) Ocular gene therapy: a review of nonviral strategies. *Mol Vis* **12:** 1334-1347

Auricchio A (2003) Pseudotyped AAV vectors for constitutive and regulated gene expression in the eye. *Vision research* **43:** 913-918

Auricchio A, Hildinger M, O'Connor E, Gao GP, Wilson JM (2001a) Isolation of highly infectious and pure adeno-associated virus type 2 vectors with a single-step gravity-flow column. *Human gene therapy* **12:** 71-76

Auricchio A, Kobinger G, Anand V, Hildinger M, O'Connor E, Maguire AM, Wilson JM, Bennett J (2001b) Exchange of surface proteins impacts on viral vector cellular specificity and transduction characteristics: the retina as a model. *Human molecular genetics* **10:** 3075-3081

Azarian SM, Megarity CF, Weng J, Horvath DH, Travis GH (1998) The human photoreceptor rim protein gene (ABCR): genomic structure and primer set information for mutation analysis. *Human genetics* **102:** 699-705

Azarian SM, Travis GH (1997) The photoreceptor rim protein is an ABC transporter encoded by the gene for recessive Stargardt's disease (ABCR). *FEBS letters* **409:** 247-252

Bainbridge JW, Smith AJ, Barker SS, Robbie S, Henderson R, Balaggan K, Viswanathan A, Holder GE, Stockman A, Tyler N, Petersen-Jones S, Bhattacharya SS, Thrasher AJ, Fitzke FW, Carter BJ, Rubin GS, Moore AT, Ali RR (2008) Effect of gene

therapy on visual function in Leber's congenital amaurosis. *The New England journal of medicine* **358:** 2231-2239

Bainbridge JW, Tan MH, Ali RR (2006) Gene therapy progress and prospects: the eye. *Gene therapy* **13:** 1191-1197

Ben-Shabat S, Parish CA, Vollmer HR, Itagaki Y, Fishkin N, Nakanishi K, Sparrow JR (2002) Biosynthetic studies of A2E, a major fluorophore of retinal pigment epithelial lipofuscin. *The Journal of biological chemistry* **277:** 7183-7190

Bennett J, Tanabe T, Sun D, Zeng Y, Kjeldbye H, Gouras P, Maguire AM (1996) Photoreceptor cell rescue in retinal degeneration (rd) mice by in vivo gene therapy. *Nature medicine* **2:** 649-654

Berns KI, Giraud C (1996) Biology of adeno-associated virus. *Current topics in microbiology and immunology* **218:** 1-23

Blanks JC (2001) *Morphology and Topography of the retina*, St. Louis: Mosby.

Campbell RE, Tour O, Palmer AE, Steinbach PA, Baird GS, Zacharias DA, Tsien RY (2002) A monomeric red fluorescent protein. *Proc Natl Acad Sci U S A* **99:** 7877-7882

Cideciyan AV, Hauswirth WW, Aleman TS, Kaushal S, Schwartz SB, Boye SL, Windsor EA, Conlon TJ, Sumaroka A, Roman AJ, Byrne BJ, Jacobson SG (2009a) Vision 1 year after gene therapy for Leber's congenital amaurosis. *The New England journal of medicine* **361:** 725-727

Cideciyan AV, Swider M, Aleman TS, Tsybovsky Y, Schwartz SB, Windsor EA, Roman AJ, Sumaroka A, Steinberg JD, Jacobson SG, Stone EM, Palczewski K (2009b) ABCA4 disease progression and a proposed strategy for gene therapy. *Human molecular genetics* **18:** 931-941

Colella P, Cotugno G, Auricchio A (2009) Ocular gene therapy: current progress and future prospects. *Trends Mol Med* **15:** 23-31

Conley SM, Cai X, Makkia R, Wu Y, Sparrow JR, Naash MI (2012) Increased cone sensitivity to ABCA4 deficiency provides insight into macular vision loss in Stargardt's dystrophy. *Biochimica et biophysica acta* **1822:** 1169-1179

Dalkara D, Byrne LC, Klimczak RR, Visel M, Yin L, Merigan WH, Flannery JG, Schaffer DV (2013) In vivo-directed evolution of a new adeno-associated virus for therapeutic outer retinal gene delivery from the vitreous. *Science translational medicine* **5:** 189ra176

Dalkara D, Kolstad KD, Caporale N, Visel M, Klimczak RR, Schaffer DV, Flannery JG (2009) Inner limiting membrane barriers to AAV-mediated retinal transduction from the vitreous. *Molecular therapy : the journal of the American Society of Gene Therapy* **17:** 2096-2102

Daya S, Berns KI (2008) Gene therapy using adeno-associated virus vectors. *Clinical microbiology reviews* **21:** 583-593

Dean M (2003) Approaches to identify genes for complex human diseases: lessons from Mendelian disorders. *Human mutation* **22:** 261-274

Dean M, Allikmets R (2001) Complete characterization of the human ABC gene family. *Journal of bioenergetics and biomembranes* **33:** 475-479

Dean M, Annilo T (2005) Evolution of the ATP-binding cassette (ABC) transporter superfamily in vertebrates. *Annual review of genomics and human genetics* **6:** 123-142

Dejneka NS, Surace EM, Aleman TS, Cideciyan AV, Lyubarsky A, Savchenko A, Redmond TM, Tang W, Wei Z, Rex TS, Glover E, Maguire AM, Pugh EN, Jr., Jacobson SG, Bennett J (2004) In utero gene therapy rescues vision in a murine model of congenital blindness. *Molecular therapy : the journal of the American Society of Gene Therapy* **9:** 182-188

Delori FC, Staurenghi G, Arend O, Dorey CK, Goger DG, Weiter JJ (1995) In vivo measurement of lipofuscin in Stargardt's disease--Fundus flavimaculatus. *Investigative ophthalmology & visual science* **36:** 2327-2331

Di Pasquale G, Davidson BL, Stein CS, Martins I, Scudiero D, Monks A, Chiorini JA (2003) Identification of PDGFR as a receptor for AAV-5 transduction. *Nature medicine* **9:** 1306-1312

Dinculescu A, Glushakova L, Min SH, Hauswirth WW (2005) Adeno-associated virus-vectored gene therapy for retinal disease. *Human gene therapy* **16:** 649-663

Dong B, Nakai H, Xiao W (2010a) Characterization of genome integrity for oversized recombinant AAV vector. *Molecular therapy : the journal of the American Society of Gene Therapy* **18:** 87-92

Dong X, Tian W, Wang G, Dong Z, Shen W, Zheng G, Wu X, Xue J, Wang Y, Chen J (2010b) Establishment of an AAV reverse infection-based array. *PloS one* **5:** e13479

Drittanti L, Rivet C, Manceau P, Danos O, Vega M (2000) High throughput production, screening and analysis of adeno-associated viral vectors. *Gene therapy* **7:** 924-929

Dryja T (2001) Retinitis Pigmentosa and stationary night blindness. In *The Online Metabolic & Molecular Bases of Inherited Diseases* Scriver C, Beaudet A, Sly W, Valle D (eds), Vol.

Vol IV Eigth edn, pp 5903-5933. New York, NY: McGraw-Hill

Duan D, Sharma P, Yang J, Yue Y, Dudus L, Zhang Y, Fisher KJ, Engelhardt JF (1998) Circular intermediates of recombinant adeno-associated virus have defined structural characteristics responsible for long-term episomal persistence in muscle tissue. *Journal of virology* **72:** 8568-8577

Duan D, Yue Y, Engelhardt JF (2001) Expanding AAV packaging capacity with trans-splicing or overlapping vectors: a quantitative comparison. *Molecular therapy : the journal of the American Society of Gene Therapy* **4:** 383-391

Eldred GE, Lasky MR (1993) Retinal age pigments generated by self-assembling lysosomotropic detergents. *Nature* **361:** 724-726

Esumi N, Oshima Y, Li Y, Campochiaro PA, Zack DJ (2004) Analysis of the VMD2 promoter and implication of E-box binding factors in its regulation. *The Journal of biological chemistry* **279:** 19064-19073

Finnemann SC, Leung LW, Rodriguez-Boulan E (2002) The lipofuscin component A2E selectively inhibits phagolysosomal degradation of photoreceptor phospholipid by the retinal pigment epithelium. *Proceedings of the National Academy of Sciences of the United States of America* **99:** 3842-3847

Fishel ML, Vasko MR, Kelley MR (2007) DNA repair in neurons: so if they don't divide what's to repair? *Mutation research* **614:** 24-36

Fishman GA, Farbman JS, Alexander KR (1991) Delayed rod dark adaptation in patients with Stargardt's disease. *Ophthalmology* **98:** 957-962

Fishman GA, Stone EM, Grover S, Derlacki DJ, Haines HL, Hockey RR (1999) Variation of clinical expression in patients with Stargardt dystrophy and sequence variations in the ABCR gene. *Archives of ophthalmology* **117:** 504-510

Flannery JG (2001) *Structure and functions of rod photoreceptors*, St.Louis: Mosby.

Flotte TR, Afione SA, Solow R, Drumm ML, Markakis D, Guggino WB, Zeitlin PL, Carter BJ (1993) Expression of the cystic fibrosis transmembrane conductance regulator from a novel adeno-associated virus promoter. *The Journal of biological chemistry* **268:** 3781-3790

Fu Y (1995) Phototransduction in Rods and Cones. In *Webvision: The Organization of the Retina and Visual System*, Kolb H, Fernandez E, Nelson R (eds). Salt Lake City (UT)

Fujinami K, Sergouniotis PI, Davidson AE, Wright G, Chana RK, Tsunoda K, Tsubota K, Egan CA, Robson AG, Moore AT, Holder GE, Michaelides M, Webster AR (2013) Clinical and molecular analysis of Stargardt disease with preserved foveal structure and function. *American journal of ophthalmology* **156:** 487-501 e481

Fumagalli A, Ferrari M, Soriani N, Gessi A, Foglieni B, Martina E, Manitto MP, Brancato R, Dean M, Allikmets R, Cremonesi L (2001) Mutational scanning of the ABCR gene with double-gradient denaturing-gradient gel electrophoresis (DG-DGGE) in Italian Stargardt disease patients. *Human genetics* **109:** 326-338

Gao G, Qu G, Burnham MS, Huang J, Chirmule N, Joshi B, Yu QC, Marsh JA, Conceicao CM, Wilson JM (2000) Purification of recombinant adeno-associated virus vectors by column chromatography and its performance in vivo. *Human gene therapy* **11:** 2079-2091

Gargiulo A, Bonetti C, Montefusco S, Neglia S, Di Vicino U, Marrocco E, Corte MD, Domenici L, Auricchio A, Surace EM (2009) AAV-mediated tyrosinase gene transfer restores melanogenesis and retinal function in a model of oculo-cutaneous albinism type I (OCA1). *Molecular therapy : the journal of the American Society of Gene Therapy* **17:** 1347-1354

Genead MA, Fishman GA, Stone EM, Allikmets R (2009) The natural history of stargardt disease with specific sequence mutation in the ABCA4 gene. *Investigative ophthalmology & visual science* **50:** 5867-5871

Ghosh A, Yue Y, Duan D (2006) Viral serotype and the transgene sequence influence overlapping adeno-associated viral (AAV) vector-mediated gene transfer in skeletal muscle. *The journal of gene medicine* **8:** 298-305

Ghosh A, Yue Y, Duan D (2011) Efficient transgene reconstitution with hybrid dual AAV vectors carrying the minimized bridging sequences. *Human gene therapy* **22:** 77-83

Ghosh A, Yue Y, Lai Y, Duan D (2008) A hybrid vector system expands adeno-associated viral vector packaging capacity in a transgene-independent manner. *Molecular therapy : the journal of the American Society of Gene Therapy* **16:** 124-130

Gomes NL, Greenstein VC, Carlson JN, Tsang SH, Smith RT, Carr RE, Hood DC, Chang S (2009) A comparison of fundus autofluorescence and retinal structure in patients with Stargardt disease. *Investigative ophthalmology & visual science* **50:** 3953-3959

Grieger JC, Samulski RJ (2005) Packaging capacity of adeno-associated virus serotypes: impact of larger genomes on infectivity and postentry steps. *Journal of virology* **79:** 9933-9944

Grose WE, Clark KR, Griffin D, Malik V, Shontz KM, Montgomery CL, Lewis S, Brown RH, Jr., Janssen PM, Mendell JR, Rodino-Klapac LR (2012) Homologous Recombination Mediates Functional Recovery of Dysferlin Deficiency following AAV5 Gene Transfer. *PloS one* **7:** e39233

Han Z, Conley SM, Makkia RS, Cooper MJ, Naash MI (2012) DNA nanoparticle-mediated ABCA4 delivery rescues Stargardt dystrophy in mice. *The Journal of clinical investigation* **122:** 3221-3226

Hauswirth WW, Aleman TS, Kaushal S, Cideciyan AV, Schwartz SB, Wang L, Conlon TJ, Boye SL, Flotte TR, Byrne BJ, Jacobson SG (2008) Treatment of leber congenital amaurosis due to RPE65 mutations by ocular subretinal injection of adeno-associated virus gene vector: short-term results of a phase I trial. *Human gene therapy* **19:** 979-990

Hellstrom M, Ruitenberg MJ, Pollett MA, Ehlert EM, Twisk J, Verhaagen J, Harvey AR (2009) Cellular tropism and transduction properties of seven adeno-associated viral vector serotypes in adult retina after intravitreal injection. *Gene therapy* **16:** 521-532

Hinton DR (2001) *Cell biology of the retina pigment epithelium*, St. Louis: Mosby.

Hirsch ML, Agbandje-McKenna M, Samulski RJ (2010) Little vector, big gene transduction: fragmented genome reassembly of adeno-associated virus. *Molecular therapy : the journal of the American Society of Gene Therapy* **18:** 6-8

Hirsch ML, Li C, Bellon I, Yin C, Chavala S, Pryadkina M, Richard I, Samulski RJ (2013a) Oversized AAV Transductifon Is Mediated via a DNA-PKcs-independent, Rad51C-dependent Repair Pathway. *Molecular therapy : the journal of the American Society of Gene Therapy*

Hirsch ML, Li C, Bellon I, Yin C, Chavala S, Pryadkina M, Richard I, Samulski RJ (2013b) Oversized AAV Transduction is Mediated via a DNA-PKcs Independent, Rad51C-dependent Repair Pathway. *Mol Ther*

Hirsch ML, Storici F, Li C, Choi VW, Samulski RJ (2009) AAV recombineering with single strand oligonucleotides. *PLoS One* **4:** e7705

Holz FG, Schutt F, Kopitz J, Eldred GE, Kruse FE, Volcker HE, Cantz M (1999) Inhibition of lysosomal degradative functions in RPE cells by a retinoid component of lipofuscin. *Investigative ophthalmology & visual science* **40:** 737-743

Illing M, Molday LL, Molday RS (1997) The 220-kDa rim protein of retinal rod outer segments is a member of the ABC transporter superfamily. *The Journal of biological chemistry* **272:** 10303-10310

Jacobson SG, Acland GM, Aguirre GD, Aleman TS, Schwartz SB, Cideciyan AV, Zeiss CJ, Komaromy AM, Kaushal S, Roman AJ, Windsor EA, Sumaroka A, Pearce-Kelling SE, Conlon TJ, Chiodo VA, Boye SL, Flotte TR, Maguire AM, Bennett J, Hauswirth WW (2006) Safety of recombinant adeno-associated virus type 2-RPE65 vector delivered by ocular subretinal injection. *Molecular therapy : the journal of the American Society of Gene Therapy* **13:** 1074-1084

Kaludov N, Handelman B, Chiorini JA (2002) Scalable purification of adeno-associated virus type 2, 4, or 5 using ion-exchange chromatography. *Human gene therapy* **13:** 1235-1243

Kaminski WE, Piehler A, Wenzel JJ (2006) ABC A-subfamily transporters: structure, function and disease. *Biochimica et biophysica acta* **1762:** 510-524

Kashiwakura Y, Tamayose K, Iwabuchi K, Hirai Y, Shimada T, Matsumoto K, Nakamura T, Watanabe M, Oshimi K, Daida H (2005) Hepatocyte growth factor receptor is a coreceptor for adeno-associated virus type 2 infection. *Journal of virology* **79:** 609-614

Kim SR, Jang YP, Jockusch S, Fishkin NE, Turro NJ, Sparrow JR (2007) The all-trans-retinal dimer series of lipofuscin pigments in retinal pigment epithelial cells in a recessive Stargardt disease model. *Proceedings of the National Academy of Sciences of the United States of America* **104:** 19273-19278

Kniazeva M, Chiang MF, Morgan B, Anduze AL, Zack DJ, Han M, Zhang K (1999) A new locus for autosomal dominant stargardt-like disease maps to chromosome 4. *American journal of human genetics* **64:** 1394-1399

Kumar-Singh R (2008) Barriers for retinal gene therapy: separating fact from fiction. *Vision research* **48:** 1671-1680

Lai Y, Yue Y, Duan D (2010) Evidence for the failure of adeno-associated virus serotype 5 to package a viral genome > or = 8.2 kb. *Molecular therapy : the journal of the American Society of Gene Therapy* **18:** 75-79

Lai Y, Yue Y, Liu M, Ghosh A, Engelhardt JF, Chamberlain JS, Duan D (2005) Efficient in vivo gene expression by trans-splicing adeno-associated viral vectors. *Nat Biotechnol* **23:** 1435-1439

Lakkaraju A, Finnemann SC, Rodriguez-Boulan E (2007) The lipofuscin fluorophore A2E perturbs cholesterol metabolism in retinal pigment epithelial cells. *Proceedings of the National Academy of Sciences of the United States of America* **104:** 11026-11031

Le Meur G, Stieger K, Smith AJ, Weber M, Deschamps JY, Nivard D, Mendes-Madeira A, Provost N, Pereon Y, Cherel Y, Ali RR, Hamel C, Moullier P, Rolling F (2007) Restoration of vision in RPE65-deficient Briard dogs using an AAV serotype 4 vector that specifically targets the retinal pigmented epithelium. *Gene therapy* **14:** 292-303

Lebherz C, Maguire A, Tang W, Bennett J, Wilson JM (2008) Novel AAV serotypes for improved ocular gene transfer. *The journal of gene medicine* **10:** 375-382

Lewis RA, Shroyer NF, Singh N, Allikmets R, Hutchinson A, Li Y, Lupski JR, Leppert M, Dean M (1999) Genotype/Phenotype analysis of a photoreceptor-specific ATP-binding cassette transporter gene, ABCR, in Stargardt disease. *American journal of human genetics* **64:** 422-434

Liang FQ, Anand,V., Maguire,A.M., Bennett,J. (2000) *Intraocular delivery of recombinant virus*, Vol. 47: Humana Press Inc, Totowa, NJ.

.

Lipinski DM, Thake M, MacLaren RE (2013) Clinical applications of retinal gene therapy. *Prog Retin Eye Res* **32:** 22-47

Lois N, Holder GE, Bunce C, Fitzke FW, Bird AC (2001) Phenotypic subtypes of Stargardt macular dystrophy-fundus flavimaculatus. *Archives of ophthalmology* **119:** 359-369

Lopes VS, Boye SE, Louie CM, Boye S, Dyka F, Chiodo V, Fofo H, Hauswirth WW, Williams DS (2013) Retinal gene therapy with a large MYO7A cDNA using adeno-associated virus. *Gene therapy*

Lotery AJ, Yang GS, Mullins RF, Russell SR, Schmidt M, Stone EM, Lindbloom JD, Chiorini JA, Kotin RM, Davidson BL (2003) Adeno-associated virus type 5: transduction efficiency and cell-type specificity in the primate retina. *Human gene therapy* **14:** 1663-1671

Ma L, Kaufman Y, Zhang J, Washington I (2011) C20-D3-vitamin A slows lipofuscin accumulation and electrophysiological retinal degeneration in a mouse model of Stargardt disease. *The Journal of biological chemistry* **286:** 7966-7974

Maguire AM, High KA, Auricchio A, Wright JF, Pierce EA, Testa F, Mingozzi F, Bennicelli JL, Ying GS, Rossi S, Fulton A, Marshall KA, Banfi S, Chung DC, Morgan JI, Hauck B, Zelenaia O, Zhu X, Raffini L, Coppieters F, De Baere E, Shindler KS, Volpe NJ, Surace EM, Acerra C, Lyubarsky A, Redmond TM, Stone E, Sun J,

McDonnell JW, Leroy BP, Simonelli F, Bennett J (2009) Age-dependent effects of RPE65 gene therapy for Leber's congenital amaurosis: a phase 1 dose-escalation trial. *Lancet* **374:** 1597-1605

Maguire AM, Simonelli F, Pierce EA, Pugh EN, Jr., Mingozzi F, Bennicelli J, Banfi S, Marshall KA, Testa F, Surace EM, Rossi S, Lyubarsky A, Arruda VR, Konkle B, Stone E, Sun J, Jacobs J, Dell'Osso L, Hertle R, Ma JX, Redmond TM, Zhu X, Hauck B, Zelenaia O, Shindler KS, Maguire MG, Wright JF, Volpe NJ, McDonnell JW, Auricchio A, High KA, Bennett J (2008) Safety and efficacy of gene transfer for Leber's congenital amaurosis. *The New England journal of medicine* **358:** 2240-2248

Maiti P, Kong J, Kim SR, Sparrow JR, Allikmets R, Rando RR (2006) Small molecule RPE65 antagonists limit the visual cycle and prevent lipofuscin formation. *Biochemistry* **45:** 852-860

Mata NL, Tzekov RT, Liu X, Weng J, Birch DG, Travis GH (2001) Delayed dark-adaptation and lipofuscin accumulation in abcr+/- mice: implications for involvement of ABCR in age-related macular degeneration. *Investigative ophthalmology & visual science* **42:** 1685-1690

Mata NL, Weng J, Travis GH (2000) Biosynthesis of a major lipofuscin fluorophore in mice and humans with ABCR-mediated retinal and macular degeneration. *Proceedings of the National Academy of Sciences of the United States of America* **97:** 7154-7159

Maugeri A, van Driel MA, van de Pol DJ, Klevering BJ, van Haren FJ, Tijmes N, Bergen AA, Rohrschneider K, Blankenagel A, Pinckers AJ, Dahl N, Brunner HG, Deutman AF, Hoyng CB, Cremers FP (1999) The 2588G-->C mutation in the ABCR gene is a mild frequent founder mutation in the Western European population and allows the classification of ABCR mutations in patients with Stargardt disease. *American journal of human genetics* **64:** 1024-1035

Molday LL, Rabin AR, Molday RS (2000) ABCR expression in foveal cone photoreceptors and its role in Stargardt macular dystrophy. *Nature genetics* **25:** 257-258

Molday RS, Molday LL (1979) Identification and characterization of multiple forms of rhodopsin and minor proteins in frog and bovine rod outer segment disc membranes. Electrophoresis, lectin labeling, and proteolysis studies. *The Journal of biological chemistry* **254:** 4653-4660

Molday RS, Zhang K (2010) Defective lipid transport and biosynthesis in recessive and dominant Stargardt macular degeneration. *Prog Lipid Res* **49:** 476-492

Monahan PE, Lothrop CD, Sun J, Hirsch ML, Kafri T, Kantor B, Sarkar R, Tillson DM, Elia JR, Samulski RJ (2010) Proteasome inhibitors enhance gene delivery by AAV virus vectors expressing large genomes in hemophilia mouse and dog models: a strategy

for broad clinical application. *Molecular therapy : the journal of the American Society of Gene Therapy* **18:** 1907-1916

Mueller C, Ratner D, Zhong L, Esteves-Sena M, Gao G (2012) Production and discovery of novel recombinant adeno-associated viral vectors. *Curr Protoc Microbiol* **Chapter 14:** Unit14D 11

Mussolino C, della Corte M, Rossi S, Viola F, Di Vicino U, Marrocco E, Neglia S, Doria M, Testa F, Giovannoni R, Crasta M, Giunti M, Villani E, Lavitrano M, Bacci ML, Ratiglia R, Simonelli F, Auricchio A, Surace EM (2011) AAV-mediated photoreceptor transduction of the pig cone-enriched retina. *Gene therapy* **18:** 637-645

Narfstrom K, Katz ML, Bragadottir R, Seeliger M, Boulanger A, Redmond TM, Caro L, Lai CM, Rakoczy PE (2003) Functional and structural recovery of the retina after gene therapy in the RPE65 null mutation dog. *Investigative ophthalmology & visual science* **44:** 1663-1672

Nasonkin I, Illing M, Koehler MR, Schmid M, Molday RS, Weber BH (1998) Mapping of the rod photoreceptor ABC transporter (ABCR) to 1p21-p22.1 and identification of novel mutations in Stargardt's disease. *Human genetics* **102:** 21-26

Noble KG, Carr RE (1979) Stargardt's disease and fundus flavimaculatus. *Archives of ophthalmology* **97:** 1281-1285

Ogden GBVBTE (2001) *Clinical electrophysilogy*, St.Louis: Mosby.

Palfi A, Chadderton N, McKee AG, Blanco Fernandez A, Humphries P, Kenna PF, Farrar GJ (2012) Efficacy of codelivery of dual AAV2/5 vectors in the murine retina and hippocampus. *Human gene therapy* **23:** 847-858

Papaioannou VE, Fox JG (1993) Efficacy of tribromoethanol anesthesia in mice. *Lab Anim Sci* **43:** 189-192

Papermaster DS, Reilly P, Schneider BG (1982) Cone lamellae and red and green rod outer segment disks contain a large intrinsic membrane protein on their margins: an ultrastructural immunocytochemical study of frog retinas. *Vision research* **22:** 1417-1428

Papermaster DS, Schneider BG, Zorn MA, Kraehenbuhl JP (1978) Immunocytochemical localization of a large intrinsic membrane protein to the incisures and margins of frog rod outer segment disks. *The Journal of cell biology* **78:** 415-425

Petrs-Silva H, Dinculescu A, Li Q, Deng WT, Pang JJ, Min SH, Chiodo V, Neeley AW, Govindasamy L, Bennett A, Agbandje-McKenna M, Zhong L, Li B, Jayandharan GR, Srivastava A, Lewin AS, Hauswirth WW (2011) Novel properties of tyrosine-mutant

AAV2 vectors in the mouse retina. *Molecular therapy : the journal of the American Society of Gene Therapy* **19:** 293-301

Petrs-Silva H, Dinculescu A, Li Q, Min SH, Chiodo V, Pang JJ, Zhong L, Zolotukhin S, Srivastava A, Lewin AS, Hauswirth WW (2009) High-efficiency transduction of the mouse retina by tyrosine-mutant AAV serotype vectors. *Molecular therapy : the journal of the American Society of Gene Therapy* **17:** 463-471

Poincelot RP, Millar PG, Kimbel RL, Jr., Abrahamson EW (1969) Lipid to protein chromophore transfer in the photolysis of visual pigments. *Nature* **221:** 256-257

Qing K, Mah C, Hansen J, Zhou S, Dwarki V, Srivastava A (1999) Human fibroblast growth factor receptor 1 is a co-receptor for infection by adeno-associated virus 2. *Nature medicine* **5:** 71-77

Rabinowitz JE, Rolling F, Li C, Conrath H, Xiao W, Xiao X, Samulski RJ (2002) Cross-packaging of a single adeno-associated virus (AAV) type 2 vector genome into multiple AAV serotypes enables transduction with broad specificity. *Journal of virology* **76:** 791-801

Radu RA, Mata NL, Bagla A, Travis GH (2004) Light exposure stimulates formation of A2E oxiranes in a mouse model of Stargardt's macular degeneration. *Proceedings of the National Academy of Sciences of the United States of America* **101:** 5928-5933

Radu RA, Yuan Q, Hu J, Peng JH, Lloyd M, Nusinowitz S, Bok D, Travis GH (2008) Accelerated accumulation of lipofuscin pigments in the RPE of a mouse model for ABCA4-mediated retinal dystrophies following Vitamin A supplementation. *Investigative ophthalmology & visual science* **49:** 3821-3829

Reich SJ, Auricchio A, Hildinger M, Glover E, Maguire AM, Wilson JM, Bennett J (2003) Efficient trans-splicing in the retina expands the utility of adeno-associated virus as a vector for gene therapy. *Human gene therapy* **14:** 37-44

Rivera A, White K, Stohr H, Steiner K, Hemmrich N, Grimm T, Jurklies B, Lorenz B, Scholl HP, Apfelstedt-Sylla E, Weber BH (2000) A comprehensive survey of sequence variation in the ABCA4 (ABCR) gene in Stargardt disease and age-related macular degeneration. *American journal of human genetics* **67:** 800-813

Rotenstreich Y, Fishman GA, Anderson RJ (2003) Visual acuity loss and clinical observations in a large series of patients with Stargardt disease. *Ophthalmology* **110:** 1151-1158

Sambrook J, Russell DW (2001) *Molecular Cloning: a laboratory manual*, Third edition edn.: Cold Spring Harbor Laboratory Press, New York.

Schlichtenbrede FC, da Cruz L, Stephens C, Smith AJ, Georgiadis A, Thrasher AJ, Bainbridge JW, Seeliger MW, Ali RR (2003) Long-term evaluation of retinal function in Prph2Rd2/Rd2 mice following AAV-mediated gene replacement therapy. *The journal of gene medicine* **5:** 757-764

Shroyer NF, Lewis RA, Allikmets R, Singh N, Dean M, Leppert M, Lupski JR (1999) The rod photoreceptor ATP-binding cassette transporter gene, ABCR, and retinal disease: from monogenic to multifactorial. *Vision research* **39:** 2537-2544

Simonelli F, Maguire AM, Testa F, Pierce EA, Mingozzi F, Bennicelli JL, Rossi S, Marshall K, Banfi S, Surace EM, Sun J, Redmond TM, Zhu X, Shindler KS, Ying GS, Ziviello C, Acerra C, Wright JF, McDonnell JW, High KA, Bennett J, Auricchio A (2010) Gene therapy for Leber's congenital amaurosis is safe and effective through 1.5 years after vector administration. *Molecular therapy : the journal of the American Society of Gene Therapy* **18:** 643-650

Smith AJ, Bainbridge JW, Ali RR (2009) Prospects for retinal gene replacement therapy. *Trends in genetics : TIG* **25:** 156-165

Smith AJ, Schlichtenbrede FC, Tschernutter M, Bainbridge JW, Thrasher AJ, Ali RR (2003) AAV-Mediated gene transfer slows photoreceptor loss in the RCS rat model of retinitis pigmentosa. *Molecular therapy : the journal of the American Society of Gene Therapy* **8:** 188-195

Smith RH (2008) Adeno-associated virus integration: virus versus vector. *Gene therapy* **15:** 817-822

Sohocki MM, Daiger SP, Bowne SJ, Rodriquez JA, Northrup H, Heckenlively JR, Birch DG, Mintz-Hittner H, Ruiz RS, Lewis RA, Saperstein DA, Sullivan LS (2001) Prevalence of mutations causing retinitis pigmentosa and other inherited retinopathies. *Human mutation* **17:** 42-51

Sparrow JR, Boulton M (2005) RPE lipofuscin and its role in retinal pathobiology. *Experimental eye research* **80:** 595-606

Sparrow JR, Cai B, Fishkin N, Jang YP, Krane S, Vollmer HR, Zhou J, Nakanishi K (2003) A2E, a fluorophore of RPE lipofuscin: can it cause RPE degeneration? *Advances in experimental medicine and biology* **533:** 205-211

Sparrow JR, Kim SR, Cuervo AM, Bandhyopadhyayand U (2008) A2E, a pigment of RPE lipofuscin, is generated from the precursor, A2PE by a lysosomal enzyme activity. *Advances in experimental medicine and biology* **613:** 393-398

Sparrow JR, Nakanishi K, Parish CA (2000) The lipofuscin fluorophore A2E mediates blue light-induced damage to retinal pigmented epithelial cells. *Investigative ophthalmology & visual science* **41:** 1981-1989

Stargardt K (1909) Über familiäre, progressive Degeneration in der Maculagegend des Auges. *Albrecht von Graefes Arch Ophthalmol* **71:** 534-550

Stieger K, Colle MA, Dubreil L, Mendes-Madeira A, Weber M, Le Meur G, Deschamps JY, Provost N, Nivard D, Cherel Y, Moullier P, Rolling F (2008) Subretinal delivery of recombinant AAV serotype 8 vector in dogs results in gene transfer to neurons in the brain. *Molecular therapy : the journal of the American Society of Gene Therapy* **16:** 916-923

Stieger K, Cronin T, Bennett J, Rolling F (2011) Adeno-associated virus mediated gene therapy for retinal degenerative diseases. *Methods in molecular biology* **807:** 179-218

Stone EM, Nichols BE, Kimura AE, Weingeist TA, Drack A, Sheffield VC (1994) Clinical features of a Stargardt-like dominant progressive macular dystrophy with genetic linkage to chromosome 6q. *Archives of ophthalmology* **112:** 765-772

Summerford C, Bartlett JS, Samulski RJ (1999) AlphaVbeta5 integrin: a co-receptor for adeno-associated virus type 2 infection. *Nature medicine* **5:** 78-82

Sun H, Molday RS, Nathans J (1999) Retinal stimulates ATP hydrolysis by purified and reconstituted ABCR, the photoreceptor-specific ATP-binding cassette transporter responsible for Stargardt disease. *The Journal of biological chemistry* **274:** 8269-8281

Sun H, Nathans J (1997) Stargardt's ABCR is localized to the disc membrane of retinal rod outer segments. *Nature genetics* **17:** 15-16

Surace EM, Auricchio A (2008) Versatility of AAV vectors for retinal gene transfer. *Vision research* **48:** 353-359

Surace EM, Domenici L, Cortese K, Cotugno G, Di Vicino U, Venturi C, Cellerino A, Marigo V, Tacchetti C, Ballabio A, Auricchio A (2005) Amelioration of both functional and morphological abnormalities in the retina of a mouse model of ocular albinism following AAV-mediated gene transfer. *Molecular therapy : the journal of the American Society of Gene Therapy* **12:** 652-658

Testa F, Maguire AM, Rossi S, Pierce EA, Melillo P, Marshall K, Banfi S, Surace EM, Sun J, Acerra C, Wright JF, Wellman J, High KA, Auricchio A, Bennett J, Simonelli F (2013) Three-year follow-up after unilateral subretinal delivery of adeno-associated virus in patients with Leber congenital Amaurosis type 2. *Ophthalmology* **120:** 1283-1291

Testa F, Rossi S, Sodi A, Passerini I, Di Iorio V, Della Corte M, Banfi S, Surace EM, Menchini U, Auricchio A, Simonelli F (2012) Correlation between photoreceptor layer integrity and visual function in patients with Stargardt disease: implications for gene therapy. *Investigative ophthalmology & visual science* **53:** 4409-4415

Tsybovsky Y, Molday RS, Palczewski K (2010) The ATP-binding cassette transporter ABCA4: structural and functional properties and role in retinal disease. *Advances in experimental medicine and biology* **703:** 105-125

van Driel MA, Maugeri A, Klevering BJ, Hoyng CB, Cremers FP (1998) ABCR unites what ophthalmologists divide(s). *Ophthalmic genetics* **19:** 117-122

Vandenberghe LH, Auricchio A (2012) Novel adeno-associated viral vectors for retinal gene therapy. *Gene therapy* **19:** 162-168

Vandenberghe LH, Bell P, Maguire AM, Cearley CN, Xiao R, Calcedo R, Wang L, Castle MJ, Maguire AC, Grant R, Wolfe JH, Wilson JM, Bennett J (2011) Dosage thresholds for AAV2 and AAV8 photoreceptor gene therapy in monkey. *Science translational medicine* **3:** 88ra54

Vandenberghe LH, Wilson JM, Gao G (2009) Tailoring the AAV vector capsid for gene therapy. *Gene therapy* **16:** 311-319

Venables VN, Ripley BD (2002) *Modern Applied Statistics with S*, New York, USA: Springer Science+Business Media.

Vives-Bauza C, Anand M, Shirazi AK, Magrane J, Gao J, Vollmer-Snarr HR, Manfredi G, Finnemann SC (2008) The age lipid A2E and mitochondrial dysfunction synergistically impair phagocytosis by retinal pigment epithelial cells. *The Journal of biological chemistry* **283:** 24770-24780

von Ruckmann A, Fitzke FW, Bird AC (1995) Distribution of fundus autofluorescence with a scanning laser ophthalmoscope. *The British journal of ophthalmology* **79:** 407-412

Walia S, Fishman GA (2009) Natural history of phenotypic changes in Stargardt macular dystrophy. *Ophthalmic genetics* **30:** 63-68

Wang Y, Ling C, Song L, Wang L, Aslanidi GV, Tan M, Ling C, Srivastava A (2012) Limitations of encapsidation of recombinant self-complementary adeno-associated viral genomes in different serotype capsids and their quantitation. *Human gene therapy methods* **23:** 225-233

Weleber RG (1994) Stargardt's macular dystrophy. *Archives of ophthalmology* **112:** 752-754

Weng J, Mata NL, Azarian SM, Tzekov RT, Birch DG, Travis GH (1999) Insights into the function of Rim protein in photoreceptors and etiology of Stargardt's disease from the phenotype in abcr knockout mice. *Cell* **98:** 13-23

Westerfeld C, Mukai S (2008) Stargardt's disease and the ABCR gene. *Seminars in ophthalmology* **23:** 59-65

Wright AF, Chakarova CF, Abd El-Aziz MM, Bhattacharya SS (2010) Photoreceptor degeneration: genetic and mechanistic dissection of a complex trait. *Nature reviews Genetics* **11:** 273-284

Wright JF (2008) Manufacturing and characterizing AAV-based vectors for use in clinical studies. *Gene therapy* **15:** 840-848

Wu J, Zhao W, Zhong L, Han Z, Li B, Ma W, Weigel-Kelley KA, Warrington KH, Srivastava A (2007) Self-complementary recombinant adeno-associated viral vectors: packaging capacity and the role of rep proteins in vector purity. *Human gene therapy* **18:** 171-182

Wu L, Nagasaki T, Sparrow JR (2010a) Photoreceptor cell degeneration in Abcr (-/-) mice. *Advances in experimental medicine and biology* **664:** 533-539

Wu Y, Fishkin NE, Pande A, Pande J, Sparrow JR (2009) Novel lipofuscin bisretinoids prominent in human retina and in a model of recessive Stargardt disease. *The Journal of biological chemistry* **284:** 20155-20166

Wu Z, Asokan A, Samulski RJ (2006) Adeno-associated virus serotypes: vector toolkit for human gene therapy. *Molecular therapy : the journal of the American Society of Gene Therapy* **14:** 316-327

Wu Z, Yang H, Colosi P (2010b) Effect of genome size on AAV vector packaging. *Molecular therapy : the journal of the American Society of Gene Therapy* **18:** 80-86

Yan Z, Lei-Butters DC, Zhang Y, Zak R, Engelhardt JF (2007) Hybrid adeno-associated virus bearing nonhomologous inverted terminal repeats enhances dual-vector reconstruction of minigenes in vivo. *Hum Gene Ther* **18:** 81-87

Yan Z, Zak R, Zhang Y, Engelhardt JF (2005) Inverted terminal repeat sequences are important for intermolecular recombination and circularization of adeno-associated virus genomes. *Journal of virology* **79:** 364-379

Yan Z, Zhang Y, Duan D, Engelhardt JF (2000) Trans-splicing vectors expand the utility of adeno-associated virus for gene therapy. *Proceedings of the National Academy of Sciences of the United States of America* **97:** 6716-6721

Yang GS, Schmidt M, Yan Z, Lindbloom JD, Harding TC, Donahue BA, Engelhardt JF, Kotin R, Davidson BL (2002) Virus-mediated transduction of murine retina with adeno-associated virus: effects of viral capsid and genome size. *Journal of virology* **76:** 7651-7660

Young RW (1976) Visual cells and the concept of renewal. *Investigative ophthalmology & visual science* **15:** 700-725

Zernant J, Schubert C, Im KM, Burke T, Brown CM, Fishman GA, Tsang SH, Gouras P, Dean M, Allikmets R (2011) Analysis of the ABCA4 gene by next-generation sequencing. *Investigative ophthalmology & visual science* **52:** 8479-8487

Zhang Y, Chirmule N, Gao G, Wilson J (2000) CD40 ligand-dependent activation of cytotoxic T lymphocytes by adeno-associated virus vectors in vivo: role of immature dendritic cells. *Journal of virology* **74:** 8003-8010

Zhong L, Li B, Mah CS, Govindasamy L, Agbandje-McKenna M, Cooper M, Herzog RW, Zolotukhin I, Warrington KH, Jr., Weigel-Van Aken KA, Hobbs JA, Zolotukhin S, Muzyczka N, Srivastava A (2008) Next generation of adeno-associated virus 2 vectors: point mutations in tyrosines lead to high-efficiency transduction at lower doses. *Proceedings of the National Academy of Sciences of the United States of America* **105:** 7827-7832

Zolotukhin S (2005) Production of recombinant adeno-associated virus vectors. *Human gene therapy* **16:** 551-557

APPENDIX

Research Article

TRANSPARENT PROCESS OPEN ACCESS

EMBO Molecular Medicine

Effective delivery of large genes to the retina by dual AAV vectors

Ivana Trapani[1,†], Pasqualina Colella[1,†], Andrea Sommella[1], Carolina Iodice[1], Giulia Cesi[1], Sonia de Simone[1], Elena Marrocco[1], Settimio Rossi[2], Massimo Giunti[3], Arpad Palfi[4], Gwyneth J Farrar[4], Roman Polishchuk[1] & Alberto Auricchio[1,5,*]

Abstract

Retinal gene therapy with adeno-associated viral (AAV) vectors is safe and effective in humans. However, AAV's limited cargo capacity prevents its application to therapies of inherited retinal diseases due to mutations of genes over 5 kb, like Stargardt's disease (STGD) and Usher syndrome type IB (USH1B). Previous methods based on 'forced' packaging of large genes into AAV capsids may not be easily translated to the clinic due to the generation of genomes of heterogeneous size which raise safety concerns. Taking advantage of AAV's ability to concatemerize, we generated dual AAV vectors which reconstitute a large gene by either splicing (trans-splicing), homologous recombination (overlapping), or a combination of the two (hybrid). We found that dual trans-splicing and hybrid vectors transduce efficiently mouse and pig photoreceptors to levels that, albeit lower than those achieved with a single AAV, resulted in significant improvement of the retinal phenotype of mouse models of STGD and USH1B. Thus, dual AAV trans-splicing or hybrid vectors are an attractive strategy for gene therapy of retinal diseases that require delivery of large genes.

Keywords AAV; ABCA4; gene therapy; MYO7A; retina
Subject Categories Genetics, Gene Theraphy & Genetic Disease; Neuroscience
DOI 10.1002/emmm.201302948 | Received 18 May 2013 | Revised 10 October 2013 | Accepted 14 October 2013

Introduction

Inherited retinal degenerations (IRDs), with an overall global prevalence of 1/2000 (Sohocki *et al*, 2001), are a major cause of blindness worldwide. Among the most frequent and severe IRDs are retinitis pigmentosa (RP), Leber congenital amaurosis (LCA), and Stargardt's disease (STGD), which are most often inherited as monogenic conditions. The majority of mutations causing IRDs occur in genes expressed in neuronal photoreceptors (PR), rods and/or cones in the retina (Dryja, 2001). No therapy is currently available for these blinding diseases.

Gene therapy holds great promise for the treatment of IRDs. Among the available gene transfer vectors, those based on the small adeno-associated virus (AAV) are most efficient at targeting both PR and retinal pigment epithelium (RPE) for long-term treatment upon a single subretinal administration (Colella *et al*, 2009; Vandenberghe & Auricchio, 2012). Recently, we and others have demonstrated that subretinal administration of AAV is well-tolerated and effective for improving vision in patients affected with type 2 LCA, which is caused by mutations in *RPE65*, a gene expressed in the RPE (Bainbridge *et al*, 2008; Maguire *et al*, 2008, 2009; Cideciyan *et al*, 2009; Simonelli *et al*, 2010). These results bode well for the treatment of other forms of LCA and IRDs in general. The availability of AAV vector serotypes such as AAV2/8, which efficiently targets PR (Allocca *et al*, 2007; Natkunarajah *et al*, 2008; Auricchio, 2011; Mussolino *et al*, 2011; Vandenberghe *et al*, 2011) and RPE, further supports this approach. However, a major limitation of AAV is its cargo capacity, which is thought to be limited to around 5 kb, the size of the parental viral genome (Hermonat *et al*, 1997; Dong *et al*, 2010a; Lai *et al*, 2010; Wu *et al*, 2010b; Wang *et al*, 2012). This limits the application of AAV gene therapy approaches for common IRDs that are caused by mutations in genes whose coding sequence (CDS) is larger than 5 kb (herein referred to as large genes). These include: (i) STGD (MIM#248200), the most common form of inherited macular degeneration caused by mutations in the *ABCA4* gene (CDS: 6822 bp; Allikmets, 1997), which encodes the all-trans retinal transporter located in the PR outer segment (Allikmets, 1997; Molday & Zhang, 2010); (ii) Usher syndrome type IB (USH1B; MIM#276900), the most severe form of RP and deafness caused by mutations in the *MYO7A* gene (CDS: 6648 bp; Millan *et al*, 2011) encoding the unconventional MYO7A, an actin-based motor expressed in both PR and RPE within the retina (Hasson *et al*, 1995; Liu *et al*, 1997; Gibbs *et al*, 2010).

1 Telethon Institute of Genetics and Medicine (TIGEM), Naples, Italy
2 Department of Ophthalmology, Second University of Naples, Naples, Italy
3 Department of Veterinary Morphophysiology and Animal Production, University of Bologna, Bologna, Italy
4 The School of Genetics & Microbiology, Trinity College Dublin, Dublin, Ireland
5 Medical Genetics, Department of Translational Medicine, Federico II University, Naples, Italy
* Corresponding author: Tel: +39 081 6132228; Fax: +39 081 5790919; E-mail: auricchio@tigem.it
† These authors contributed equally to this work.

Various strategies have been investigated to overcome the limitation of AAV cargo capacity. Several groups, including our own, have attempted to 'force' large genes into one of the many AAV capsids available by developing the so-called oversize vectors (Grieger & Samulski, 2005; Wu *et al*, 2007; Allocca *et al*, 2008). Although administration of oversize AAV vectors achieves therapeutically-relevant levels of transgene expression in rodent and canine models of human inherited diseases (Allocca *et al*, 2008; Monahan *et al*, 2010; Grose *et al*, 2012; Lopes *et al*, 2013), including the retina of the *Abca4*$^{-/-}$ and *shaker 1* (*sh1*) mouse models of STGD and USH1B (Allocca *et al*, 2008; Lopes *et al*, 2013), the mechanism underlying oversize AAV-mediated transduction remains elusive. In contrast to what we and others originally proposed (Grieger & Samulski, 2005; Wu *et al*, 2007; Allocca *et al*, 2008), oversize AAV vectors do not contain a pure population of intact large size genomes but rather a heterogeneous mixture of mostly truncated genomes ≤5 kb in length (Dong *et al*, 2010a; Lai *et al*, 2010; Wu *et al*, 2010b; Wang *et al*, 2012). Following infection, re-assembly of these truncated genomes in the target cell nucleus has been proposed as a mechanism for oversize AAV vector transduction (Dong *et al*, 2010a; Hirsch *et al*, 2010, 2013; Lai *et al*, 2010; Wu *et al*, 2010b). Independent of transduction mechanism and *in vivo* efficacy, the heterogeneity in oversize AAV genome sizes is a major limitation for their application in human gene therapy.

Alternatively, the inherent ability of AAV genomes to undergo intermolecular concatemerization (Duan *et al*, 1998) is exploited to transfer large genes *in vivo* by splitting a large gene expression cassette into halves (<5 kb in size), each contained in one of two separate (dual) AAV vectors (Yan *et al*, 2000; Duan *et al*, 2001; Ghosh *et al*, 2008). In the dual AAV trans-splicing strategy, a splice donor (SD) signal is placed at the 3′ end of the 5′-half vector and a splice acceptor (SA) signal is placed at the 5′ end of the 3′-half vector (Fig 1). Upon co-infection of the same cell by the dual AAV vectors and inverted terminal repeat (ITR)-mediated head-to-tail concatemerization of the two halves, trans-splicing results in the production of a mature mRNA and full-size protein (Yan *et al*, 2000). Trans-splicing has been successfully used to express large genes in muscle and retina (Reich *et al*, 2003; Lai *et al*, 2005). Alternatively, the two halves of a large transgene expression cassette contained in dual AAV vectors may contain homologous overlapping sequences (at the 3′ end of the 5′-half vector and at the 5′ end of the 3′-half vector, dual AAV overlapping), which will mediate reconstitution of a single large genome by homologous recombination (Duan *et al*, 2001). This strategy depends on the recombinogenic properties of the transgene overlapping sequences (Ghosh *et al*, 2006). A third dual AAV strategy (hybrid) is based on adding a highly recombinogenic region from an exogenous gene [i.e. alkaline phosphatase, AP (Ghosh *et al*, 2008, 2011)] to the trans-splicing vectors. The added region is placed downstream of the SD signal in the 5′-half vector and upstream of the SA signal in the 3′-half vector (Fig 1) in order to increase recombination between the dual AAVs.

To determine which AAV-based strategy most efficiently transduces large genes in the retina, we compared them side-by-side in HEK293 cells and in mouse and pig retina using *EGFP*, *ABCA4* or *MYO7A*. We then used the dual AAV trans-splicing and hybrid strategies, which were the most efficient for transducing PR as well as RPE, to rescue the retinal phenotype of the *Abca4*$^{-/-}$ and *sh1* mouse models of STGD and USH1B.

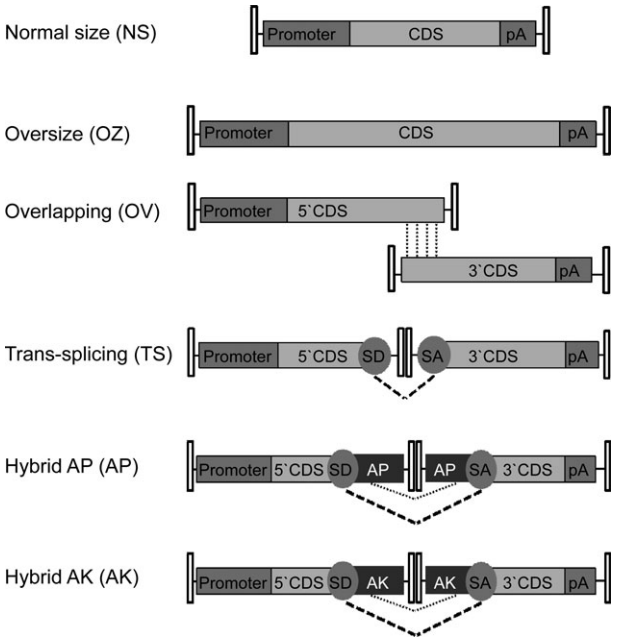

Figure 1. Schematic representation of AAV-based strategies for large gene transduction. CDS, coding sequence; pA, poly-adenylation signal; SD, splicing donor signal; SA, splicing acceptor signal; AP, alkaline phosphatase recombinogenic region; AK, F1 phage recombinogenic region. Pointed lines show overlapping regions available for homologous recombination, dotted lines show the splicing occurring between SD and SA.

Results

Generation of normal size, oversize and dual AAV vectors

We generated AAV oversize (OZ), dual AAV overlapping (OV), trans-splicing (TS) and hybrid vectors that included the therapeutic ABCA4-3xflag and MYO7A-HA coding sequences. The recombinogenic sequences included in the dual AAV hybrid vectors were based on either a previously reported region of the alkaline phosphatase transgene (AP, dual AAV hybrid AP; Ghosh *et al*, 2011) or a 77 bp sequence from the F1 phage genome (AK, dual AAV hybrid AK) that we found to be recombinogenic in previous *in vitro* experiments (Colella and Auricchio, unpublished data). We additionally generated AAV OZ and dual AAV vectors including the reporter EGFP sequence with the exception of the dual AAV OV approach since its efficiency relies on transgene-specific overlaps for reconstitution (Ghosh *et al*, 2006) and therefore can not be extrapolated from one gene to another. For EGFP we additionally generated single AAV vectors of normal size (NS) to compare levels of transgene expression from the various strategies. The constructs generated for production of all AAV vectors used in this study are listed in supplementary Table S1 and a schematic representation of the various approaches is depicted in Fig 1.

We used AAV2/2 vectors for the *in vitro* experiments, with the ubiquitous cytomegalovirus (CMV) or chicken beta-actin (CBA) pro-

moters, which efficiently transduce HEK293 cells (Dong *et al*, 2010b). In the experiments performed *in vivo* in the retina, we used AAV2/8 vectors, which efficiently transduce RPE and PR (Allocca *et al*, 2007; Mussolino *et al*, 2011; Vandenberghe *et al*, 2011) but poorly infect HEK293 cells, and either the ubiquitous CBA and CMV promoters (Mussolino *et al*, 2011), or the RPE-specific vitelliform macular dystrophy 2 (VMD2; Esumi *et al*, 2004) or the PR-specific Rhodopsin (RHO) and Rhodopsin kinase (RHOK) promoters (Allocca *et al*, 2007; supplementary Table S1).

Dual AAV vectors allow high levels of transduction *in vitro*

We initially compared the efficiency of the various OZ, dual AAV OV, TS and hybrid AP and AK strategies for AAV-mediated large gene transduction *in vitro* by infecting HEK293 cells with the AAV2/2 vectors [multiplicity of infection, m.o.i.: 10^5 genome copies (GC)/cell of each vector] with ubiquitous promoters (CMV for ABCA4-3xflag, CBA for MYO7A-HA). Cell lysates were analyzed by Western blot with anti-3xflag (to detect ABCA4-3xflag, Fig 2A) or anti-Myo7a (Fig 2B) antibodies. All strategies resulted in the expression of proteins of the expected size. As predicted, no bands of the expected size were observed when only one of the dual AAV vectors was used for infection (Fig 2A and B). Quantification of ABCA4 and MYO7A expression (Fig 2D and E) showed that the dual AAV hybrid AP approach resulted in the lowest levels of transgene expression, while the dual AAV OV, TS and hybrid AK approaches were more efficient than the AAV OZ approach. We then confirmed this using the *EGFP* transgene. For this purpose we selected the best performing dual AAV strategies (TS and hybrid AK; we did not use the transgene-specific OV strategy with *EGFP*, which is a reporter gene) and further compared them to AAV OZ. We thus produced AAV2/2-CMV-OZ-EGFP vectors and for comparison -TS- and -AK-EGFP-L in which the combined dual AAV vector genome length is similar to that of AAV

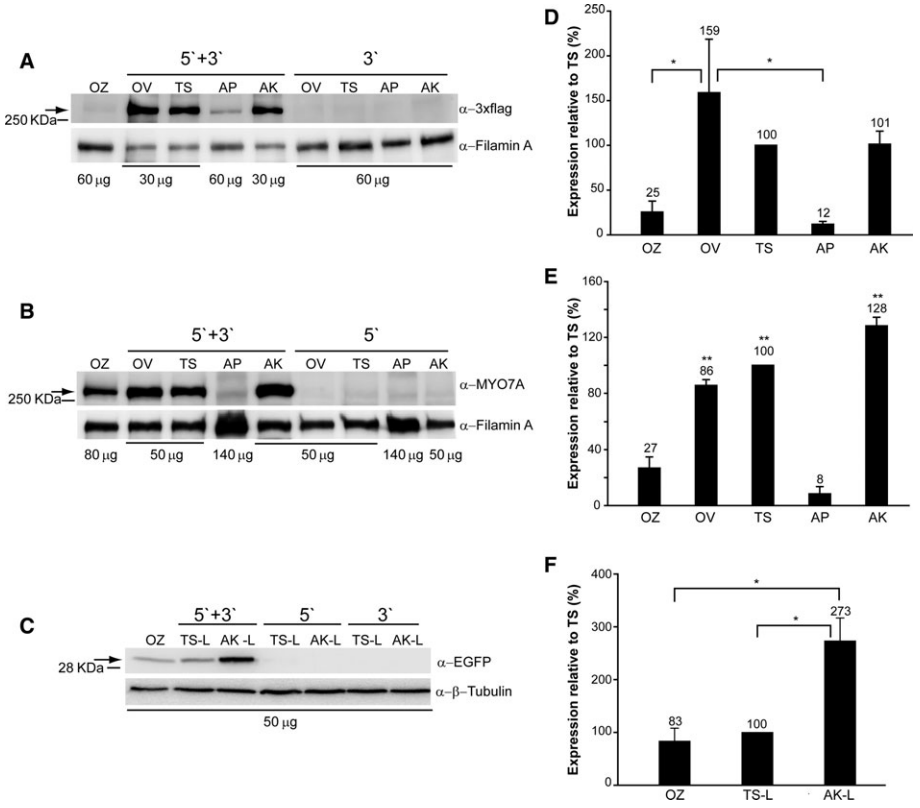

Figure 2. Dual AAV overlapping, trans-splicing and hybrid AK vectors efficiently transduce large genes *in vitro*.

A–F Western blot analysis of HEK293 cells infected with AAV2/2 vectors encoding for ABCA4 (A, D), MYO7A (B, E) and EGFP (C, F). The Western blot images (A-C) are representative of and the quantifications (D-F) are from $n = 4$ (A, C, D, F) or $n = 3$ (B, E) independent experiments. OZ, AAV oversize; OV, dual AAV overlapping; TS, dual AAV trans-splicing; AP, dual AAV hybrid AP; AK, dual AAV hybrid AK; TS-L, dual AAV trans-splicing EGFP with a combined genome size similar to OZ-EGFP; AK-L, dual AAV hybrid AK EGFP with a combined genome size similar to OZ-EGFP; 5′+3′: cells co-infected with 5′- and 3′-half vectors; 5′: control cells infected with the 5′-half vector; 3′: control cells infected with the 3′-half vector; α-EGFP: Western blot with anti-EGFP antibody; α-3xflag: Western blot with anti-3xflag antibody; α-Myo7a: Western blot with anti-Myo7a antibody; α-β-Tubulin: Western blot with anti-β-Tubulin antibody, used as loading control; α-Filamin A: Western blot with anti-Filamin A antibody, used as loading control. *P ANOVA < 0.05; **P ANOVA < 0.001.

A–C The arrows indicate full-length proteins, the micrograms of proteins loaded are depicted under each lane, the molecular weight ladder is depicted on the left.

D–F Quantification of ABCA4 (D), MYO7A (E) and EGFP (F) protein bands. The intensity of the ABCA4, MYO7A and EGFP bands was divided by the intensity of the Filamin A (D, E) or Tubulin (F) bands. The histograms show the expression of proteins as a percentage relative to dual AAV trans-splicing (TS) vectors, the mean value is depicted above the corresponding bar. Values are represented as mean ± standard error of the mean (s.e.m.).

Data information: (E) The asterisks represent significant differences with both OZ and AP. (D–F) More details on the TS and TS-L variability as well as on the statistical analysis including specific statistical values can be found in the Western blot and Statistical analysis paragraphs of the Materials and methods section, respectively.

OZ (supplementary Table S1). We infected HEK293 cells with AAV2/2-CMV-EGFP vectors [multiplicity of infection, m.o.i.: 10^5 genome copies (GC)/cell of each vector] and performed Western blot analysis of cell lysates with anti-EGFP antibodies (Fig 2C). Similarly to what observed with the ABCA4 and MYO7A transgenes, quantification of EGFP expression (Fig 2F) showed that dual AAV TS and hybrid AK approaches are more efficient than AAV OZ.

Then, we compared the efficiency of single AAV NS-EGFP to that of dual AAV TS and hybrid AK of similar size (supplementary Fig S1) by Western blot analysis of infected HEK293 cells. Quantification of EGFP expression showed that the levels achieved with dual AAV TS and hybrid AK were about 13–25-fold lower (7–4%) than with AAV NS (supplementary Fig S1).

Dual AAV TS and hybrid AK but not OV vectors transduce mouse and pig photoreceptors

The enclosed and small subretinal space should favour co-infection and transduction of the same cell by two independent AAV vectors. To test this, we injected subretinally WT mice with AAV2/8-CMV-EGFP, AAV2/8-CMV-DsRed or a mixture of both vectors (dose of each vector/eye: 3×10^9 GC) and harvested the eyes transduced by single or both vectors 3 weeks post-injection. Neural retinas, separated from the RPE, were dissociated and analyzed by flow cytometry. We found that $36 \pm 6\%$ of the labelled cells were positive for both EGFP and DsRed. However, since the number of $DsRed^+$ only cells ($8 \pm 5\%$) was lower than the number of $EGFP^+$ only cells ($56 \pm 8\%$) by counting the number of $EGFP^+/DsRed^+$ cells over the total number of transduced cells we may have under-estimated the co-transduction efficiency of the two vectors. Indeed, if we analyze the DsRed-positive cell populations, 82% of these were also EGFP-positive. This co-transduction efficiency is similar to that which we have reported previously (Palfi *et al*, 2012). To determine the co-transduction efficiency specifically in PR, and to test another red fluorescent reporter possibly more potent than DsRed, we repeated the injection in mice with a mixture of AAV2/8-CMV-EGFP and -RFP vectors (dose of each vector/eye: 1.4×10^9 GC/eye) and analyzed co-transduction on retinal cryosections which allow to unequivocably identify PR from RPE (supplementary Fig S2). We found that $24 \pm 2\%$ of transduced PR expressed both EGFP and RFP. However, the number of RFP^+ cells was still lower than the number of $EGFP^+$ cells due to weaker RFP fluorescence compared to EGFP, and the percentage of co-transduction reaches $53 \pm 4\%$ when we consider the number of RFP^+ cells that are also $EGFP^+$.

We then evaluated the best *in vitro* performing AAV-based systems for large gene transduction in the mouse retina. To test the dual AAV OV, which is transgene-specific, we used the therapeutic *ABCA4* and *MYO7A* genes (Fig 3 and data not shown). We used *EGFP* to evaluate the AAV OZ and the dual AAV TS and hybrid AK approaches (supplementary Fig S4).

Western blot analysis on retinal lysates, 1 month after subretinal delivery in C57BL/6 mice of the dual AAV OV vectors (dose of each vector/eye: 1.3×10^9 GC), encoding ABCA4-3xflag from the ubiquitous CMV promoter, revealed robust protein expression (Fig 3A). To determine which cell type in the retina expressed ABCA4, we used dual AAV OV vectors (dose of each vector/eye: 1×10^9 GC) that contained either the PR-specific RHO and RHOK, or the RPE-specific VMD2 promoters. We detected ABCA4 protein expression in retinas injected with the VMD2 but not with the RHO and RHOK

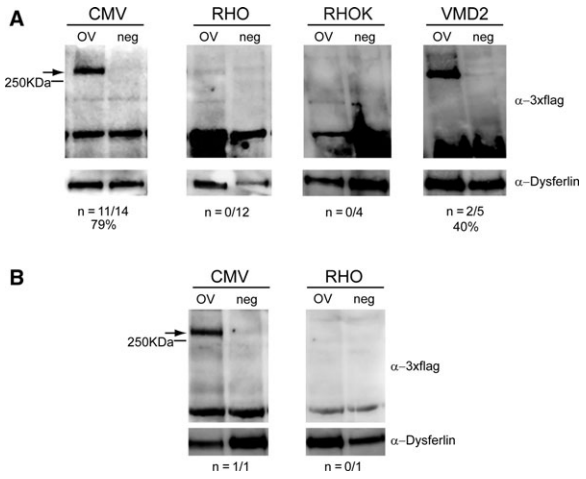

Figure 3. Dual AAV overlapping vectors transduce RPE but not photoreceptors in the mouse and pig retina.

A–B Representative Western blot analysis of C57BL/6 (A) and Large White pig (B) retinal lysates 1 month following injection of dual AAV2/8 overlapping vectors encoding for ABCA4-3xflag (OV) or AAV2/8 vectors expressing EGFP (neg), under the control of the ubiquitous cytomegalovirus (CMV) promoter, the PR-specific Rhodopsin (RHO) and Rhodopsin kinase (RHOK) promoters, or the RPE-specific vitelliform macular dystrophy 2 (VMD2) promoter. The arrows indicate full-length proteins, the molecular weight ladder is depicted on the left, 150 μg of proteins were loaded in each lane. The number (*n*) and percentage of ABCA4-positive retinas out of total retinas analyzed is depicted; α-3xflag, Western blot with anti-3xflag antibody; α-Dysferlin, Western blot with anti-Dysferlin antibody, used as loading control.

promoters (Fig 3A). These results were also confirmed in the Large White pig retina (Fig 3B). The pig retina is an excellent model to evaluate vector efficiency because of its size, which is similar to the human retina, and because it is enriched with cones that are concentrated in a streak-like region whose cone density is comparable to that of the primate macula (Mussolino *et al*, 2011). We injected Large White pig subretinally with dual AAV OV vectors encoding ABCA4-3xflag (dose of each vector/eye: 1×10^{10} GC), and observed ABCA4 protein expression with the CMV but not the RHO promoter (Fig 3B). Similarly, subretinal administration of dual AAV OV vectors encoding MYO7A-HA resulted in weak MYO7A protein expression in the mouse retina with the ubiquitous CBA (dose of each vector/eye: 2.5×10^9 GC) and no detectable expression with the RHO (dose of each vector/eye: 3.2×10^9 GC) promoter (data not shown). To rule out that this was due to a lower transcriptional activity from either the RHO or RHOK promoters compared to CMV, we injected subretinally C57BL/6 mice with 1.5×10^9 GC/eye of AAV2/8 vectors expressing *EGFP* from each of the promoters and found that CMV and RHO drive similarly robust PR transgene expression (supplementary Fig S3). Overall, these data suggest that the dual AAV OV approach is more efficient for large gene transfer to RPE than to PR.

To find an AAV-based strategy that efficiently transduces large genes in PR, which are a major target of gene therapy for IRDs including STGD and USH1B, we compared the retinal transduction properties of the AAV OZ with those of dual AAV TS and hybrid AK approaches, which in addition to dual AAV OV were the best

performing dual AAV approaches *in vitro*. We used EGFP, which allowed us to easily localize transgene expression in the various retinal cell types, including PR, as well as to properly compare the levels of AAV-based large transgene transduction to those of a single AAV NS vector. C57BL/6 mice were initially injected subretinally with AAV OZ and dual AAV TS-L and hybrid AK-L vectors (dose of each vector/eye: 1.7×10^9 GC), all encoding EGFP under the transcriptional control of the CMV promoter. One month later, fundus photographs showed that the highest levels of fluorescence were obtained with the dual AAV TS and hybrid AK approaches (supplementary Fig S4A). Fluorescence microscope analysis of retinal cryosections showed that detectable levels of RPE and PR transduction could be achieved with all approaches when combining the two half-vectors but not with each of them separately (supplementary Figs S4B and S5). However the levels of expression were higher, although variable, in the eyes injected with dual AAV TS-L and hybrid AK-L than in the eyes injected with AAV OZ vectors (supplementary Fig S4).

To test whether the levels and consistency of dual AAV-mediated transduction obtained can be improved by varying the ratio between the 5′- and 3′-half vectors, we injected subretinally C57BL/6 mice with dual AAV TS and hybrid AK vectors with different doses of 5′- and 3′-half vectors (supplementary Fig S6). We set as 1:1 the dose of 2.5×10^8 GC/eye which is submaximal considering that the titers of our AAV preps range around 10^9 GC/μl (supplementary Table S2) and that 1 μl is the maximum volume tolerated by the mouse subretinal space. Thus, 2.5×10^9 GC/eye which is the high 1:1 dose (10:10) is the maximum dose which we can administer to the murine eye. We show that none of the various ratios tested outperforms the 1:1 ratio of the high dose of vectors (10:10) used so far (supplementary Fig S6). Therefore we used the optimal 10:10 dose and ratio in our following experiments.

We then assessed PR-specific transduction levels in C57BL/6 mice following subretinal administration of dual AAV TS and hybrid AK vectors, which appears the most promising for large gene reconstitution in PR, as well as AAV NS vectors for comparison (dose of

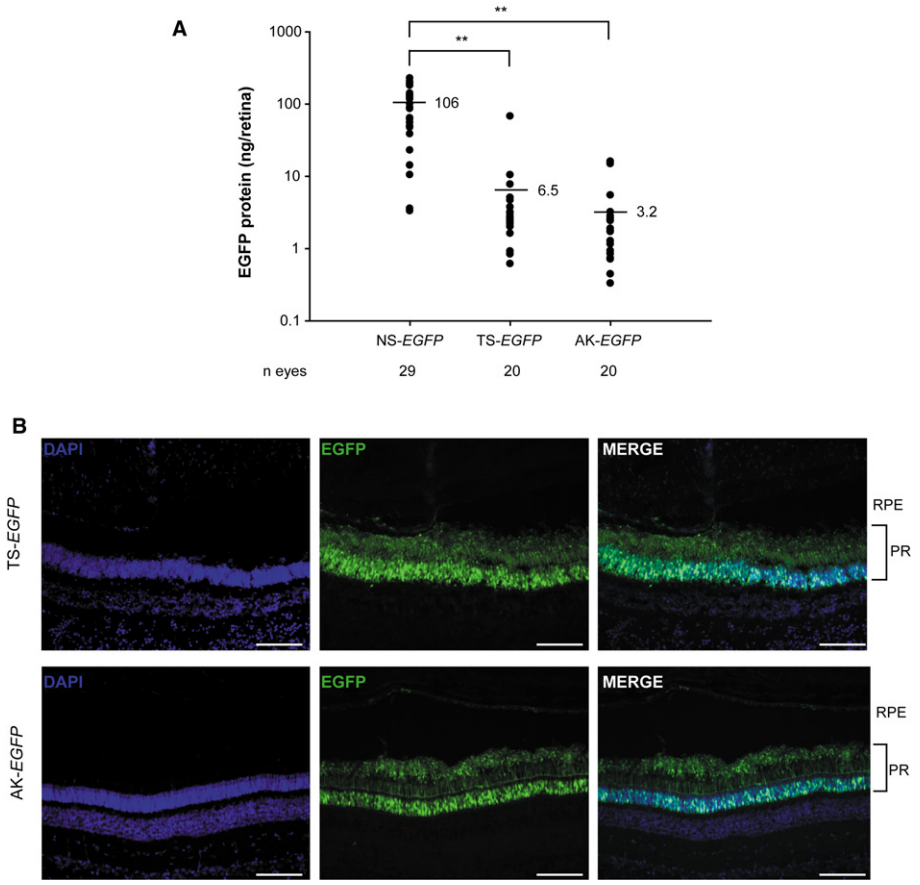

Figure 4. Dual AAV trans-splicing and hybrid AK vectors efficiently transduce mouse and pig photoreceptors.

A EGFP protein quantification by ELISA of retinas from C57BL/6 mice 1 month following subretinal injection of AAV2/8 vectors encoding for EGFP under the control of the PR-specific Rhodopsin (RHO) promoter. The scatter plot depicts EGFP protein levels from each retina; the mean value for each group is depicted and indicated with a solid line. The number (*n*) of eyes analyzed is depicted under the *x* axis. ***P* ANOVA<0.001. More details on the statistical analysis including specific statistical values can be found in the Statistical analysis paragraph of the Materials and methods section.

B Fluorescence analysis of retinal cryosections from Large White pigs 1 month following subretinal injection of AAV2/8 vectors encoding for EGFP under the control of the PR-specific RHO promoter. The pictures are representative of: $n = 4$ or $n = 3$ eyes injected with dual AAV TS or hybrid AK, respectively. The scale bar (100 μm) is depicted in the figure. NS, AAV normal size; TS, dual AAV trans-splicing; AK, dual AAV hybrid AK; DAPI, 4′,6′-diamidino-2-phenylindole staining; EGFP, native EGFP fluorescence; Merge, overlay of DAPI and EGFP pictures; RPE, retinal pigmented epithelium; PR, photoreceptors.

each vector/eye: 2.4×10^9 GC). All vectors encoded EGFP under the transcriptional control of the PR-specific RHO promoter. One month after vector administration whole retina lysates were analyzed by ELISA to quantify EGFP protein levels (Fig 4A). Dual AAV TS and hybrid AK vectors reconstituted consistent EGFP expression in PR at levels on average about 16–33-fold lower (6–3%) than with AAV NS. However, these levels were variable, similarly to what observed in retinal histological sections (supplementary Fig S4B), and some of the eyes treated with dual AAV vectors had EGFP levels in the range of those achieved with AAV NS (Fig 4A). As expected, no detectable EGFP expression was measured by ELISA in injected retinas when only one of the dual AAV vectors encoding for EGFP was used ($n = 9$: five eyes injected with 5′-half and four eyes with 3′-half; data not shown).

Thus, we conclude that dual AAV TS and hybrid AK strategies allow efficient mouse PR transduction although at levels which are lower than those obtained with an AAV NS. We then confirmed that subretinal administration of dual AAV TS and hybrid AK vectors transduced PR of Large White pigs (Fig 4B; dose of each vector/eye: 1×10^{11} GC).

Dual AAV vectors improve the retinal phenotype of STGD and USH1B mouse models

To understand whether the levels of PR transduction obtained with the dual AAV TS and hybrid AK approaches may be therapeutically relevant, we investigated them in the retina of two mouse models of IRDs, STGD and USH1B, caused by mutations in the large *ABCA4* and *MYO7A* genes, respectively.

Although the *Abca4*$^{-/-}$ mouse model does not undergo severe PR degeneration (Wu *et al*, 2010a), the absence of the ABCA4-encoded all-trans retinal transporter in PR outer segments (Illing *et al*, 1997; Sun & Nathans, 1997) causes an accumulation of lipofuscin in PR as well as in RPE, as result of PR phagocytosis by RPE (Weng *et al*, 1999; Mata *et al*, 2001). As a consequence, both the number of lipofuscin granules in the RPE and the thickness of RPE cells are greater in *Abca4*$^{-/-}$ mice than in control mice (Allocca *et al*, 2008; Radu *et al*, 2008; Ma *et al*, 2011; Conley *et al*, 2012; Han *et al*, 2012). In addition, *Abca4*$^{-/-}$ mice also show delayed recovery from light desensitization (Weng *et al*, 1999; Maiti *et al*, 2006; Allocca *et al*, 2008; Radu *et al*, 2008; Han *et al*, 2012). Since *ABCA4* is expressed specifically in PR, we generated dual AAV TS and hybrid AK vectors encoding ABCA4-3xflag under the transcriptional control of the RHO promoter. These vectors were subretinally injected in wild-type C57BL/6 mice (dose of each vector/eye: 3–5×10^9 GC) and 1 month later retinas were lysed and analyzed by Western blot with anti-3xflag antibodies (Fig 5A). Both approaches resulted in robust yet variable levels of ABCA4-3xflag expression. ABCA4-3xflag expression levels were more consistent in retinas treated with the dual AAV hybrid AK vectors (Fig 5A). No truncated and/or aberrant ABCA4 proteins were detected by Western blot analysis of C57BL/6 eyecups treated with dual AAV TS and hybrid AK vectors using anti-3xflag antibodies although two proteins (>100 KDa) smaller than the full length are produced *in vitro* following infection with either the single 5′- or 3′-half of both dual AAV approaches (supplementary Figs S7 and S8). In addition no evident signs of retinal toxicity were observed in *Abca4*$^{-/-}$ mice at 8 months after treatment with dual AAV TS and hybrid AK vectors by conventional histological analysis (supplementary Fig S9A).

To evaluate the biological and therapeutic activity of the recombinant ABCA4 protein produced by dual AAV vectors, 1 month-old albino *Abca4*$^{-/-}$ mice were injected subretinally with the dual AAV TS and hybrid AK RHO-*ABCA4*-HA vectors (dose of each vector/eye: 1–3×10^9 GC). Three months later, eyes were harvested and immuno-electron microscopy analysis with anti-hemagglutinin (HA) antibodies of retinal sections confirmed that immunogold particles were correctly localized in PR outer segments only in animals that were injected with the combination of 5′ and 3′ dual AAV TS and hybrid AK vectors (Fig 5B). To assess the functionality of the ABCA4 protein expressed by the dual AAV vectors, we measured *Abca4*$^{-/-}$ retinal lipofuscin accumulation and recovery from light desensitization. To assess the former we performed transmission electron microscopy analysis to measure the number of RPE lipofuscin granules (Fig 5C and D) and RPE thickness (Fig 6A and B). Both were greater in the retina of *Abca4*$^{-/-}$ mice injected with control vectors (independently of the size of the control constructs, supplementary Fig S10) than in the retina of wild-type, age-matched BALB/c controls, and were significantly reduced or normalized in the eyes injected either with the therapeutic dual AAV TS or hybrid AK vectors (Figs 5C and D and 6A and B). We additionally attempted at measuring A2E, the major component of lipofuscin granules, by HPLC (Parish *et al*, 1998; Ben-Shabat *et al*, 2002; Allocca *et al*, 2008), however these measurements were inconsistent, even between affected and normal retinas (data not shown), thus we were not able to use these techniques in our rescue experiments. Importantly, the eyes treated with dual AAV TS and hybrid AK vectors showed improved recovery from light desensitization when compared to eyes treated with control vectors (dose of each vector/eye: 1.2×10^9 GC, Fig 6C), independently of the size of the control constructs [Student's *t*-test *P* value of dual AAV-EGFP-L ($n = 2$ TS-L, $n = 4$ AK-L; total $n = 6$) versus dual AAV-EGFP ($n = 5$ TS, $n = 4$ AK; total $n = 9$): 0.23].

We then tested the efficacy of dual AAV-mediated *MYO7A* gene transfer in the retina of *sh1* mice, the most commonly used model of USH1B (Liu *et al*, 1997, 1998, 1999; Lillo *et al*, 2003; Gibbs *et al*, 2010). In *sh1* mice, a deficiency in the motor Myo7a causes the mis-localization of RPE melanosomes (Liu *et al*, 1998), which do not enter into the RPE apical microvilli, and the accumulation of rhodopsin at the PR connecting cilium (Liu *et al*, 1999). *MYO7A* is highly expressed in the RPE and to a lesser extent in PR (Hasson *et al*, 1995; Liu *et al*, 1997), therefore we used dual AAV TS and hybrid AK vectors expressing MYO7A-HA under the transcriptional control of the ubiquitous CBA promoter. One month-old wild-type C57BL/6 mice were injected with the dual AAV vectors (dose of each vector/eye: 1.7×10^9 GC) and eyecup lysates were evaluated 1 month later using Western blot analysis with anti-HA antibodies. Results showed similarly robust and consistent levels of MYO7A expression in retinas treated with both approaches (Fig 7A). Taking advantage of our anti-Myo7a antibody able to recognize both murine and human MYO7A (although with potentially different affinity for the two orthologous proteins), we compared the levels of MYO7A achieved following delivery of dual AAV vectors to the *sh1*$^{-/-}$ eye to those expressed endogenously in the *sh1*$^{+/-}$ eye (Fig 7B). The levels of human MYO7A driven by the CBA promoter 1 month after treatment (Fig 7B; dose of each vector/eye: 1.7×10^9 GC) were 19–21% of endogenous Myo7a expressed in both RPE and PR

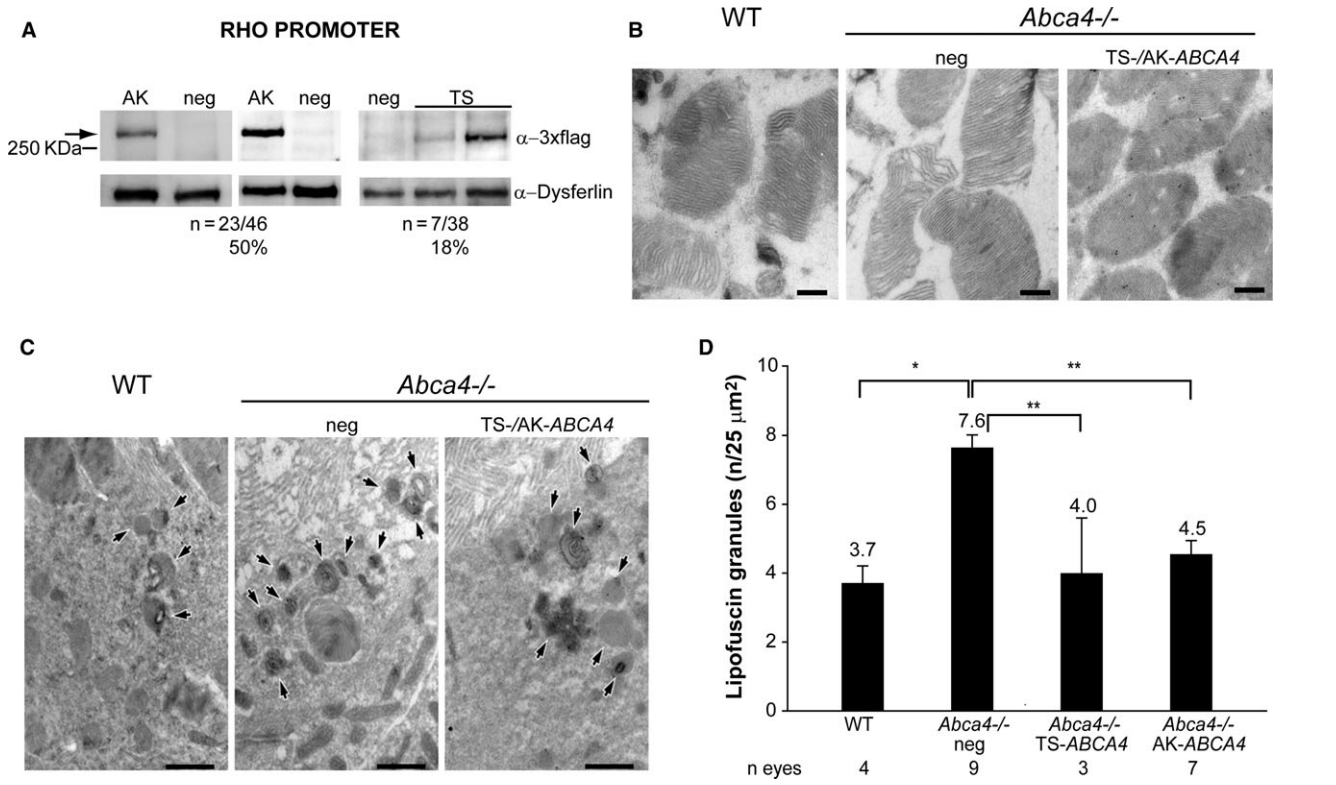

Figure 5. Subretinal administration of dual AAV vectors results in ABCA4 expression in mouse photoreceptors and reduction in the accumulation of lipofuscin granules in *Abca4*$^{-/-}$ mice.

A Representative Western blot analysis of C57BL/6 retinal lysates 1 month following the injection of dual AAV trans-splicing (TS) and hybrid AK (AK) vectors encoding for ABCA4 under the control of the PR-specific Rhodopsin promoter (RHO PROMOTER). The arrow points at full-length proteins, the molecular weight ladder is depicted on the left, 150 μg of protein were loaded in each lane. The number (*n*) and percentage of ABCA4-positive retinas out of total retinas analyzed is depicted. AK, retinas injected with dual AAV hybrid AK vectors; TS, retinas injected with dual AAV TS vectors; neg: retinas injected with AAV vectors expressing *EGFP*, as negative controls; α-3xflag: Western blot with anti-3xflag antibody; α-Dysferlin: Western blot with anti-Dysferlin antibody, used as loading control.

B Representative pictures of immuno-electron microscopy analysis with anti-HA antibody of retinal sections from wild-type BALB/c (WT) and *Abca4*$^{-/-}$ mice injected with either dual AAV or with negative control vectors. The black dots represent the immuno-gold labelling of the ABCA4-HA protein. The scale bar (200 nm) is depicted in the figure.

C Representative pictures of transmission electron microscopy analysis showing lipofuscin granules content in the RPE of WT and *Abca4*$^{-/-}$ mice injected with either dual AAV or negative control vectors. The black arrows indicate lipofuscin granules. The scale bar (1.6 μm) is depicted in the figure.

D Quantification of the mean number of lipofuscin granules counted in at least 30 fields (25 μm^2) for each sample. The number (*n*) of eyes analyzed is depicted below each bar. The mean value is depicted above the corresponding bar. Values are represented as mean ± standard error of the mean (s.e.m.). **P* ANOVA < 0.05; ***P* ANOVA < 0.001. More details on the statistical analysis including specific statistical values can be found in the Statistical analysis paragraph of the Materials and methods section.

Data information: (B-D) WT, BALB/c eyes; Abca4$^{-/-}$ neg, Abca4$^{-/-}$ eyes injected with either AAV vectors expressing EGFP (*n* = 2) or the 5′- (*n* = 3) or 3′- (*n* = 4) half of the dual AAV hybrid AK vectors, as negative control (neg total n = 9); Abca4$^{-/-}$ AK-ABCA4: mice injected with dual AAV hybrid AK vectors; Abca4$^{-/-}$ TS-ABCA4: mice injected with dual AAV TS vectors.

(Fig 7B) and these remained similar at 9 months after vector delivery (MYO7A retinal levels after subretinal delivery of dual AAV-TS, quantified on Western blot of eyecup lysates as in Fig 7B: 19 ± 6% of endogenous Myo7a, $n = 5$). Notably, subretinal delivery of dual AAV TS and hybrid AK resulted in efficient expression of human MYO7A specifically in PR when using the RHO promoter (supplementary Fig S11). No MYO7A proteins of size different from the full-length were detected by Western blot analysis of *sh1*$^{-/-}$ eyecups treated with either dual AAV TS or hybrid AK vectors. However, two proteins smaller than the full length MYO7A (<130 KDa) are detected *in vitro* following infection with either the single 5′- or 3′-half of both dual AAV approaches (supplementary Fig S12 and S13).

To test the ability of MYO7A expressed from dual AAV vectors to rescue the defects of the *sh1*$^{-/-}$ retina, we evaluated RPE melanosome (Fig 8A and B) and rhodopsin localization (Fig 8C) following subretinal injection of dual AAV TS and hybrid AK CBA-*MYO7A* vectors (dose of each vector/eye: 1.7 × 10^9 GC) in 1 month-old *sh1*$^{-/-}$ mice. Unlike in unaffected mice, the *sh1*$^{-/-}$ melanosomes do not enter the RPE apical microvilli (Fig 8A and B), this was significantly improved after the delivery of either dual AAV TS or hybrid AK vectors encoding *MYO7A* (Fig 8A and B).

We also found that the number of rhodopsin particles at the connecting cilium is greater in *sh1*$^{-/-}$ retinas treated with control vectors (independently of the size of the control constructs, supplementary Fig S14) than in unaffected *sh1* (Fig 8C and sup-

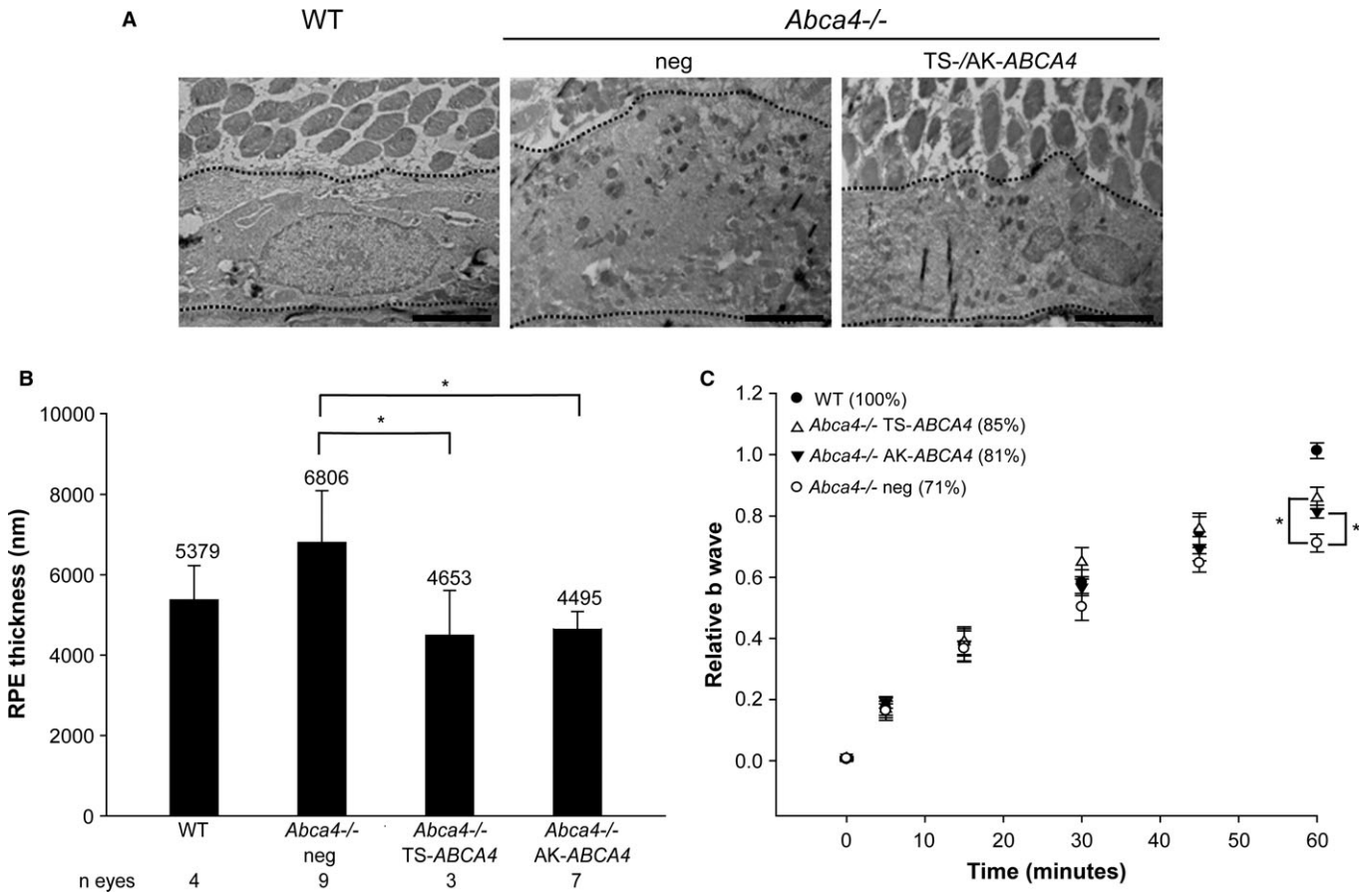

Figure 6. Subretinal injection of dual AAV vectors reduces the thickness of the RPE and improves recovery from light desensitization in *Abca4*$^{-/-}$ mice.

A Representative pictures of transmission electron microscopy analysis of retinal sections from wild-type BALB/c (WT) and *Abca4*$^{-/-}$ mice injected with dual AAV trans-splicing (TS-*ABCA4*) and hybrid AK vectors (AK-*ABCA4*) or with either AAV vectors expressing *EGFP* or 5′- or 3′-half of the dual hybrid AK vectors (neg), as negative controls. The dotted lines indicate the edges of RPE cells. The scale bar (3.8 μm) is depicted in the figure.

B Quantification of the mean RPE thickness counted in at least 30 fields for each sample. The number (*n*) of eyes analyzed is depicted below each bar. *Abca4*$^{-/-}$ neg includes *Abca4*$^{-/-}$ mice injected with either AAV vectors expressing *EGFP* (*n* = 2) or 5′- (*n* = 3) or 3′- (*n* = 4) half of the dual hybrid AK vectors (neg total *n* = 9). The mean value is depicted above the corresponding bar. Values are represented as mean ± standard error of the mean (s.e.m.). **P* ANOVA < 0.05.

C Recovery from light desensitization in 3 month-old *Abca4*$^{-/-}$ and BALB/c mice at 6 weeks post-injection. The relative b-wave is the ratio between the post- and the pre-desensitization b-wave amplitudes both evoked by 1 cd s/m^2. The time refers to the minutes post-desensitization. The mean recovery (%) at 60 min is depicted. WT, BALB/c eyes (*n* = 4); *Abca4*$^{-/-}$ TS-*ABCA4*, eyes injected with dual AAV TS vectors (*n* = 5); *Abca4*$^{-/-}$ AK-*ABCA4*: mice injected with dual AAV hybrid AK vectors (*n* = 5); *Abca4*$^{-/-}$ neg: *Abca4*$^{-/-}$ mice either not injected (*n* = 2) or injected with the 5′-half of the dual AAV TS (*n* = 3) or hybrid AK (*n* = 2) vectors (neg total *n* = 7). Values are represented as mean ± standard error of the mean (s.e.m.). **P* ANOVA < 0.05. More details on the statistical analysis including specific statistical values can be found in the Statistical analysis paragraph of the Materials and methods section.

plementary Fig S14). This was reduced in *sh1*$^{-/-}$ retinas treated with dual AAV TS and hybrid AK vectors expressing MYO7A, although the differences were not statistically significant (Fig 8C). Notably, the improvement of the *sh1*$^{-/-}$ retinal defects is associated with a normal retinal architecture (supplementary Fig S9B) which further suggests that subretinal delivery of dual AAV TS and hybrid AK vectors does not induce evident retinal toxicity.

Discussion

While AAV-mediated gene therapy is effective in animal models and in patients with inherited blinding conditions (Jacobson *et al*, 2006; Bainbridge *et al*, 2008; Maguire *et al*, 2008, 2009; Cideciyan *et al*, 2009; Simonelli *et al*, 2010), its application to diseases affecting the retina and requiring a transfer of genes larger than 5 kb (referred to as large genes) is inhibited by AAV limited cargo capacity. To overcome this, we compared the efficiency of various AAV-based strategies for large gene transduction including: AAV OZ and dual AAV OV, TS, hybrid AP and AK approaches *in vitro* and in mouse and pig retina. Our *in vitro* and *in vivo* results show that the dual AAV strategies we tested (with the exception of the dual AAV hybrid AP) outperform AAV OZ vectors in terms of transduction levels. This may be explained by: (i) the homogeneous size of the dual AAV genome population when compared to AAV OZ genomes, which may favour the generation of transcriptionally active large transgene expression cassettes; (ii) the small volume of the subretinal space,

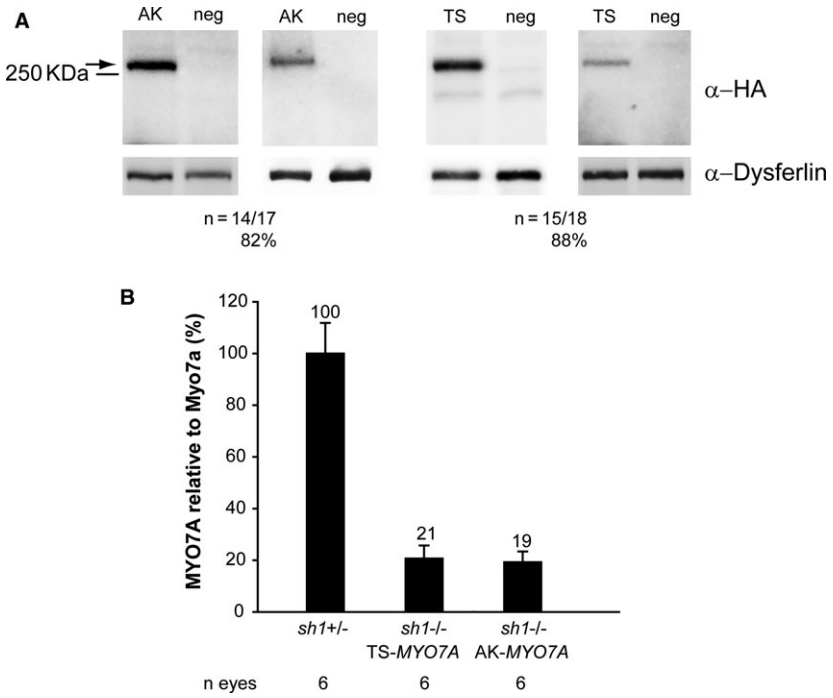

Figure 7. Subretinal administration of dual AAV trans-splicing and hybrid AK vectors results in robust MYO7A expression in mice.

A Representative Western blot analysis of C57BL/6 eyecups 1 month following the injection of dual AAV trans-splicing (TS) and hybrid AK (AK) vectors encoding for MYO7A-HA under the control of the ubiquitous chicken beta-actin (CBA) promoter. The arrow indicates full-length proteins, the molecular weight ladder is depicted on the left, 100 μg of proteins were loaded in each lane. The number (*n*) and percentage of MYO7A-positive eyecups out of total eyecups analyzed is depicted. AK: eyes injected with dual AAV hybrid AK vectors; TS: eyes injected with dual AAV TS vectors; neg: eyes injected with either 5′- or 3′-half of the dual AAV TS and hybrid AK vectors; α-HA: Western blot with anti-hemagglutinin (HA) antibody; α-Dysferlin: Western blot with anti-Dysferlin antibody, used as loading control.

B Quantification of MYO7A levels expressed from dual AAV vectors in $sh1^{-/-}$ eyecups relative to endogenous Myo7a expressed in littermate $sh1^{+/-}$ eyecups. $sh1^{-/-}$ eyes were injected with dual AAV TS and hybrid AK vectors encoding MYO7A under the control of the CBA promoter and analyzed 1.5 months later. $sh1^{+/-}$ eyes were injected with AAV vectors expressing EGFP. The number (*n*) of eyes analyzed is depicted below each bar. The quantification was performed by Western blot analysis using the anti-Myo7a antibody and measurements of MYO7A and Myo7a band intensities normalized to Dysferlin. The histograms show the expression of MYO7A protein as percentage relative to $sh1^{+/-}$ Myo7a; the mean value is depicted above the corresponding bars. Values are represented as mean ± standard error of the mean (s.e.m.).

which we show favours infection and transduction of the same cell by two independent AAV vectors. Although this has been suggested by previous work in the retina with either dual AAV TS vectors carrying the lacZ reporter gene (Reich *et al*, 2003) or with two single vectors encoding different fluorescent reporter proteins (Palfi *et al*, 2012), our study represents the first comprehensive comparison in the retina of the dual AAV strategies reported so far, as well as the first demonstration of their efficacy in animal models of common inherited blinding conditions.

The dual AAV OV approach is particularly interesting when compared to the TS or hybrid AK approaches, which appear similarly efficient *in vitro*, as dual AAV OV vectors only contain sequences belonging to the therapeutic transgene expression cassette. However, when we administered dual AAV OV vectors to the subretinal space of adult mice and pigs, we were able to detect expression of the large ABCA4 and MYO7A proteins only when the ubiquitous or the RPE-specific promoters, but not the PR-specific promoters, were used. This may suggest that the homologous recombination required for dual AAV OV reconstitution is more efficient in RPE than PR. This is consistent with the low levels of homologous recombination reported in post-mitotic neurons (Fishel *et al*, 2007) and may partially explain the low levels of dual AAV OV-mediated MYO7A transduction recently reported by other groups (Lopes *et al*, 2013). We conclude that subretinal administration of dual AAV OV vectors should not be used for large gene transfer to PR, although we can not exclude that sequences that are more recombinogenic than those included in our dual AAV OV *ABCA4* and *MYO7A* vectors may allow efficient homologous recombination in PR.

Dual AAV TS and hybrid AK approaches efficiently transduce mouse and pig PR, differently from what we observed with dual AAV OV. This is consistent with the knowledge that the mechanism of large gene reconstitution mediated by dual AAV TS and hybrid AK approaches may be via ITR-mediated head-to-tail rejoining (Duan *et al*, 1998; Yan *et al*, 2005; Ghosh *et al*, 2008) rather than homologous recombination.

The transduction levels provided by the dual hybrid AK are superior to those of the TS approach in mouse PR but not RPE. This was evident when using the large *ABCA4* and *MYO7A* but not the small *EGFP* transgene, suggesting an advantage of

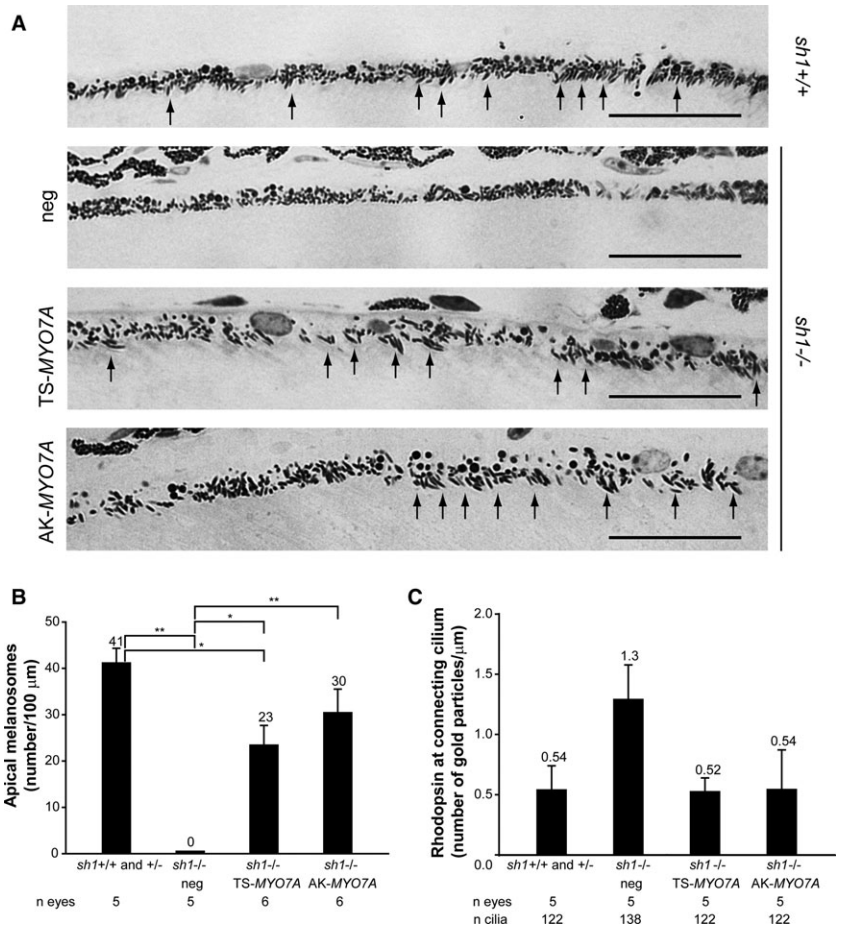

Figure 8. Subretinal administration of dual AAV vectors rescues melanosome and rhodopsin localization in *sh1*$^{-/-}$ retinas.

A Semi-thin retinal sections representative of both *sh1*$^{+/+}$ and *sh1*$^{+/-}$ eyes (*sh1*$^{+/+}$) injected with AAV vectors expressing *EGFP* and of *sh1*$^{-/-}$ eyes injected with dual AAV trans-splicing (TS-*MYO7*A), hybrid AK (AK-*MYO7*A) or the 5′- or 3′-half vectors (neg), as negative controls. The arrows point at correctly localized melanosomes, the scale bar (10 μm) is depicted in the figure.

B Quantification of melanosome localization in the RPE villi of *sh1* mice 2–3 months following subretinal delivery of dual AAV vectors. The *n* of eyes analyzed is depicted below each bar. The quantification is depicted as the mean number of apical melanosomes/100 μm, the mean value is depicted above the corresponding bar. *sh1*$^{-/-}$ neg includes *sh1*$^{-/-}$ eyes injected with AAV vectors expressing either 5′- (*n* = 1) or 3′- (*n* = 2) half of the dual TS vectors, or 5′-half (*n* = 2) of the dual hybrid AK vectors (neg total *n* = 5). Values are represented as mean ± standard error of the mean (s.e.m.). **P* ANOVA < 0.05, ***P* ANOVA < 0.001.

C Quantification of the number of rhodopsin gold particles at the PR connecting cilium of *sh1* mice 2–3 months following subretinal delivery of dual AAV vectors. The *n* of eyes and connecting cilia analyzed is depicted below each bar. *sh1*$^{-/-}$ neg includes *sh1*$^{-/-}$ eyes injected with AAV vectors expressing either 5′-half of the dual TS vectors (*n* = 3) or 5′-half (*n* = 2) of the dual hybrid AK vectors (neg total *n* = 5). The quantification is depicted as the mean number of gold particles per length of connecting cilium, the mean value is depicted above the corresponding bar. Values are represented as mean ± standard error of the mean (s.e.m.). More details on the statistical analysis including specific statistical values can be found in the Statistical analysis paragraph of the Materials and methods section.

including the AK sequence for large transgene reconstitution in cells like PR which are more difficult to target by AAV2/8 than RPE.

Differently from what we have observed, Hirsch *et al* (2013) have recently shown that AAV OZ vectors can reconstitute a large reporter gene (6.2 kb) in the retina of mice more efficiently than dual AAV TS vectors. The following factors may account for this: (i) the design of the dual AAV vectors which may result in lower transduction levels in Hirsch *et al* than in our case; (ii) the purification of the AAV OZ vectors by Hirsch *et al* that may promote the selection in the viral preparation of genomes with higher transduction properties than in our preparations; (iii) the use of a shorter transgene by Hirsch *et al* than by us that gives rise to genomes with longer overlaps which can positively influence AAV OZ transduction. Our results also differ from those of another group that has reported that dual AAV hybrid AP outperforms TS (Ghosh *et al*, 2011). While we have generated our dual hybrid AP vectors based on the description provided in that publication, it is possible that minor differences in the AP sequences used may account for the different transduction levels we have observed.

The levels of mouse PR transduction we achieved with dual AAV TS and hybrid AK are lower than with single NS vectors. However, we show that in the case of MYO7A, retinal transgene expression levels are about 20% of endogenous. These may be effective for

treating inherited blinding conditions that require relatively low levels of transgene expression, i.e. diseases inherited as autosomal recessive. Indeed, we show that subretinal delivery of dual AAV TS and hybrid AK improves and even normalizes the retinal defects of two animal models of IRDs, STGD and USH1B, which are due to mutations in large genes and are attractive targets of gene therapy. Importantly, both levels and consistency of dual AAV-mediated large transgene expression could be improved by directing the productive head-to-tail genome concatemerization by either using heterologous ITRs (Yan *et al*, 2007) or by adding oligos to the injection solution (Hirsch *et al*, 2009).

Single normal size AAV vectors ensure multi-year retinal gene expression after a single vector administration (Testa *et al*, 2013). The data we have obtained so far from dual AAV vectors up to 9 months after retinal gene delivery, the last time point of our analysis, suggest that longevity of transgene expression may be similar between single normal size and dual AAV vectors.

The genome size of dual AAV vectors is homogeneous, which means identity and safety issues related to their use should be less considerable than those related to AAV OZ vectors, which have heterogeneous genome sizes. However, the possibility that delivery of dual AAV vectors results in the production of aberrant proteins in the retina, i.e. truncated proteins from the 5′-half vector that contains the promoter sequence and/or from the 3′-half vector due to the low promoter activity of the ITRs (Flotte *et al*, 1993) must be considered. Our results show that proteins smaller than the full-length are produced from the 5′- and 3′-halves of dual AAV vectors *in vitro* but not *in vivo* in the retina where only full-length ABCA4 and MYO7A proteins are detected. The production of properly spliced full length proteins by dual AAV vectors is corroborated by the successful amplification of the full size ABCA4 and MYO7A mRNA retro transcribed from cells infected with dual AAV TS and hybrid AK vectors (data not shown). Indeed the transcript sequences confirmed that intermolecular AAV joining and splicing occurred correctly (data not shown), as expected by the size of the full length proteins detected by Western blot. In addition, we detected neither ERG (data not shown) nor retinal histological abnormalities in both *Abca4*$^{-/-}$ and *sh1*$^{-/-}$ mice that we followed up to 3–8 months after dual AAV vector delivery. Future long-term safety studies as well as sensitive proteomic profiling will help to better define if any toxicity derives from intraocular administration of dual AAV vectors.

In conclusion, we found that dual AAV vectors are efficient both *in vitro* and in the retina *in vivo*. While dual AAV OV vectors efficiently transduce RPE, they do not transduce PR, whereas dual AAV TS and hybrid AK approaches drive efficient large gene reconstitution in both cell types. Administration of dual AAV TS and hybrid AK approaches improved the retinal phenotype of mouse models of STGD and USH1B, providing evidence of the efficacy of these strategies for gene therapy of these and other blinding conditions, which require large gene transfer to PR as well as RPE.

Materials and Methods

Generation of AAV vector plasmids

The plasmids used for AAV vector production were derived from either the pZac2.1 (Gao *et al*, 2000) or pAAV2.1 (Auricchio *et al*, 2001) plasmids that contain the inverted terminal repeats (ITRs) of AAV serotype 2 (supplementary Table S1). Normal size and oversize AAV vector plasmids contained full length expression cassettes including the promoter, the full-length transgene CDS and the polyadenylation signal (pA; supplementary Table S1). The two separate AAV vector plasmids (5′ and 3′) required to generate dual AAV vectors contained either the promoter followed by the N-terminal portion of the transgene CDS (5′ plasmid) or the C-terminal portion of the transgene CDS followed by the pA signal (3′ plasmid, supplementary Table S1). Normal size EGFP plasmids were generated by cloning the EGFP CDS of pAAV2.1-CMV-EGFP plasmid (720 bp; Auricchio *et al*, 2001) in pZac2.1 (Gao *et al*, 2000); oversize EGFP was generated from pAAV2.1-CMV-EGFP (Auricchio *et al*, 2001) by inserting a DNA stuffer sequence of 3632 bp from human *ABCA4* (NM_000350.2, bp 1960-5591) upstream of the CMV promoter and a second DNA stuffer sequence of 3621 bp, composed of: murine *ABCA4* (NM_007378.1, 1066-1 and 7124-6046 bp; 2145 total bp) and human *Harmonin* (NM_153676.3 131-1606 bp; 1476 total bp), downstream of the pA signal. To generate dual AAV vector plasmids, the EGFP CDS (720 bp) was split into two constructs: one containing the N-terminal CDS (PMID: 9759496, bp 1-393) and the other containing the C-terminal CDS (PMID: 9759496, bp 394-720). The stuffer sequences flanking the EGFP expression cassette in the EGFP OZ plasmid were used to generate dual AAV-TS-L and dual AAV-AK-L plasmids (supplementary Table S1) with a combined (5′+3′) genome length similar to the EGFP OZ construct size.

The oversize *ABCA4* plasmids contained the full-length human *ABCA4* CDS (NM_000350.2, bp 105-6926), while the oversize *MYO7A* plasmids contained the full-length human *MYO7A* CDS from isoform 1 (NM_000260.3, bp 273-6920). To generate plasmids for dual AAV OV vectors the *ABCA4* and *MYO7A* CDS were split into two constructs, one containing N-terminal CDS (*ABCA4*: NM_000350.2, bp 105-3588; *MYO7A*: NM_000260.3, bp 273-3782) and the other containing C-terminal CDS (*ABCA4*: NM_000350.2, bp 2819-6926; *MYO7A*: NM_000260.3, bp 2913-6920). Therefore, the region of homology shared by overlapping vector plasmids was 770 bp for *ABCA4* and 870 bp for *MYO7A*. To generate trans-splicing and hybrid vector plasmids the *ABCA4* and *MYO7A* CDS were split at a natural exon-exon junction. *ABCA4* was split between exons 19-20 (5′ half: NM_000350.2, 105-3022 bp; 3′ half: NM_000350.2, bp 3023-6926) and *MYO7A* was split between exons 24-25 (5′ half: NM_000260.3, bp 273-3380; 3′ half: NM_000260.3, bp 3381-6926). The ABCA4 and MYO7A proteins were both tagged at their C-terminus: ABCA4 with either the 3xflag or hemagglutinin (HA) tag; MYO7A with the HA tag only. In addition, the ABCA4 protein was tagged at both N- (amino acidic position 590) and C-termini with the 3xflag tag for the experiments shown in supplementary Figs S7 and S8. The splice donor (SD) and splice acceptor (SA) signals contained in dual trans-splicing and hybrid AAV vector plasmids are as follows: 5′-GTAAGTATCAAGGTTACAAGACAGGTTT AAGGAGACCAATAGAAACTGGGCTTGTCGAGACAGAGAAGACTCTTG CGTTTCT-3′ (SD); 5′-GATAGGCACCTATTGGTCTTACTG ACATCC ACTTTGCCTTTCTCTCCACAG-3′ (SA). The recombinogenic sequence contained in hybrid AP vector plasmids was derived from alkaline phosphatase (AP) gene (NM_001632, bp 823-1100), as previously described (Ghosh *et al*, 2011). The recombinogenic sequence contained in hybrid AK vector plasmids was derived from the phage F1 genome (Gene Bank accession number: J02448.1; bp

5850-5926). The AK sequence is: 5′-GGGATTTTGCC GATTTCGGCC TATTGGTTAAAAAATGAGCTGATTTAACAAAAATT TAACGCGAATT TTAACAAAAT-3′. To generate the pZac2.1-CMV-RFP plasmid, the monomeric RFP CDS (Campbell *et al*, 2002; 675 bp) was amplified and cloned in pZac2.1-CMV-EGFP plasmid using EcoRI and BamHI restriction sites. The pAAV2.1-CMV-DsRed plasmid (Palfi *et al*, 2012) was obtained by cloning the DsRed gene from the pDsRed-Express2 plasmid (Clontech, Saint-Germain-en-Laye, France) in the pAAV-MCS plasmid (Stratagene, La Jolla, CA, USA).

The ubiquitous CMV promoter is that contained in pZac2.1 (Gao *et al*, 2000) or pAAV2.1-CMV-EGFP (Auricchio *et al*, 2001); the ubiquitous CBA promoter was derived from pAAV2.1-CBA-EGFP (Mussolino *et al*, 2011), the PR-specific human RHO and RHOK promoters were derived from pAAV2.1-RHO-EGFP and pAAV2.1-RHOK-EGFP, respectively (Allocca *et al*, 2007); the RPE-specific VMD2 promoter (NG_009033.1, bp 4870-5470) corresponds to the previously described EcoRI-XcmI promoter fragment (Esumi *et al*, 2004) and was amplified by human genomic DNA. The details of cloning strategies as well as plasmid sequences are available upon request.

AAV vector production and characterization

AAV vectors were produced by the TIGEM AAV Vector Core by triple transfection of HEK293 cells followed by two rounds of $CsCl_2$ purification (Doria *et al*, 2013). For each viral preparation, physical titers [genome copies (GC)/ml] were determined by averaging the titer achieved by dot-blot analysis (Drittanti *et al*, 2000) and by PCR quantification using TaqMan (Applied Biosystems, Carlsbad, CA, USA; Doria *et al*, 2013). The probes used for dot-blot and PCR analyzes were designed to anneal with either the ITRs or regions within 1 kb from the ITRs. No statistically significant differences were found in the titers (GC/ml) of NS AAV2/2 or AAV2/8 compared to those of dual AAV OV, TS and hybrid vectors (supplementary Table S2). In addition alkaline Southern blot analysis of viral DNA extracted from several dual AAV OV, TS and hybrid AK preps showed that the AAV genome is homogeneous and its size corresponds to that expected independently of the presence of recombinogenic elements in the dual AAV vectors (supplementary Fig S15). However, since recombination is sequence-specific, the conclusions from supplementary Fig S15 can not be directly extrapolated to other vectors. The alkaline Southern blot analysis shown in supplementary Fig S15 was carried out as follows: 3×10^{10} GC of viral DNA were extracted from AAV particles. To digest unpackaged genomes, the vector solution was resuspended in 240 μl of PBS pH 7.4 1× (GIBCO; Invitrogen S.R.L., Milan, Italy) and then incubated with 1 U/μl of DNase I (Roche, Milan, Italy) in a total volume of 300 μl containing 40 mM TRIS–HCl, 10 mM NaCl, 6 mM MgCl2, 1 mM $CaCl_2$ pH 7.9 for 2 h at 37°C. The DNase I was then inactivated with 50 mM EDTA, followed by incubation with proteinase K and 2.5% *N*-lauroyl-sarcosil solution at 50°C for 45 min to lyse the capsids. The DNA was extracted twice with phenol-chloroform and precipitated with two volumes of ethanol 100 and 10% sodium acetate (3 M, pH 7). Alkaline agarose gel electrophoresis and blotting were performed as previously described (Sambrook & Russell, 2001). Ten microlitres of the 1 kb DNA ladder (N3232L; New England Biolabs, Ipswich, MA, USA) were loaded as molecular weight marker. Three different double strand DNA fragments were radio-labelled with [α-32]-CTP using the Amersham Rediprime II DNA labelling System (GE Healthcare Europe, GmbH, Milan, Italy) and used as probes. The 5′ probe (875 bp) was generated by digestion of the pZac2.1-CMV-*ABCA4_5′* plasmid with EagI; the 3′ probe (880 bp) was generated by double digestion of the pZac2.1-*ABCA4_3′_3xflag*_SV40 plasmid with StuI and NcoI; the EGFP probe (735 bp) was generated by digestion of the pAAV2.1-CMV-EGFP plasmid with NotI and BamHI. Prehybridization and hybridization were performed at 65°C in Church buffer (Sambrook & Russell, 2001) for 1 h and overnight, respectively. Then, the membrane (Whatman Nytran N, charged nylon membrane; Sigma-Aldrich, Milan, Italy) was washed for 30 min in SSC 2×-0.1% SDS and for 30 min in SSC 0.5×-0.1% SDS at 65°C, and then for 30 min in SSC 0.1×-0.1% SDS at 37°C. The membrane was then analyzed by X-ray autoradiography using Amersham Hyperfilm™ MP (GE Healthcare Europe, GmbH).

AAV infection of HEK293 cells

HEK293 cells were maintained in Dulbecco's modified Eagle's medium (DMEM) containing 10% fetal bovine serum and 2 mM L-glutamine (GIBCO; Invitrogen S.R.L.). Cells were plated in six-well plates at a density of 2×10^6 cells/well and transfected 16 h later with 1.3 μg of pDeltaF6 helper plasmid which contains the Ad helper genes (Zhang *et al*, 2000) using the calcium phosphate method. After 5 h, cells were washed once with serum-free DMEM and incubated with AAV2/2 vectors (m.o.i: 5×10^4 GC/cell of each vector; 1:1 co-infection with dual AAV vectors resulted in 1×10^5 total GC/cell) in a final volume of 700 μl serum-free DMEM. Two hours later 2 ml of complete DMEM were added to the cells. Cells were harvested 72 h following infection for Western blot analysis.

Animal models

Mice were housed at the Institute of Genetics and Biophysics animal house (Naples, Italy) and maintained under a 12-h light/dark cycle (10–50 lux exposure during the light phase). C57BL/6 and BALB/c mice were purchased from Harlan Italy SRL (Udine, Italy). Albino *Abca4*$^{-/-}$ mice were generated through successive crosses and backcrosses with BALB/c mice (homozygous for Rpe65 Leu450; Radu *et al*, 2004) and maintained inbred. Breeding was performed crossing homozygous mice. Pigmented *shaker1 4626SB/4626SB* (referred to as *sh1*$^{-/-}$) mice were imported from the Wellcome Trust Sanger Institute (Cambridge, UK, a kind gift of Dr Karen Steel) and back-crossed twice with CBA/Ca mice purchased from Harlan Italy SRL to obtain heterozygous *shaker1*$^{+}$*/4626SB* (referred to as *sh1*$^{+/-}$) mice to expand the colony. The mice were maintained intercrossed; breeding was performed crossing heterozygous females with heterozygous males. The pigmented *sh1* mice used in this study were either affected (*sh1*$^{-/-}$) or unaffected (*sh1*$^{+/-}$ and *sh1*$^{+/+}$). Albino *shaker1 4626SB/4626SB* mice (referred as *sh1*$^{-/-}$) were imported from the Medical Research Council Institute of Hearing Research (Nottingham, UK) and maintained inbred; breedings were performed crossing heterozygous female with homozygous males. The albino *sh1* mice used in this study were either affected (*sh1*$^{-/-}$) or unaffected (*sh1*$^{+/-}$). Figure 7B and supplementary Figs S13 and S14 show data from albino *sh1*$^{-/-}$ mice. The genotype for the *MYO7A*^{4626SB} allele was performed by PCR analysis of genomic DNA (extracted from the mouse tail tip) followed by DNA sequencing. The primers used for the PCR amplification are as follows: Fw1 (GTGGAGCTTGACATCTACTTGACC) and Rev3 (AGC TGACCCTCATGACTCTGC), which generate a product of 712 bp

that was sequenced with the Fw1 primer. The Large White Female pigs used in this study were registered as purebred in the LWHerd Book of the Italian National Pig Breeders' Association (Azienda Agricola Pasotti, Imola, Italy).

Subretinal injection of AAV vectors in mice and pigs

This study was carried out in accordance with the Association for Research in Vision and Ophthalmology Statement for the Use of Animals in Ophthalmic and Vision Research and with the Italian Ministry of Health regulation for animal procedures. All procedures on mice were submitted to the Italian Ministry of Health; Department of Public Health, Animal Health, Nutrition and Food Safety on October 17th, 2011. The Ministry of Health approved the procedures by silence/consent, as per article 7 of the 116/92 Ministerial Decree. Surgery was performed under anesthesia and all efforts were made to minimize suffering.

Mice (4–5 week-old) were anesthetized with an intraperitoneal injection of 2 ml/100 g body weight of avertin [1.25% w/v of 2,2,2-tribromoethanol and 2.5% v/v of 2-methyl-2-butanol (Sigma-Aldrich)] (Papaioannou & Fox, 1993), then AAV2/8 vectors were delivered subretinally via a trans-scleral trans-choroidal approach as described by Liang *et al* (2000). All eyes were treated with 1 μl of vector solution. The AAV2/8 doses (GC/eye) delivered vary across the different mouse experiments as it is described in the Results section. To compare dual AAV to single AAV NS vectors (supplementary Fig S1 and Fig 4A) we used the same dose of each vector because we considered that one GC of the 5′-vector plus one GC of the 3′-vector of dual AAVs are required to re-constitute one full-size functional genome as that contained in one particle of AAV NS. To exclude competition between dual AAV capsids at the entry step which may lead us to over-estimate the efficiency of AAV NS, we evaluated EGFP expression after subretinal delivery of either 1.7×10^9 GC of AAV2/8 NS-EGFP or 1.7×10^9 GC of AAV2/8-NS-EGFP + 1.7×10^9 GC of an AAV2/8 vector carrying an unrelated genome (AAV-unrelated, supplementary Fig S16). Notably, we found no significant differences in the levels of EGFP expression whether the unrelated AAV was added or not (supplementary Fig S16), proving that the double dose of dual AAV capsids administered when compared to AAV-NS does not affect dual AAV-mediated transduction.

AAV2/1-VMD2-*human Tyrosinase* (Gargiulo *et al*, 2009; dose: $2–5 \times 10^8$ GC/eye) or AAV2/5-CMV-*EGFP* (encoding normal size EGFP, dose: 4×10^8 GC/eye) were added to the AAV2/8 vector solution that was subretinally delivered to albino mice (*Abca4*$^{-/-}$, BALB/c, and *sh1*; Figs 5B, C and D and 6A and B; supplementary Figs S10 and S14) or pigmented *sh1* mice (Fig 8), respectively. This allowed us to mark the RPE within the transduced part of the eyecup, which was subsequently dissected and analyzed. Subretinal delivery of AAV vectors to the pig retina was performed as previously described (Mussolino *et al*, 2011). All eyes were treated with 100 μl of AAV2/8 vector solution. The AAV2/8 dose was 1×10^{10} (Fig 3B) or 1×10^{11} GC of each vector/eye (Fig 4B) and co-injection of dual AAV vectors resulted in a total dose of 2×10^{10} GC/eye or 2×10^{11} GC/eye, respectively.

Western blot analysis and ELISA

Samples [HEK293 cells, retinas or eyecups (cups + retinas)] for Western blot analysis were lysed in RIPA buffer (50 mM Tris–HCl pH 8.0, 150 mM NaCl, 1% NP40, 0.5% Na-Deoxycholate, 1 mM EDTA pH 8.0, 0.1% SDS) to extract EGFP and MYO7A proteins from HEK293 cells and eyecups, or in SIE buffer (250 mM sucrose, 3 mM imidazole pH 7.4, 1% ethanol, and 1% NP-40) to extract MYO7A from retinas and ABCA4 protein. Lysis buffers were supplemented with protease inhibitors (Complete Protease inhibitor cocktail tablets; Roche) and 1 mM phenylmethylsulfonyl. After lysis EGFP and MYO7A samples were denatured at 99°C for 5 min in 1X Laemli sample buffer; ABCA4 samples were denatured at 37°C for 15 min in 1X Laemli sample buffer supplemented with 4 M urea. Lysates were separated by 7% (ABCA4 and MYO7A samples) or 12% (EGFP samples) SDS–polyacrylamide gel electrophoresis. The antibodies used for immuno-blotting are as follows: anti-EGFP (1:500, sc-8334; Santa Cruz, Dallas, TX, USA); anti-3xflag (1:1000, A8592; Sigma-Aldrich); anti-Myo7a (1:500, polyclonal; Primm Srl, Milan, Italy) generated using a peptide corresponding to aminoacids 941–1070 of the human MYO7A protein; anti-HA antibody (1:2000, PRB-101P-200, HA.11; Covance, Princeton, NJ, USA); anti-β Tubulin (1:10 000, T5201; Sigma Aldrich); anti-Filamin A (1:1000, catalog#4762; Cell Signaling Technology, Danvers, MA, USA); anti-Dysferlin (1:500, Dysferlin, clone Ham1/7B6, MONX10795; Tebu-bio, Le Perray-en-Yveline, France). The quantification of EGFP, ABCA4 and MYO7A bands detected by Western blot was performed using ImageJ software (free download is available at http://rsbweb.nih.gov/ij/). ABCA4 and MYO7A expression was normalized to Filamin A or Dysferlin for the *in vitro* and *in vivo* experiments, respectively. EGFP expression was normalized to β-Tubulin. Different proteins were used for normalization based on the similarity of their molecular weight to those of the different transgene products. The TS (Fig 2D and E), TS-L (Fig 2F) and NS (supplementary Fig S1) histogram do not have standard error bars as only one TS, TS-L or NS sample has been loaded on each SDS–PAGE and used as internal reference sample in each independent experiment. To show the internal variability of TS, TS-L and NS samples we calculated the expression of proteins as percentage relative to the AK sample (set to 100%) which are the following: Fig 2D: TS = 106 ± 16%; Fig 2E: TS = 78 ± 4%; Fig 2F: TS-L = 39 ± 6%; supplementary Fig S1: NS = 906 ± 281%. The ELISA was performed on retina or eyecup lysates using the Max Discovery Green Fluorescent Protein Kit ELISA (Bioo Scientific Corporation, Austin, TX, USA).

Fundus photography

The fundus live-imaging was performed by dilating the eye of C57BL/6 with a drop of tropicamide 1% (Visufarma, Rome, Italy) and subsequent eye stimulation with a 300W flash. Fundus photographs were taken using a Topcon TRC-50IX retinal camera, with a FITC filter, connected to a charge-coupled-device Nikon D1H digital camera (Topcon Medical System, Oakland, NJ, USA).

Histology, light and fluorescence microscopy

To evaluate EGFP expression in histological sections, eyes from C57BL/6 mice or Large White pigs (Mussolino *et al*, 2011) were enucleated 1 month after AAV2/8 injection. Mouse eyes were fixed in 4% paraformaldehyde over-night and infiltrated with 30% sucrose over-night; the cornea and the lens were then dissected and the eyecups were embedded in optimal cutting temperature compound (O.C.T. matrix; Kaltek, Padua, Italy). PR co-transduction fol-

lowing subretinal combined delivery of AAV2/8-CMV-*EGFP* and -*RFP* vectors has been evaluated as follows: retinal cryosections from $n = 6$ eyes were analyzed under a fluorescent microscope using either the FITC (to visualize $EGFP^+$ cells) or Rhodamine (to visualize RFP^+ cells) filters. For each eye RFP^+ PR contained in one field at 20× magnification (at least 100) and the corresponding $EGFP^+$ PR (at least 200) were photographed and then counted. PR expressing both EGFP and RFP were unequivocally identified based on their identical shape on picture micrographs of the same field taken under either the FITC or Rhodamine filter. To calculate the percentage of co-transduced PR, the number of PR expressing both EGFP and RFP was divided by the total number of transduced PR, i.e. PR expressing at least one of the two reporter genes.

Pig eyes were fixed in 4% paraformaldehyde for 48 h, infiltrated with 10% sucrose for 4 h, 20% sucrose for 4 h and finally 30% sucrose overnight. Then, the cornea, the lens, and the vitreous body were dissected and the EGFP-positive portions of the eyecups were embedded in optimal cutting temperature compound (O.C.T. matrix; Kaltek). Serial cryosections (12 μm thick) were cut along the horizontal meridian and progressively distributed on slides. Retinal histology pictures were captured using a Zeiss Axiocam (Carl Zeiss, Oberkochen, Germany). Subretinal delivery in pigs of AAV vectors encoding for EGFP under the control of the Rhodopsin promoter resulted in PR transduction in: 100% of the retinas injected with: dual AAV TS (4/4), and dual AAV hybrid AK (3/3, Fig 4B).

To analyze melanosome localization in the RPE of pigmented *sh1* mice, eyes were enucleated 2–3 months following the AAV injection, fixed in 2% glutaraldehyde-2% paraformaldehyde in 0.1 M phosphate buffer over-night, rinsed in 0.1 M phosphate buffer and dissected under a florescence microscope. The EGFP-positive portions of the eyecups were embedded in Araldite 502/EMbed 812 (catalog #13940, Araldite 502/EMbed 812 KIT; Electron Microscopy Sciences, Hatfield, PA, USA). Semi-thin (0.5 μm) sections were transversally cut on a Leica Ultratome RM2235 (Leica Microsystems, Bannockburn, IL, USA), mounted on slides and stained with Epoxy tissue stain (catalog #14950; Electron Microscopy Sciences). Melanosomes were counted by a masked operator in about 10 different fields/eye under a light microscope at 100× magnification. Retinal pictures were captured using a Zeiss Axiocam (Carl Zeiss).

Flow cytometry

Flow cytometry analysis was carried out as described (Palfi *et al*, 2012). Briefly, eyes in adult 129 mice were subretinally injected with 3 μl of a 1:1 mixture of 3×10^9 GC of AAV2/8-EGFP and 3×10^9 GC of AAV2/8-DsRed. Control retinas were injected with 3 μl of either 3×10^9 GC of AAV2/8-EGFP or 3 μl of 3×10^9 GC of AAV2/8-DsRed or were left un-injected. Three weeks post-injection, retinas were dissociated in trypsin/HBSS, stained with DRAQ5 (Biostatus, Shepshed, UK) and EGFP (488:530/40), DsRed (564:615/20) and DRAQ5 (633: 665/20) fluorescence signals analyzed in the live cells using a Beckman Coulter Cyan ADP flow cytometer (Beckman Coulter Diagnostics Limited, Lismeehan, Ireland) modified by Propel Labs (Fort Collins, CO, USA). The analysis was carried out using Summit v4.3 (Beckman Coulter) software. Nucleated events were selected by gating the brightest DRAQ5 events in a bivariate density plot of the forward light scatter (FSC) versus DRAQ5. A second selection was done in the bivariate histogram of forward versus side scatter (FSC versus SSC), selecting the homogeneous and perfectly well defined population of events. Between 10 000 and 25 000 events were analyzed per sample.

Electron microscopy and immuno-gold labelling

For electron microscopy analyzes eyes were harvested from *Abca4*$^{-/-}$ or *sh1* mice at 3 and 2–3 months after AAV injection, respectively. Eyes were fixed in 0.2% glutaraldehyde-2% paraformaldehyde in 0.1 M PHEM buffer pH 6.9 (240 mM PIPES, 100 mM HEPES, 8 mM $MgCl_2$, 40 mM EGTA) for 2 h and then rinsed in 0.1 M PHEM buffer. Eyes were then dissected under light or fluorescence microscope to select the Tyrosinase- or EGFP-positive portions of the eyecups of albino (*Abca4*$^{-/-}$, BALB/c and *sh1*$^{-/-}$) and pigmented *sh1* mice, respectively. The transduced portion of the eyecups were subsequently embedded in 12% gelatin, infused with 2.3 M sucrose and frozen in liquid nitrogen. Cryosections (50 nm) were cut using a Leica Ultramicrotome EM FC7 (Leica Microsystems) and extreme care was taken to align PR connecting cilia longitudinally. To avoid bias in the attribution of morphological data to the various experimental groups, measurements of RPE thickness and counts of lipofuscin granules in *Abca4*$^{-/-}$ eyes were performed by a masked operator (Roman Polishchuk) using the iTEM software (Olympus SYS, Hamburg, Germany). Briefly, RPE thickness was measured in at least 30 different areas along the specimen length using the 'Arbitrary Line' tool of iTEM software. The 'Touch count' module of the iTEM software was utilized to count the number of lipofuscin granules in the 25 μm^2 areas distributed randomly across the RPE layer. The granule density was expressed as number of granules per 25 μm^2. The immuno-gold analysis aimed at testing the expression of ABCA4-HA in *Abca4*$^{-/-}$ samples after AAV vector delivery was performed by incubating cryosections successively with monoclonal anti-HA antibody (MMS-101P-50; Covance, 1:50), rabbit anti-mouse IgG, and 10-nm gold particle-conjugated protein A. To quantify rhodopsin localization to the connecting cilium of *sh1* PR, cryosections of *sh1* mice were successively incubated with anti-rhodopsin antibody (1D4, ab5417; Abcam, Cambridge, UK, 1:100), rabbit anti-mouse IgG, and 10-nm gold particle-conjugated protein A. The quantification of gold density of rhodospin in the connecting cilia was performed by a masked operator using iTEM software (Olympus SYS). Briefly, the 'Touch count' module of the iTEM software was used to count the number of gold particles per cilium that were then normalized to the cilium perimeter (nm) measured using the 'Closed polygon tool'. Gold density was expressed as gold particles/μm. Immunogold labelled cryosections were analyzed under FEI Tecnai-12 (FEI, Eindhoven, The Netherlands) electron microscope equipped with a Veletta CCD camera (Soft Imaging Systems, Munster, Germany) for digital image acquisition.

A2E measurement in *Abca4*$^{-/-}$ mice

To further evaluate lipofuscin accumulation in *Abca4*$^{-/-}$ mice, we attempted at measuring by either HPLC in combination with mass spectrometry (Gutierrez *et al*, 2010) or by HPLC alone (Parish *et al*, 1998; Ben-Shabat *et al*, 2002; Allocca *et al*, 2008) the A2E content of *Abca4*$^{-/-}$ eyecups which is reported to be increased compared to wild-type controls (Weng *et al*, 1999; Radu *et al*, 2004; Allocca *et al*, 2008).

Electrophysiological analyzes

To assess the recovery from light desensitization eyes were stimulated with three light flashes of 1 cd s/m^2 and then desensitized by exposure to constant light (300 cd/m^2) for 3 min. Then, eyes were stimulated over time using the pre-desensitization flash (1 cd s/m^2) at 0, 5, 15, 30, 45 and 60 min post-desensitization. The recovery of rod activity was evaluated by performing the ratio between the b-wave generated post-desensitization (at the different time points) and that generated pre-desensitization.

RNA extraction, cDNA production and reverse transcription analyzes

RNA was extracted at 72 h after HEK293 cells infection with dual AAV2/2 TS and hybrid AK vectors encoding for either *ABCA4* or *MYO7A* (5′+3′halves) and as negative controls with either the 5′or 3′ half of dual AAV2/2 vectors or with a single NS AAV2/2 *EGFP* vector.

Total RNA was extracted using the RT–PCR RNeasy MiniKit (Qiagen, Milan, Italy). One microgram of RNA was submitted to DNase I digestion (RNase Free DNase set; Qiagen) and cDNA was generated using the QuantiTect reverse transcription kit (Qiagen). To amplify the *ABCA4* mRNA region corresponding to the exon-intron junction used in dual AAV TS and hybrid AK vectors, 1 μl of cDNA and the following primers were used: Abca4_RT_Fw 5′-GCTGGGAAAAC CACCACC-3′ and Abca4_RT_Rev 5′-GTGGACACATGCCAAGGC-3′. A PCR product of the expected size (130 bp) was then sequenced. Five microlitres of cDNA were insted used to amplify the full-length *ABCA4* mRNA (6.9 kb) with a long-range PCR using TaKaRa LA Taq DNA polymerase kit (TaKaRa, Kioto, Japan), and the following primers: ATGFw 5′-GGTACCTCTAGAGTCGACCCGG-3′, which anneals upstream of the ATG start codon and SV40polyA-Rev 5′-ACTCAT CAATGTATCTTATCATGTC TG-3′. To amplify the MYO7A mRNA region corresponding to the exon-intron junction used in dual AAV TS and hybrid AK vectors, 1.5 μl of cDNA and the following primers were used: Fw 5′-AGG GGACAACTACGCACTC-3′ Rev 5′- GTC TTCTTGCCCAGGGTCTC-3′. A PCR product of the expected size (218 bp) was then sequenced. Two micrograms of total RNA were instead retro-transcribed using SuperScript® III First-Strand Synthesis System (Invitrogen) and 1 μl of cDNA was used to amplify the full-length *MYO7A* mRNA (6.7 kb) with a long-range PCR using TaKaRa LA Taq DNA polymerase kit (TaKaRa) and the following primers: ATGFw 5′-GCGGC CGCCATGGTGATTCTTCAGCAG-3′ and BgHpolyA-Rev 5′-TGGGA GTGGCACCTTCCA-3′.

Statistical analysis

Statistical P values ≤ 0.05 were considered significant. One-way ANOVA with *post-hoc* Multiple Comparison Procedure was used to compare data depicted in: Fig 2 (P ANOVA = A. 0.012; B. 1×10^{-7}; C. 0.002); Fig 4A (P ANOVA = 1.9×10^{-12}); Fig 6B (P ANOVA = 0.00126); Fig 6C (P ANOVA = 2.2×10^{-5}); Fig 8B (P ANOVA = 1.2×10^{-5}); Fig 8C (P ANOVA = 0.11); supplementary Fig S1 (P ANOVA = 2.3×10^{-8}); supplementary Fig S6 (P ANOVA = A: 0.13; B: 0.16); supplementary Table S2 (2/2 preps: P ANOVA = 0.0698; 2/8 preps: P ANOVA = 0.0767). As the counts of lipofuscin granules (Fig 5D) are expressed as discrete numbers, these were analyzed by deviance from a Negative Binomial generalized linear models (Venables & Ripley, 2002) (P value analysis of deviance: Fig 5D: 1.7×10^{-7}). The statistically significant differences between groups determined with the *post-hoc* Multiple Comparison Procedure are the following: Fig 2D: OV versus OZ $P = 0.03$; OV versus AP $P = 0.016$. Fig 2E: OV versus OZ $P = 0.0001$; OV versus AP $P = 1.1 \times 10^{-5}$; OV versus AK $P = 0.0017$; TS versus OZ $P = 1.8 \times 10^{-5}$; TS versus AP $P = 2.3 \times 10^{-6}$; TS versus AK $P = 0.026$; AK versus OZ $P = 9 \times 10^{-7}$; AK versus AP $P = 2 \times 10^{-7}$. Fig 2F: AK-L versus OZ $P = 0.003$; AK-L versus TS-L $P = 0.005$. Fig 4A: NS-*EGFP* versus TS-*EGFP* $P = 0$; NS-*EGFP* versus AK-*EGFP* $P = 0$. Fig 5D: WT versus $Abca4^{-/-}$ neg $P = 0.016$; WT versus $Abca4^{-/-}$ AK-*ABCA4* $P = 0.03$; $Abca4^{-/-}$ neg versus $Abca4^{-/-}$ TS-*ABCA4* $P = 0.0005$; $Abca4^{-/-}$ neg versus $Abca4^{-/-}$ AK-*ABCA4* $P = 9 \times 10^{-8}$. Fig 6B: $Abca4^{-/-}$ neg versus $Abca4^{-/-}$ TS-*ABCA4* $P = 0.012$; $Abca4^{-/-}$ neg versus $Abca4^{-/-}$ AK-*ABCA4* $P = 0.002$. Fig 6C (60 min): $Abca4^{-/-}$ neg versus $Abca4^{-/-}$ AK-*ABCA4*: 0.05; $Abca4^{-/-}$ neg versus $Abca4^{-/-}$ TS-*ABCA4*: 0.009; $Abca4^{-/-}$ AK-*ABCA4* versus WT: 0.002; $Abca4^{-/-}$ TS-*ABCA4* versus WT: 0.02 $Abca4^{-/-}$ neg versus WT 1×10^{-5}. Fig 8B: $sh1^{+/+}$ and $sh1^{+/-}$ versus $sh1^{-/-}$ neg $P = 7.7 \times 10^{-6}$; $sh1^{+/+}$ and $sh1^{+/-}$ versus $sh1^{-/-}$ TS-*MYO7A* $P = 0.025$; $sh1^{-/-}$ neg versus $sh1^{-/-}$ TS-*MYO7A* $P = 0.0028$; $sh1^{-/-}$ neg versus $sh1^{-/-}$ AK-*MYO7A* $P = 0.0002$. Supplementary Fig S1: NS-*EGFP* versus TS-*EGFP* $P = 0$; NS-*EGFP* versus AK-*EGFP* $P = 1 \times 10^{-7}$.

The Student's t-test was used to compare data depicted in supplementary Fig S10, S14 and S16. The data in the manuscript are depicted as mean ± standard error of the mean (s.e.m.). The s.e.m has been calculated using the number of independent *in vitro* experiments or eyes (not replicate measurements of the same sample).

Supplementary information for this article is available online: www.embomolmed.org

Acknowledgements

We thank Annamaria Carissimo and Luisa Cutillo (Bioinformatics Core, TIGEM, Naples, Italy) for the statistical analyzes; Enrico M. Surace (TIGEM, Naples, Italy), Maria L. Bacci (Department of Veterinary Morphophysiology and Animal Production, University of Bologna, Bologna, Italy) and Michele Della Corte (Department of Ophthalmology, Second University of Naples, Naples, Italy) for support with work in pigs; Elena Polishchuk and Simona Iacobacci (Advanced Microscopy and Imaging Core, TIGEM, Naples, Italy) for help with the immuno-electron microscopy analysis; Monica Doria and Antonella Ferrara (AAV Vector Core, TIGEM, Naples, Italy) for AAV vector production; Andrea Ballabio, Nicola Brunetti-Pierri (TIGEM, Naples, Italy), Ellen Abrams and Graciana Diez-Roux (Scientific Office, TIGEM, Naples, Italy) for the critical reading of this manuscript. Funding: The work of AA was supported by the following: the European Research Council/ERC Grant agreement no 282085 'RetGeneTx'; the European Community's Seventh Framework Programme (FP7/2007–2013) under Grant agreement no 242013 'Treatrush'; the NIH (grant R24 RY019861-01A); the Italian Telethon Foundation (grant TGM11MT1). We also thank the following agencies for support to GJF: Science Foundation Ireland (SFI) and the Health Research Board of Ireland/Fighting Blindness Ireland (MRCG).

Author contributions

The study was conceived and designed by AA, IT and PC. The manuscript was written by AA with contribution from PC. Most data were generated by IT and PC, IT performed *in vitro* and *in vivo* experiments with the ABCA4 gene, PC performed *in vitro* and *in vivo* experiments with the MYO7A gene, the *in vitro* and *in vivo* experiments with the EGFP gene were conducted by both IT and PC.

The paper explained

Problem
Inherited retinal degenerations (IRDs) are a common cause of blindness worldwide. Gene therapy with AAV vectors is safe and effective in patients with a childhood form of IRD. One of the major limitations to extend this clinical success to other blinding conditions is that many are caused by mutations in genes with large coding sequences that exceed AAV DNA cargo capacity.

Results
We have generated dual AAV vectors each containing one half of a large transgene which is reconstituted upon target cell co-infection by either splicing (trans-splicing, TS), homologous recombination (overlapping, OV) or a combination of the two (hybrid). We show that the delivery of dual AAV TS and hybrid vectors to the retina results in efficient reconstitution of large transgenes in mouse and pig photoreceptors, the major cell target of IRDs. Although the levels of transgene expression achieved with dual AAV vectors are lower than those achieved with a single normal size AAV, they result in significant improvement of the retinal disease of two mouse models of common IRDs due to mutations in large genes, Stargardt's disease (STGD) and Usher syndrome type IB (USH1B).

Impact
Our results provide proof-of-concept of gene therapy for STGD and USH1B using dual AAV vectors. Importantly, dual AAV vectors expand AAV cargo capacity for gene therapy of IRDs requiring transfer of large genes.

The data analyzes were performed by IT and PC with contributions from AS. AS, GC, CI and SdS performed retinal histology and contributed to the generation of plasmid constructs; CI performed subretinal injections in mice; EM performed the electrophysiological recordings and helped with work in pigs; SR performed subretinal injections in pigs; MG performed anesthesia in pigs; AP and GJF performed the EGFP- DsRed- co-trasduction experiments; RP performed immune-electron microscopy analyzes.

Conflict of interest
The authors declare that they have no conflict of interest.

For more information
Stargardt's disease: http://www.macular.org/stargardts.htm
Online Mendelian Inheritance in Man (OMIM): http://www.ncbi.nlm.nih.gov/omim
Retinal Information Network (RetNet): https://sph.uth.tmc.edu/retnet/
Author's website: http://www.tigem.it/en/research/researchers/alberto-auricchio

References

Allikmets R (1997) A photoreceptor cell-specific ATP-binding transporter gene (ABCR) is mutated in recessive Stargardt macular dystrophy. *Nat Genet* 17: 122

Allocca M, Doria M, Petrillo M, Colella P, Garcia-Hoyos M, Gibbs D, Kim SR, Maguire A, Rex TS, Di Vicino U *et al* (2008) Serotype-dependent packaging of large genes in adeno-associated viral vectors results in effective gene delivery in mice. *J Clin Invest* 118: 1955 – 1964

Allocca M, Mussolino C, Garcia-Hoyos M, Sanges D, Iodice C, Petrillo M, Vandenberghe LH, Wilson JM, Marigo V, Surace EM *et al* (2007) Novel adeno-associated virus serotypes efficiently transduce murine photoreceptors. *J Virol* 81: 11372 – 11380

Auricchio A (2011) Fighting blindness with adeno-associated virus serotype 8. *Hum Gene Ther* 22: 1169 – 1170

Auricchio A, Hildinger M, O'Connor E, Gao GP, Wilson JM (2001) Isolation of highly infectious and pure adeno-associated virus type 2 vectors with a single-step gravity-flow column. *Hum Gene Ther* 12: 71 – 76

Bainbridge JW, Smith AJ, Barker SS, Robbie S, Henderson R, Balaggan K, Viswanathan A, Holder GE, Stockman A, Tyler N *et al* (2008) Effect of gene therapy on visual function in Leber's congenital amaurosis. *N Engl J Med* 358: 2231 – 2239

Ben-Shabat S, Parish CA, Vollmer HR, Itagaki Y, Fishkin N, Nakanishi K, Sparrow JR (2002) Biosynthetic studies of A2E, a major fluorophore of retinal pigment epithelial lipofuscin. *J Biol Chem* 277: 7183 – 7190

Campbell RE, Tour O, Palmer AE, Steinbach PA, Baird GS, Zacharias DA, Tsien RY (2002) A monomeric red fluorescent protein. *Proc Natl Acad Sci USA* 99: 7877 – 7882

Cideciyan AV, Hauswirth WW, Aleman TS, Kaushal S, Schwartz SB, Boye SL, Windsor EA, Conlon TJ, Sumaroka A, Roman AJ *et al* (2009) Vision 1 year after gene therapy for Leber's congenital amaurosis. *N Engl J Med* 361: 725 – 727

Colella P, Cotugno G, Auricchio A (2009) Ocular gene therapy: current progress and future prospects. *Trends Mol Med* 15: 23 – 31

Conley SM, Cai X, Makkia R, Wu Y, Sparrow JR, Naash MI (2012) Increased cone sensitivity to ABCA4 deficiency provides insight into macular vision loss in Stargardt's dystrophy. *Biochim Biophys Acta* 1822: 1169 – 1179

Dong B, Nakai H, Xiao W (2010a) Characterization of genome integrity for oversized recombinant AAV vector. *Mol Ther* 18: 87 – 92

Dong X, Tian W, Wang G, Dong Z, Shen W, Zheng G, Wu X, Xue J, Wang Y, Chen J (2010b) Establishment of an AAV reverse infection-based array. *PLoS One* 5: e13479

Doria M, Ferrara A, Auricchio A (2013) AAV2/8 vectors purified from culture medium with a simple and rapid protocol transduce murine liver, muscle, and retina efficiently. *Hum Gene Ther Methods*. DOI: 10.1089/hgtb.2013.155

Drittanti L, Rivet C, Manceau P, Danos O, Vega M (2000) High throughput production, screening and analysis of adeno-associated viral vectors. *Gene Ther* 7: 924 – 929

Dryja T (2001) Retinitis pigmentosa and stationary night blindness. In *The Online Metabolic and Molecular Bases of Inherited Diseases*, Scriver C, Beaudet A, Sly W, Valle D (eds), pp 5903 – 5933. New York, NY: McGraw-Hill

Duan D, Sharma P, Yang J, Yue Y, Dudus L, Zhang Y, Fisher KJ, Engelhardt JF (1998) Circular intermediates of recombinant adeno-associated virus have defined structural characteristics responsible for long-term episomal persistence in muscle tissue. *J Virol* 72: 8568 – 8577

Duan D, Yue Y, Engelhardt JF (2001) Expanding AAV packaging capacity with trans-splicing or overlapping vectors: a quantitative comparison. *Mol Ther* 4: 383 – 391

Esumi N, Oshima Y, Li Y, Campochiaro PA, Zack DJ (2004) Analysis of the VMD2 promoter and implication of E-box binding factors in its regulation. *J Biol Chem* 279: 19064 – 19073

Fishel ML, Vasko MR, Kelley MR (2007) DNA repair in neurons: so if they don't divide what's to repair? *Mutat Res* 614: 24 – 36

Flotte TR, Afione SA, Solow R, Drumm ML, Markakis D, Guggino WB, Zeitlin PL, Carter BJ (1993) Expression of the cystic fibrosis transmembrane conductance regulator from a novel adeno-associated virus promoter. *J Biol Chem* 268: 3781 – 3790

Gao G, Qu G, Burnham MS, Huang J, Chirmule N, Joshi B, Yu QC, Marsh JA, Conceicao CM, Wilson JM (2000) Purification of recombinant adeno-associated virus vectors by column chromatography and its performance in vivo. *Hum Gene Ther* 11: 2079 – 2091

Gargiulo A, Bonetti C, Montefusco S, Neglia S, Di Vicino U, Marrocco E, Corte MD, Domenici L, Auricchio A, Surace EM (2009) AAV-mediated tyrosinase gene transfer restores melanogenesis and retinal function in a model of oculo-cutaneous albinism type I (OCA1). *Mol Ther* 17: 1347 – 1354

Ghosh A, Yue Y, Duan D (2006) Viral serotype and the transgene sequence influence overlapping adeno-associated viral (AAV) vector-mediated gene transfer in skeletal muscle. *J Gene Med* 8: 298 – 305

Ghosh A, Yue Y, Duan D (2011) Efficient transgene reconstitution with hybrid dual AAV vectors carrying the minimized bridging sequences. *Hum Gene Ther* 22: 77 – 83

Ghosh A, Yue Y, Lai Y, Duan D (2008) A hybrid vector system expands adeno-associated viral vector packaging capacity in a transgene-independent manner. *Mol Ther* 16: 124 – 130

Gibbs D, Diemer T, Khanobdee K, Hu J, Bok D, Williams DS (2010) Function of MYO7A in the human RPE and the validity of shaker1 mice as a model for Usher syndrome 1B. *Invest Ophthalmol Vis Sci* 51: 1130 – 1135

Grieger JC, Samulski RJ (2005) Packaging capacity of adeno-associated virus serotypes: impact of larger genomes on infectivity and postentry steps. *J Virol* 79: 9933 – 9944

Grose WE, Clark KR, Griffin D, Malik V, Shontz KM, Montgomery CL, Lewis S, Brown RH Jr, Janssen PM, Mendell JR *et al* (2012) Homologous recombination mediates functional recovery of dysferlin deficiency following AAV5 gene transfer. *PLoS One* 7: e39233

Gutierrez DB, Blakeley L, Goletz PW, Schey KL, Hanneken A, Koutalos Y, Crouch RK, Ablonczy Z (2010) Mass spectrometry provides accurate and sensitive quantitation of A2E. *Photochem Photobiol Sci* 9: 1513 – 1519

Han Z, Conley SM, Makkia RS, Cooper MJ, Naash MI (2012) DNA nanoparticle-mediated ABCA4 delivery rescues Stargardt dystrophy in mice. *J Clin Invest* 122: 3221 – 3226

Hasson T, Heintzelman MB, Santos-Sacchi J, Corey DP, Mooseker MS (1995) Expression in cochlea and retina of myosin VIIa, the gene product defective in Usher syndrome type 1B. *Proc Natl Acad Sci USA* 92: 9815 – 9819

Hermonat PL, Quirk JG, Bishop BM, Han L (1997) The packaging capacity of adeno-associated virus (AAV) and the potential for wild-type-plus AAV gene therapy vectors. *FEBS Lett* 407: 78 – 84

Hirsch ML, Agbandje-McKenna M, Samulski RJ (2010) Little vector, big gene transduction: fragmented genome reassembly of adeno-associated virus. *Mol Ther* 18: 6 – 8

Hirsch ML, Li C, Bellon I, Yin C, Chavala S, Pryadkina M, Richard I, Samulski RJ (2013) Oversized AAV transduction is mediated via a DNA-PKcs Independent, Rad51C-dependent repair pathway. *Mol Ther*. DOI: 10.1038/mt.2013.184

Hirsch ML, Storici F, Li C, Choi VW, Samulski RJ (2009) AAV recombineering with single strand oligonucleotides. *PLoS One* 4: e7705

Illing M, Molday LL, Molday RS (1997) The 220-kDa rim protein of retinal rod outer segments is a member of the ABC transporter superfamily. *J Biol Chem* 272: 10303 – 10310

Jacobson SG, Acland GM, Aguirre GD, Aleman TS, Schwartz SB, Cideciyan AV, Zeiss CJ, Komaromy AM, Kaushal S, Roman AJ *et al* (2006) Safety of recombinant adeno-associated virus type 2-RPE65 vector delivered by ocular subretinal injection. *Mol Ther* 13: 1074 – 1084

Lai Y, Yue Y, Duan D (2010) Evidence for the failure of adeno-associated virus serotype 5 to package a viral genome $\geq$ 8.2 kb. *Mol Ther* 18: 75 – 79

Lai Y, Yue Y, Liu M, Ghosh A, Engelhardt JF, Chamberlain JS, Duan D (2005) Efficient in vivo gene expression by trans-splicing adeno-associated viral vectors. *Nat Biotechnol* 23: 1435 – 1439

Liang FQ, Anand V, Maguire AM, Bennett J (2000) Intraocular delivery of recombinant virus. In *Methods in Molecular Medicine: Vision Research Protocols*, Rakoczy PE (ed.), pp 125 – 139. Totowa, NJ, USA: Humana Press Inc

Lillo C, Kitamoto J, Liu X, Quint E, Steel KP, Williams DS (2003) Mouse models for Usher syndrome 1B. *Adv Exp Med Biol* 533: 143 – 150

Liu X, Ondek B, Williams DS (1998) Mutant myosin VIIa causes defective melanosome distribution in the RPE of shaker-1 mice. *Nat Genet* 19: 117 – 118

Liu X, Udovichenko IP, Brown SD, Steel KP, Williams DS (1999) Myosin VIIa participates in opsin transport through the photoreceptor cilium. *J Neurosci* 19: 6267 – 6274

Liu X, Vansant G, Udovichenko IP, Wolfrum U, Williams DS (1997) Myosin VIIa, the product of the Usher 1B syndrome gene, is concentrated in the connecting cilia of photoreceptor cells. *Cell Motil Cytoskeleton* 37: 240 – 252

Lopes VS, Boye SE, Louie CM, Boye S, Dyka F, Chiodo V, Fofo H, Hauswirth WW, Williams DS (2013) Retinal gene therapy with a large MYO7A cDNA using adeno-associated virus. *Gene Ther* 20: 824 – 833

Ma L, Kaufman Y, Zhang J, Washington I (2011) C20-D3-vitamin A slows lipofuscin accumulation and electrophysiological retinal degeneration in a mouse model of Stargardt disease. *J Biol Chem* 286: 7966 – 7974

Maguire AM, High KA, Auricchio A, Wright JF, Pierce EA, Testa F, Mingozzi F, Bennicelli JL, Ying GS, Rossi S *et al* (2009) Age-dependent effects of RPE65 gene therapy for Leber's congenital amaurosis: a phase 1 dose-escalation trial. *Lancet* 374: 1597 – 1605

Maguire AM, Simonelli F, Pierce EA, Pugh EN Jr, Mingozzi F, Bennicelli J, Banfi S, Marshall KA, Testa F, Surace EM *et al* (2008) Safety and efficacy of gene transfer for Leber's congenital amaurosis. *N Engl J Med* 358: 2240 – 2248

Maiti P, Kong J, Kim SR, Sparrow JR, Allikmets R, Rando RR (2006) Small molecule RPE65 antagonists limit the visual cycle and prevent lipofuscin formation. *Biochemistry (Mosc)* 45: 852 – 860

Mata NL, Tzekov RT, Liu X, Weng J, Birch DG, Travis GH (2001) Delayed dark-adaptation and lipofuscin accumulation in abcr+/- mice: implications for involvement of ABCR in age-related macular degeneration. *Invest Ophthalmol Vis Sci* 42: 1685 – 1690

Millan JM, Aller E, Jaijo T, Blanco-Kelly F, Gimenez-Pardo A, Ayuso C (2011) An update on the genetics of usher syndrome. *J Ophthalmol* 2011: 417217

Molday RS, Zhang K (2010) Defective lipid transport and biosynthesis in recessive and dominant Stargardt macular degeneration. *Prog Lipid Res* 49: 476 – 492

Monahan PE, Lothrop CD, Sun J, Hirsch ML, Kafri T, Kantor B, Sarkar R, Tillson DM, Elia JR, Samulski RJ (2010) Proteasome inhibitors enhance gene delivery by AAV virus vectors expressing large genomes in hemophilia mouse and dog models: a strategy for broad clinical application. *Mol Ther* 18: 1907 – 1916

Mussolino C, della Corte M, Rossi S, Viola F, Di Vicino U, Marrocco E, Neglia S, Doria M, Testa F, Giovannoni R *et al* (2011) AAV-mediated photoreceptor transduction of the pig cone-enriched retina. *Gene Ther* 18: 637 – 645

Natkunarajah M, Trittibach P, McIntosh J, Duran Y, Barker SE, Smith AJ, Nathwani AC, Ali RR (2008) Assessment of ocular transduction using single-stranded and self-complementary recombinant adeno-associated virus serotype 2/8. *Gene Ther* 15: 463 – 467

Palfi A, Chadderton N, McKee AG, Blanco Fernandez A, Humphries P, Kenna PF, Farrar GJ (2012) Efficacy of codelivery of dual AAV2/5 vectors in the murine retina and hippocampus. *Hum Gene Ther* 23: 847 – 858

Papaioannou VE, Fox JG (1993) Efficacy of tribromoethanol anesthesia in mice. *Lab Anim Sci* 43: 189 – 192

Parish CA, Hashimoto M, Nakanishi K, Dillon J, Sparrow J (1998) Isolation and one-step preparation of A2E and iso-A2E, fluorophores from human retinal pigment epithelium. *Proc Natl Acad Sci USA* 95: 14609 – 14613

Radu RA, Mata NL, Bagla A, Travis GH (2004) Light exposure stimulates formation of A2E oxiranes in a mouse model of Stargardt's macular degeneration. *Proc Natl Acad Sci USA* 101: 5928 – 5933

Radu RA, Yuan Q, Hu J, Peng JH, Lloyd M, Nusinowitz S, Bok D, Travis GH (2008) Accelerated accumulation of lipofuscin pigments in the RPE of a mouse model for ABCA4-mediated retinal dystrophies following Vitamin A supplementation. *Invest Ophthalmol Vis Sci* 49: 3821 – 3829

Reich SJ, Auricchio A, Hildinger M, Glover E, Maguire AM, Wilson JM, Bennett J (2003) Efficient trans-splicing in the retina expands the utility of adeno-
associated virus as a vector for gene therapy. *Hum Gene Ther* 14: 37 – 44

Sambrook J, Russell DW (2001) *Molecular Cloning: A Laboratory Manual*. New York, USA: Cold Spring Harbor Laboratory Press

Simonelli F, Maguire AM, Testa F, Pierce EA, Mingozzi F, Bennicelli JL, Rossi S, Marshall K, Banfi S, Surace EM *et al* (2010) Gene therapy for Leber's congenital amaurosis is safe and effective through 1.5 years after vector administration. *Mol Ther* 18: 643 – 650

Sohocki MM, Daiger SP, Bowne SJ, Rodriquez JA, Northrup H, Heckenlively JR, Birch DG, Mintz-Hittner H, Ruiz RS, Lewis RA *et al* (2001) Prevalence of mutations causing retinitis pigmentosa and other inherited retinopathies. *Hum Mutat* 17: 42 – 51

Sun H, Nathans J (1997) Stargardt's ABCR is localized to the disc membrane of retinal rod outer segments. *Nat Genet* 17: 15 – 16

Testa F, Maguire AM, Rossi S, Pierce EA, Melillo P, Marshall K, Banfi S, Surace EM, Sun J, Acerra C *et al* (2013) Three-year follow-up after unilateral subretinal delivery of adeno-associated virus in patients with Leber congenital Amaurosis type 2. *Ophthalmology* 120: 1283 – 1291

Vandenberghe LH, Auricchio A (2012) Novel adeno-associated viral vectors for retinal gene therapy. *Gene Ther* 19: 162 – 168

Vandenberghe LH, Bell P, Maguire AM, Cearley CN, Xiao R, Calcedo R, Wang L, Castle MJ, Maguire AC, Grant R *et al* (2011) Dosage thresholds for AAV2 and AAV8 photoreceptor gene therapy in monkey. *Sci Transl Med* 3: 88ra54

Venables VN, Ripley BD (2002) *Modern Applied Statistics with S*. Chambers SJ, Eddy W, Hardle W, Sheater S, Tierney L (eds). New York, NY, USA: Springer Science+Business Media

Wang Y, Ling C, Song L, Wang L, Aslanidi GV, Tan M, Srivastava A (2012) Limitations of encapsidation of recombinant self-complementary adeno-associated viral genomes in different serotype capsids and their quantitation. *Hum Gene Ther Methods* 23: 225 – 233

Weng J, Mata NL, Azarian SM, Tzekov RT, Birch DG, Travis GH (1999) Insights into the function of Rim protein in photoreceptors and etiology of Stargardt's disease from the phenotype in abcr knockout mice. *Cell* 98: 13 – 23

Wu J, Zhao W, Zhong L, Han Z, Li B, Ma W, Weigel-Kelley KA, Warrington KH, Srivastava A (2007) Self-complementary recombinant adeno-associated viral vectors: packaging capacity and the role of rep proteins in vector purity. *Hum Gene Ther* 18: 171 – 182

Wu L, Nagasaki T, Sparrow JR (2010a) Photoreceptor cell degeneration in Abcr (–/–) mice. *Adv Exp Med Biol* 664: 533 – 539

Wu Z, Yang H, Colosi P (2010b) Effect of genome size on AAV vector packaging. *Mol Ther* 18: 80 – 86

Yan Z, Lei-Butters DC, Zhang Y, Zak R, Engelhardt JF (2007) Hybrid adeno-associated virus bearing nonhomologous inverted terminal repeats enhances dual-vector reconstruction of minigenes in vivo. *Hum Gene Ther* 18: 81 – 87

Yan Z, Zak R, Zhang Y, Engelhardt JF (2005) Inverted terminal repeat sequences are important for intermolecular recombination and circularization of adeno-associated virus genomes. *J Virol* 79: 364 – 379

Yan Z, Zhang Y, Duan D, Engelhardt JF (2000) Trans-splicing vectors expand the utility of adeno-associated virus for gene therapy. *Proc Natl Acad Sci USA* 97: 6716 – 6721

Zhang Y, Chirmule N, Gao G, Wilson J (2000) CD40 ligand-dependent activation of cytotoxic T lymphocytes by adeno-associated virus vectors in vivo: role of immature dendritic cells. *J Virol* 74: 8003 – 8010

